COHERENT DETECTION OF DATA AND TIMING SIGNALS OVER OPTICAL FIBER FOR TELESCOPE NETWORKS

KETSHABILE NFANYANA

Submitted in partial fulfilment of the requirements for the degree of

MAGISTER SCIENTIAE

In the Faculty of Science at Nelson Mandela University

December 2020

Supervisor: T.B. GIBBON

Co-Supervisor: S. WASSIN

Acknowledgement

It gives me immense pleasure to thank Prof T.B Gibbon and Dr. S. Wassin for all their support and continuous guidance during both practical and theoretical phases of this thesis. I thank them for always encouraging me to give my utmost best and to present high quality and meaningful results.

I also thank my colleagues at center for broadband communication (CBC), R. Karembera, J. Jena, M. Ngungi, P. Dlamini, and V. Shumane for their love, technical and personal support. With the words of Yamada Jirokichi, “Sword and mind must be united. Technique by itself is insufficient, and spirit alone is not enough,” I thank you.

I also would like to express my deepest gratitude to SARAO, SKA, DARTCOM, NRF, CISCO and TELKOM for their direct and indirect funding towards my degree.

NELSON MANDELA
UNIVERSITY

DECLARATION BY CANDIDATE

NAME: KETSHABILE NFANYANA

STUDENT NUMBER: s221395261

QUALIFICATION: MSc PHYSICS

TITLE OF PROJECT:

COHERENT DETECTION OF DATA AND TIMING SIGNALS OVER OPTICAL FIBER FOR TELESCOPE NETWORKS

DECLARATION:

In accordance with Rule G5.11.4, I hereby declare that the above-mentioned treatise/ dissertation/ thesis is my own work and that it has not previously been submitted for assessment to another University or for another qualification.

SIGNATURE:

DATE: 18/11/2020

TABLE OF CONTENTS

Abstract

Telescope networks are increasingly being developed with networks such as the SKA telescope demanding the use of high-end technology to be incorporated. These networks require accurate clock signals to be transported to antennas as well as massive data to be transported from individual parabolic array antennas to a central computer for data analysis. To achieve this, optical fiber technology forms the backbone of these networks, proving high speed transmission and required bandwidth. For a distributed telescope network, coherent detection technology serves as the ideal optical fiber technology candidate for transport of information to a correlator. Use of this technology constitutes too many benefits. Sensitivity of the system is improved, and advanced modulation formats can be employed thereby improving spectral efficiency. Furthermore, coherent detection allows for digital signal processing algorithms to be employed for equalization of transmission impairments such as chromatic dispersion (CD), polarization mode dispersion (PMD), phase noise and nonlinear effects in the electrical domain.

CD equalization is performed in the time or frequency domain using digital filters which suppress the fibers dispersion effectively. PMD equalization is usually performed in the time domain through the use of adaptive filters which employ algorithms such as least mean squares (LMS) and constant modulus algorithm (CMA). These algorithms further equalize residual CD. In mitigation of phase noise (carrier phase recovery), feed-forward and feedback carrier phase algorithms are used. Fiber nonlinearities and other impairments are compensated using the digital backpropagation algorithm which solves for the Manakov equation and nonlinear Schrödinger equation (NLSE). Distribution of stable clock signals to individual antennas is an important aspect of telescope networks. Clock signals are used to drive the digitizers and time stamping of received antenna information. These clock signals can be distributed using coherent detection technology by phase modulating the clock so as to provide inherent phase modulation robustness to noise through the fiber.

In this thesis, we present coherent detection of non-return-to-zero pseudorandom binary sequence (PRBS-7) using binary phase shift keying (BPSK) through 26.6 km non-zero dispersion shifted fiber (NZDSF) at 10 Gbps. Digital signal processing for equalization of CD and PMD was performed offline using MATLAB software. For residual CD and PMD

equalization, the LMS algorithm was used. The performance of the system, bit error rate (BER), was compared with that of an intensity modulated on-off keying (OOK) signal at the same bit rate. Basing on receiver sensitivity performance of OOK at 10^{-9} bit error rate, BPSK achieved superior performance with receiver sensitivity improvements of 18.37 dB and 13.89 dB attained for back-to-back and transmission over fiber, respectively.

Phase modulation transmission of a 4 GHz clock signal was also conducted. Frequency instability, Allan variance and phase noise, of phase modulated clock was compared with that of intensity modulated clock. Moreover, we present an all optical clock generation scheme using frequency heterodyning technique. Allan variance values in the range of 10^{-10} were attained. The frequency instability of this clock generation scheme was quantified using the spectrum analyzer method. Furthermore, an all-photonic technique for data latency tracking of 5G networks over optical fiber is presented. The technique is spectrally efficient and is able to track latency down to the nano second timescale.

List of acronyms

4G	Fourth generation
5G	Fifth generation
ADC	Analogue to digital converter
ASE	Amplifies spontaneous emissions
BER	Bit error rate
BERT	Bit error rate tester
BPF	Band pass filter
BPSK	Binary phase shift keying
CBC	Center for broadband communication
CD	Chromatic dispersion
CMA	Constant modulus algorithm
CR	Coherent receiver
CSRZ	Carrier suppressed return to zero
DDL	Differential delay line
DFB	Distributed feedback
DGD	Differential group delay
DSP	Digital signal processing
DUT	Device under test
EDFA	Erbium doped fiber amplifier
EVM	Error vector magnitude

FEC	Forward error correction
IM	Intensity modulation
IM-DD	Intensity modulation direct detection
ITU	International telecommunications union
LMS	Least mean squares
LPF	Low pass filter
LTE	Long term evolution
MMF	Multi mode fiber
MZM	Mach-Zehnder modulator
M-PSK	Multilevel phase shift keying
M-QAM	Multilevel quadrature amplitude modulation
NLSE	Non-linear Schrödinger equation
NRZ	Non-return to zero
NTP	Network time protocol
NZDSF	Non zero dispersion shifted fiber
OSNR	Optical signal to noise ratio
OOK	On off keying
PIN	Positive intrinsic negative
PD	Photodiode
PDL	Polarization dependent loss
PM	Phase modulation

PMD	Polarization mode dispersion
PC	Polarization controller
SKA	Square kilometer array
SNR	Signal to noise ratio
VOA	Variable optical attenuator
WDM	Wavelength division multiplexing

List of figures

List of tables

Chapter 1

Fiber optic communications technologies have revolutionized the communications world. Tremendous bandwidth, high speed links and increased network reach are many of the benefits of optical fiber communication. Although this is the case, the performance of high-speed optical fiber transmission systems is greatly affected by attenuation, polarization mode dispersion, chromatic dispersion, and nonlinear effects. Coherent detection allows for equalization of these transmission impairments in the electrical domain as well as further increasing network reach and capacity through the use of complex modulation (advanced modulation) formats. In this chapter, we provide a description of the layout of the thesis. Furthermore, we provide the history of fiber optic communication. Current deployed optical fiber technologies are also provided with the evolution of the state-of-the-art coherent detection technique being briefly discussed.

1.1 Thesis outline

In this dissertation, we present a detailed study of coherent optical fiber communication in the context of telescope networks using BPSK (Binary phase shift keying) as the modulation format. We show post equalization of fiber optic transmission impairments focusing mainly on chromatic dispersion (CD) and polarization mode dispersion (PMD) with the digital signal processing (DSP) algorithm used in PMD equalization being the least mean squares algorithm (LMS). The performance of coherent BPSK is compared with OOK (On off keying) modulation. Furthermore, we present a technique for generating an all optical clock signal using classical frequency heterodyning at the photodiode. Stability, long term, and short term, of the system is investigated with results obtained being used for comparative analysis with clock systems used in real life applications.

Coherent BPSK and equalization of PMD in the digital domain were experimentally demonstrated for the first time at the center for broadband communication (CBC) at Nelson Mandela University. Moreover, a novel way of tracking data latency in 5G networks was demonstrated with findings published in the journal of optical society of America. Chapter 11 explains this in more detail.

The structure of this thesis is as follows:

Chapter 1 presents a brief introduction on the history and development of optical fiber communication systems. Current fiber optic technologies such as wavelength division multiplexing (WDM) and coherent detection are also discussed in part.

In chapter 2, concepts related to the characteristics of light as a carrier confined in optical fiber are introduced. The construction and different types of optical fiber is also presented. Transmission impairments encountered by a wave propagating in fiber are discussed extensively. The impacts posed by fiber attenuation, laser phase noise, CD, PMD, and nonlinear effects on the transmission systems are discussed. This provides insight on the fundamental principle of DSP equalization techniques for each transmission impairment.

Chapter 3 presents an in-depth overview of coherent optical fiber communication. Here, we explore the transmitter and receiver part of the communication system. Modulation formats used in fiber optics are explained in detailed. Metrics used to evaluate performance, bit error rate and error vector magnitude, of the transmission system are discussed. The configuration of a typical coherent receiver is explained in detail with DSP signal flow and algorithms for equalization of transmission impairments being explained extensively. For equalization of PMD, two algorithms are explained, constant modulus algorithm (CMA) and LMS.

In chapter 4, we discuss optical techniques used for generation of clock signals. Here, emphasis is on two techniques, frequency comb method and heterodyning. Theoretical performance of these two techniques is evaluated.

In chapter 5, an overview of optical telescope networks is presented. Networks such as the SKA, e-MERLIN and Giant meter wave telescope are described with more emphasis being on the state-of-the-art SKA and its requirements in terms of data capacity and timing. A brief description of the network architecture of the SKA is provided. The importance of timing in telescope networks is also placed into perspective in this chapter.

Chapter 6 is the first chapter of the experimental section. In this chapter, techniques used for measurement of frequency stability in relation to this work are provided. A brief description of

equipment used in fiber optic transmission is presented with the focus being on those utilized for this thesis.

In chapter 7, we experimentally demonstrate phase modulation of data using BPSK format at 10 Gbps. The modulated signal is coherently detected with equalization of transmission impairments, residual CD and PMD, being performed offline in MATLAB. We further show OOK at the same bit rate and evaluate the performance of both transmission systems using modulation metrics described in chapter 3.

In chapter 8, we experimentally generate a 4 GHz clock signal using the classical frequency heterodyning technique. The performance of the clock generation scheme is evaluated by measuring frequency instabilities, both long term and short term. Suitable applications with regard to the clock generating system are identified basing on the performance.

In chapter 9, we demonstrate phase modulation of a 4 GHz clock signal as part of telescope network timing dissemination architecture. Moreover, OOK modulation of the 4 GHz clock is performed. The frequency stability of the recovered phase or intensity modulated clock is measured. The two network clock distribution schemes are compared.

In chapter 10, we validate the significance of physical layer security associated with conveying information through optical fiber. Various techniques which pose a security breach are discussed. We experimentally demonstrate tapping of information through macro bending of the optical fiber and identify he wavelength dependence associated with the tapping scheme.

In chapter 11, we experimentally demonstrate a new way of tracking latency of data at 10 Gbps over optical fiber for 5G networks. We validate the merits of the technique which include spectral efficiency and time resolution amongst others.

Finally, chapter 12 presents a summary of our research work in this thesis. Moreover, we provide some suggestions and plans for our future investigations in coherent optical fiber technology as well as network security at the physical layer.

1.2 History of fiber optics communication

Although telecommunication using light waves was proposed in 1880 by Alexander bell, the feasibility of fiber optic communication came in the 1960s due to the invention of lasers and glass fibers [1, 2]. In 1960, the invention of a laser offered an optical source for optical fiber communication. At this time, the attenuation in optical fibers extremely high at around 1000 dB/km [3, 4]. The cornerstone in optical fiber communication occurred in 1970 when a fiber with loss around 20 dB/km was developed by Corning Glass Works [2, 3]. Even though this was high compared to today's standards, this marked the first time by which fiber produced would be suited for telecom distances.

The first generation of optical communication systems was developed in 1975, operating in the 800 nm region. These systems reached a bit rate of 45 Mbps with repeater spacing up to 10 km [4, 5]. The second generation was developed in the early 1980s. These systems operated in the 1330 nm region. The fiber loss at this time was below 1 dB/km [4]. The transmission speed was initially limited by dispersion in multimode fibers, but this soon changed through the development of single mode fibers in 1981. Systems in the second generation reached bit rates up to 1.7 Gbps with repeater spacing up to 50 km [4]. Third generation optical fiber communication systems were also concurrently developed in the 1980s. These systems operated near the 1550 nm region. The fiber loss in that region was around 0.2 dB/km [4, 6]. The problem posed by dispersion was mitigated by using dispersion shifted fibers. Third generation systems reached a bit rates up to 2.5 Gbps with repeater spacing up to 100 km [3, 4]. Optical coherent detection was also extensively researched during this period because of its high sensitivity and long reach capability. However, research on this technology soon diminished due to the development of wavelength division multiplexing systems (WDM) and invention of the erbium doped fiber amplifier (EDFA) in the 1990s. The 1990s marked the fourth generation of optical fiber communication systems. These systems employed EDFA's and WDM technologies to increase repeater spacing (reduced number of repeater stations) and increase channel capacity, respectively. In 2006, bit rates of 14 Tbps were reached over 160 km line [5]. Optical technologies first to fourth generation all employed intensity modulation direct detection (IMDD) scheme. In 2005, coherent detection regained interest [3]. This is was constituted by advances in digital signal processing.

1.3 Current fiber optics communication technologies

Dense wavelength division multiplexing (DWDM) is the most current fiber optic technology. The emphasis is to increase the channel capacity by increasing the number of channels that can be transmitted and also reducing spacing between channels. The increase in WDM bandwidth requires that all channels outside the classical EDFA band, C band window, be amplified and this is archived using Raman amplification. Moreover, a new kind of fiber, dry fiber, has been developed with the property that fiber losses are small over the 1330 to 1650 nm wavelength range [4]. The hydroxyl ion (OH) concentration in this fiber is greatly reduced to a level that the absorption peaks which occur in convectional fiber almost disappear. Coherent detection is also one technology which aims at increasing the spectral efficiency of a single WDM channel (well beyond 1 b/s/Hz) as well as improving receiver sensitivity. Coherent detection technology supports the use of complex modulation formats where information is encoded in more than one degree of freedom of the light carrier wave. The receiver sensitivity is improved by up to 20 dB compared with IMDD systems [4]. This is economically beneficial since few repeater stations and amplifiers are required in the transmission channel. Therefore, network reach is increased to several thousand kilometers. Moreover, at the receiver, the recovered signal contains all information. Therefore, DSP algorithms are performed for equalization of transmission impairments. These algorithms can be implemented at the receiver (post equalization) or transmitter (pre equalization) side. The most important technical issue is the real time operation of digital coherent receivers which depends on the computing speed of analog to digital converters and DSP components.

References

[1] J.L. Miller, "Optical Fibers," in *Optical Communications Rules of Thumb*, McGraw-Hill, 2003.
Available:https://0www.accessengineeringlibrary.com.wam.seals.ac.za/content/book/9780071387781/chapter/chapter9

[2] R.W. Waynant, and M.N. Ediger, "Optical Fibers" in *Electro-Optics Handbook*, 2nd ed. McGraw-Hill, 2000.

Available:https://0www.accessengineeringlibrary.com.wam.seals.ac.za/content/book/9780070687165/chapter/chapter12

[3] T. Xu, "DSP based Chromatic Dispersion Equalization and Carrier Phase Estimation in High Speed Coherent Optical Transmission Systems," Ph.D. dissertation, dept. of Optics and Photonics, Royal Institute of Technology, Stockholm, Sweden, 2012.

[4] G.P. Agrawal, "Introduction," in *Fiber-Optic Communication Systems*, 3rd ed. John Wiley & Sons, 2002.

[5] "Fiber-optic communication history," April.19, 2016. Accessed on July. 21, 2020. [Online]. Available: https://www.fiberoptictel.com/fiber-optic-communication-history/

[6] M.D Al-Amri, M.M. El-Gomati and M.S. Zubairy, "Optical Communication: Its History and Recent Progress," in *Optics in Our Time*, Springer, pp. 177-181, 2016. Accessed on July. 21, 2020. [Online].

Available: https://link.springer.com/chapter/10.1007/978-3-319-31903-2_8#citeas

Chapter 2

2.1 Introduction

Light is an electromagnetic wave which consists of two distinct waves oscillating perpendicular to each other. These waves are the electric field and magnetic field. Like all other electromagnetic waves, propagation of light in a waveguide such as optical fiber is explained using Maxwell's equations [1]. Maxwell's equations used to explain change in electric $\boldsymbol{E}$ and magnetic $\boldsymbol{H}$ fields in space and time are given by

$$\nabla \times \boldsymbol{E} = -\frac{\delta \boldsymbol{B}}{\delta t}$$

$$\nabla \times \boldsymbol{H} = \boldsymbol{J} + \frac{\delta \boldsymbol{D}}{\delta t} \ , \boldsymbol{J} = \eta \boldsymbol{E}$$

$$\nabla . \boldsymbol{D} = p$$

$$\nabla . \boldsymbol{B} = 0 \qquad (2.1)$$

where $\boldsymbol{B}$ and $\boldsymbol{D}$ denote magnetic flux and electric flux densities, respectively and $\boldsymbol{J}$ is the current density. The relationship between the flux densities and field vectors is given by

$$\boldsymbol{D} = \varepsilon \boldsymbol{E} + P$$

$$\boldsymbol{B} = \mu(\boldsymbol{H} + M) \qquad (2.2)$$

where P and M represent induced electric and magnetic densities. ε and μ represent permeability and permittivity in vacuum, respectively. In optical fiber medium, there is no electric charge, the volume density of electric charge is zero (p = 0). Moreover, silica is a nonmagnetic material and its conductivity is extremely low (η ≈ 0). Therefore, there is no induced magnetic density (M = 0). The induced electric density is also zero (P = 0) [1]. Therefore,

$$\nabla \times \boldsymbol{E} = -\mu \frac{\delta \boldsymbol{H}}{\delta t} \qquad (2.3)$$

$$\nabla \times \boldsymbol{H} = \varepsilon \frac{\delta \boldsymbol{E}}{\delta t} \qquad (2.4)$$

$$\nabla . \boldsymbol{E} = 0 \qquad (2.5)$$

$$\nabla . \boldsymbol{H} = 0 \qquad (2.6)$$

Equations 2.3 and 2.4 are used to generate the wave equations given by

$$\nabla^2 \boldsymbol{E} = \frac{1}{C^2}\frac{\partial^2 \boldsymbol{E}}{\partial t^2} \quad \nabla^2 \boldsymbol{H} = \frac{1}{C^2}\frac{\partial^2 \boldsymbol{H}}{\partial t^2} \tag{2.7}$$

where *c* is the speed of light. In optical fiber, the speed of the wave changes. This a consequence of the permittivity and permeability of the material being different from that of vacuum. The light wave travels at a lower speed *v*. The ratio of the speed of light in vacuum to its speed in fiber is referred to as index of refraction, *n*.

$$n = \frac{C}{V} \tag{2.8}$$

The degree of refraction of light ray as it passes from one material to the next depends on the refractive index of the material. When light passes from a medium of high refractive index to a material with lower one, light is refracted towards normal. When the angle of incidence is increased, the angle of refraction approaches 90^o with normal [2]. This is referred to as the critical angle and is given by

$$\emptyset_{critical} = \sin^{-1}\frac{n_2}{n_1} \tag{2.9}$$

When the angle of incidence is increased past the critical angle, light is totally internally reflected. Total internal reflection is the principle of propagation of a light carrier within an optical fiber. Figure 2.1 below provides a pictorial overview of total internal reflection principle.

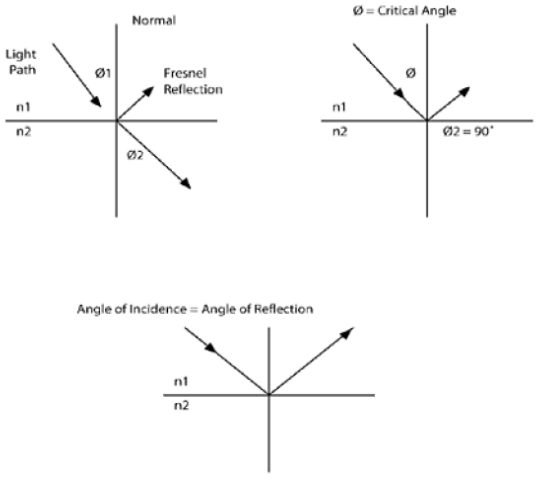

Fig. 2.1. Lightwave refraction principle [2]. n1: Refractive index of core. n2: Refractive index of cladding.

2.2 Optical fiber construction

An optical fiber is a waveguide which consist of three concentric components, inner core, outer cladding, and coating [2]. The core, cladding and coating are made of various materials. The material used for construction of the core and cladding can either be glass or plastic. The coating is always made from plastic. The core is the central region of the fiber where most of the light propagate. The cladding surrounds the core and helps confine the light in the core as well as providing additional strength. The refractive index of the inner core is higher than of the outer cladding. A light ray injected into the fiber core eventually hits the boundary between the cladding and core. When the light ray is launched into the core at an angle greater than the critical angle, it propagates through the fiber by experiencing total internal reflection. Light striking the boundary at an angle less than the critical angle, travels into the cladding and is eventually lost. The coating insulates the core and cladding form the environment and also gives fiber intrinsic strength. Figure 2.2 shows the geometry of a typical optical fiber.

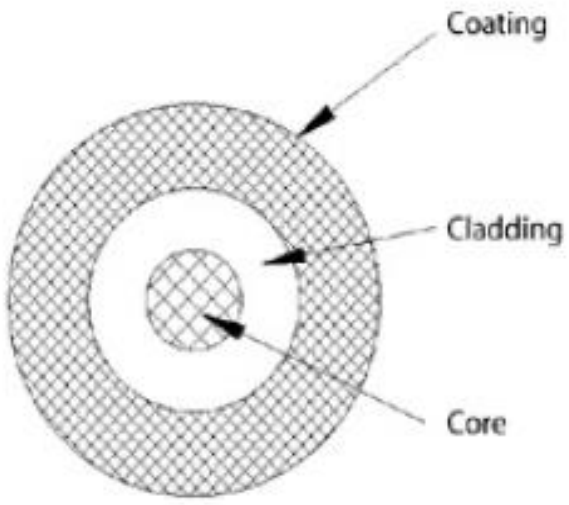

Fig. 2.2. Optical fiber geometry [2].

Propagation of light through the fiber is explained using Maxwell's equations which show that light does not travel randomly, rather, it is channeled into modes. Therefore, classification of a fiber is by both the number of modes it can support/transmit and its construction. The two types of fiber are single mode fiber (SMF) and multimode fiber (MMF).

2.2.1 Single Mode Fiber

A single mode fiber allows only one mode to propagate through the fiber. This type of fiber is commonly used in long distance fiber communication at high data rates. This is because they do not experience multimode dispersion, a phenomenon in which narrow pulses of light spread out in time as they travel through the fiber. However, at high data rates, the signal travelling in SMF suffers from chromatic dispersion, a transmission impairment later discussed in this chapter. The core of a SMF is less than 10 microns although the cladding is typically about 125 microns [3, 4]. The index profile of an SMF is step index. The schematic for this type of index profile is shown in figure 2.3. A step index profile is one which has a flat index profile for the core, constant profile for the cladding and an abrupt (sharp) change at the interface.

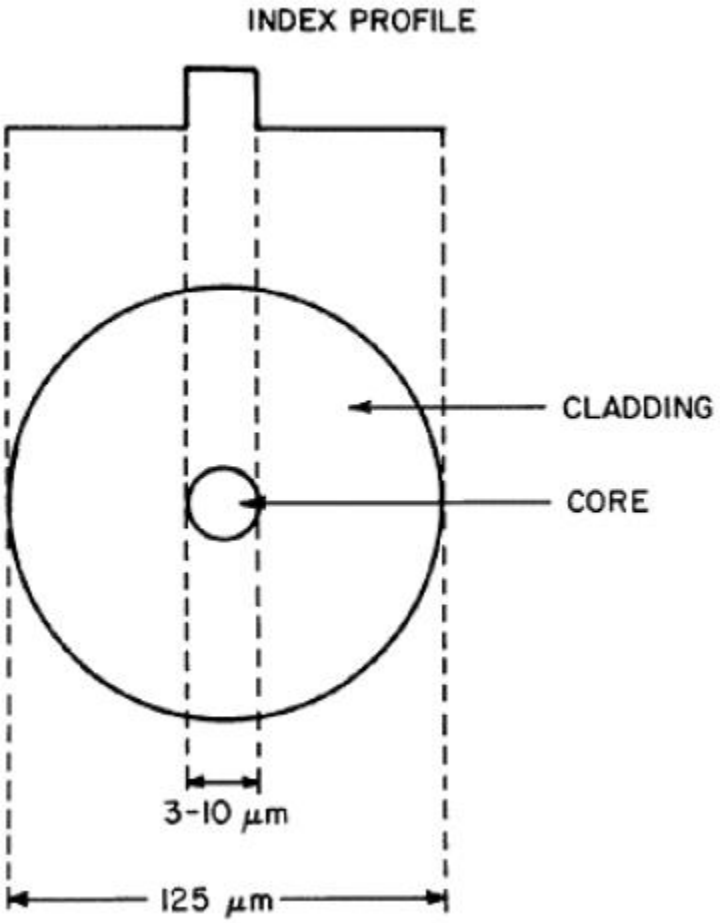

Fig. 2.3. Typical dimensions and index profile of SMF [4].

2.2.2 Multimode Fiber

Multimode fiber allows the transmission of many modes. Coupling of a light pulse onto an MMF is relatively easy compared to SMF. This is a consequence of its larger core which is typically 50 to 1000 microns [2]. MMF's are low cost. However, it suffers from low data rates for long distance transmission. Therefore, these fibers are usually used within short reach networks typically 300 m or less. There are two types of multimode fibers, graded index, and step index MMF. In graded index, the core index is not uniform. It is highest at the center of the fiber and decreases parabolically until it matches the cladding. Figure 2.4 shows characteristics of these two types of MMF.

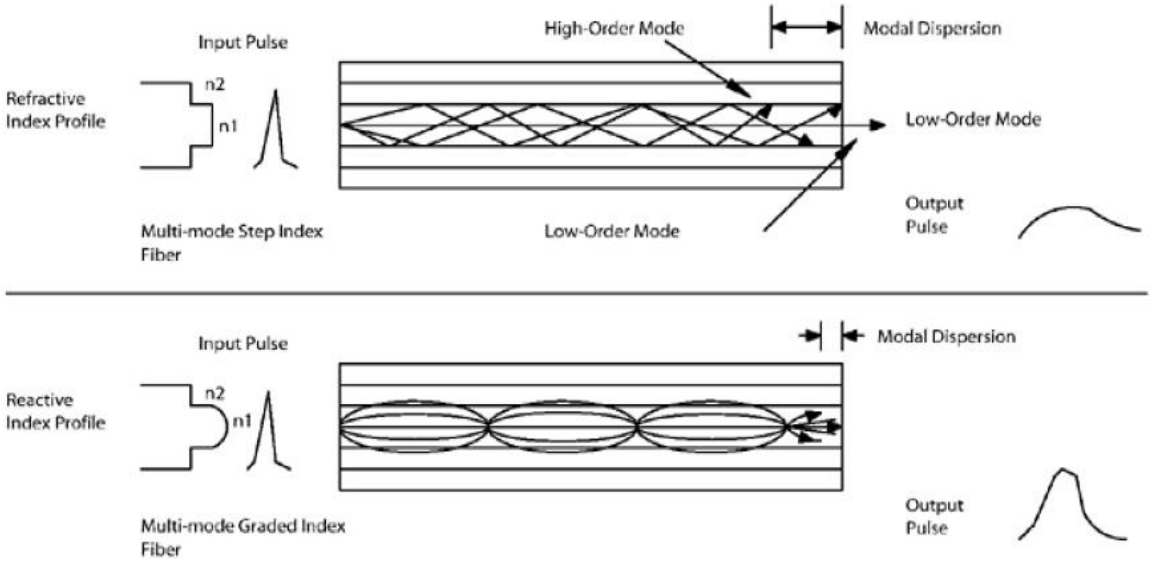

Fig. 2.4. MMF fiber index profiles and dispersion characteristics [2].

MMF suffer from modal dispersion. Modal dispersion for step index MMF is higher compared to its graded index counterpart. Like step index SMF, graded index MMF limits modal dispersion. The core in graded index MMF is a series of concentric rings each with a lower refractive index with respect to the center [2]. Since high-order modes have a faster average velocity than low-order modes and rays of light not being sharply reflected by the core-cladding interface (refracted successfully by layers of the core), all modes tend to arrive at a given point at nearly the same time.

2.3 Optical fiber transmission impairments

Optical fiber is one of the most deployed and used transmission mediums across the world. It is used as the backbone of network architectures due to its tremendous bandwidth, robustness to noise and capability to transmit information at very high data rates with low loss over long distances. However, when using this material to carry network traffic, transmission impairments are encountered due to the physical nature of the optical fiber. For long haul optical communication, these effects become severe as impairments accumulate with distance ultimately distorting the signal. These impairments can be divided into linear and non-linear effects.

2.3.1 Linear impairments

2.3.1.1 Attenuation

An optical signal travelling through optical fiber experiences attenuation. There are various processes which attribute to degradation in signal power at the receiver. Material absorption and Rayleigh scattering are predominant attenuation processes in optical fiber [5]. Rayleigh scattering is caused by small scale inhomogeneities, glass composition fluctuations, which are produced in the fiber fabrication process. This process accounts for approximately 96% of attenuation in optical fiber [6]. Absorption depends on wavelength and composition of the substance (material type). When residual hydrogen atoms interact with oxygen atoms in silica glass fiber, it produces hydroxyl (OH) ions. These ions lead to absorption peaks at 0.72μm, 0.88μm, 0.95μm, 1.13μm, 1.24μm and 1.38μm thereby constituting to higher total attenuation when wavelengths around those absorption peaks are used [6, 7]. However, OH absorption band is narrow enough that fibers can attain less than 0.2 dB/km at 1550 nm. Power at a distance z from the transmitter is given by

$$P(z) = P(0)exp^{-\alpha z} \tag{2.10}$$

where *P(0)* is the launch power and α is the loss coefficient. The loss coefficient is normally given in dB/km. A standard single mode fiber (SSMF) has an average attenuation coefficient of 0.2dB/km over the C-band spectrum [8]. In-order to compensate for attenuation and further the transmission reach with maximum distance between repeater stations, EDFA's are used. A transmission architecture which uses an EDFA is shown in figure 2.5.

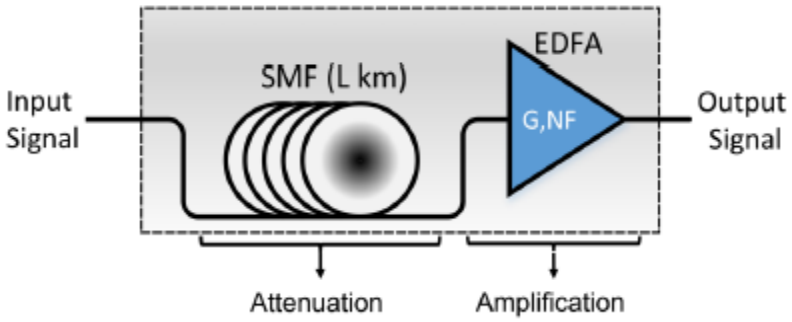

Fig. 2.5 Optical transmission system with EDFA [8].

Optical amplifiers are active sources of additive noise. Amplifiers generate background noise which arises from the nature of the amplification process. In the case of EDFAs, a small portion of erbium atoms instinctively fall from the excited state hence releasing energy as light in the form of spontaneous emission [7]. As more EDFAs are placed along the link, this noise gets amplified. Therefore, the processes of amplification inherently introduce amplified spontaneous emissions (ASE) which degrades the optical signal-to-noise ratio (OSNR) of the signal with respect to the OSNR of the input signal. The OSNR is defined by

$$OSNR = \frac{P_{sig}}{2B_{ref}N_{ASE}} \tag{2.11}$$

where P_{sig}, N_{ASE} and B_{ref} are the average signal power, amplifier noise figure in decibels and optical measurement bandwidth, respectively. The measurement bandwidth is normally chosen to be 12.5 GHz. EDFA's have noise figures in the range of 4 to 6 decibels [8].

2.3.1.2 Chromatic dispersion

Different wavelengths travel at different speeds and therefore arrive at slightly different times at the receiver. This is caused by the dependence of the phase and group velocities on the optical frequency of the light. CD imposes a delay on the frequency components of the light pulse propagating through the fiber thereby causing it to broaden in time. CD consists of material dispersion and waveguide dispersion [5]. Material dispersion is due to variations in the refractive index of the fiber core with wavelength. A portion of light travels in the cladding giving rise to waveguide dispersion. Waveguide dispersion is caused by the wavelength dependence of the propagation constant of the fiber. This is important in single mode fibers. The larger the

wavelength, the more the fundamental mode will spread from the core into the cladding causing the mode to propagate faster. Chromatic dispersion in optical fiber is an all pass filter on the electric field of the light wave [9]. The frequency response of the filter is given by

$$H(\omega) = exp^{(j\frac{\lambda_0^2 Dz}{4\pi c}\omega^2)} \tag{2.12}$$

where z is the propagation distance, c is the speed of light in vacuum and D is the dispersion parameter. For telecom fibers, the dispersion parameter at a given wavelength, λ, is expressed as

$$D = -\frac{2\pi c}{\lambda_0^2}\beta_2 \tag{2.13}$$

where β_2 is the second order dispersion parameter at carrier angular frequency. The parameter D has units ps/(nm.km). In optical communication systems, broadening of light pulses causes inter symbol interference (ISI) thereby degrading system performance. A light pulse will typically have a curved shape when observing its intensity with time. CD can be either positive or negative as shown by equation 2.13. For positive CD, shorter wavelengths travel faster than longer wavelengths such that after some time, the shorter wavelengths would have moved forward in time with respect to the longer wavelengths. Therefore, the beginning and end of a pulse in time would have spread further apart. For a 10 Gbps optical transmission system with 0.2 nm pulse spectral width using a fiber with 1 ps/(nm.km) CD, a single pulse will spread by a whole bit (100 ps) after 500 km and will be completely indistinguishable from adjacent bits. Figure 2.6 shows the effect of CD on optical communication.

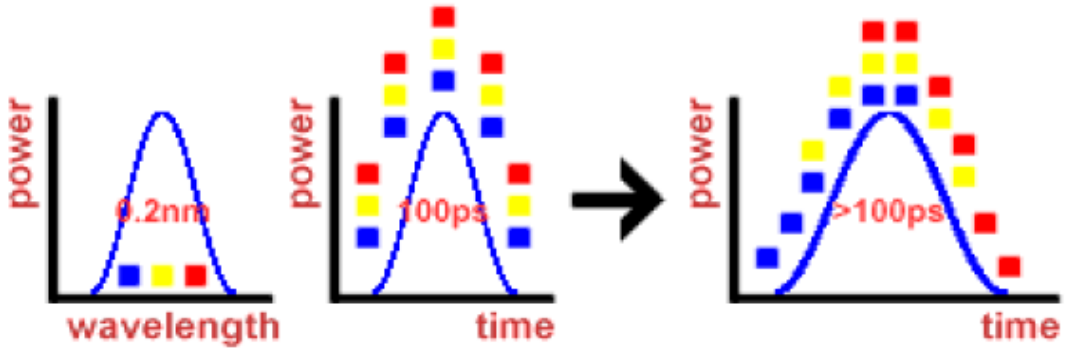

Fig. 2.6. Effect of CD on a light pulse before and after transmission [10].

The amount of CD experienced in the fiber is dependent on the wavelength of the carrier. Shorter wavelengths experience small CD compared to longer wavelengths. Equation 2.13 provides a mathematical description of this effect.

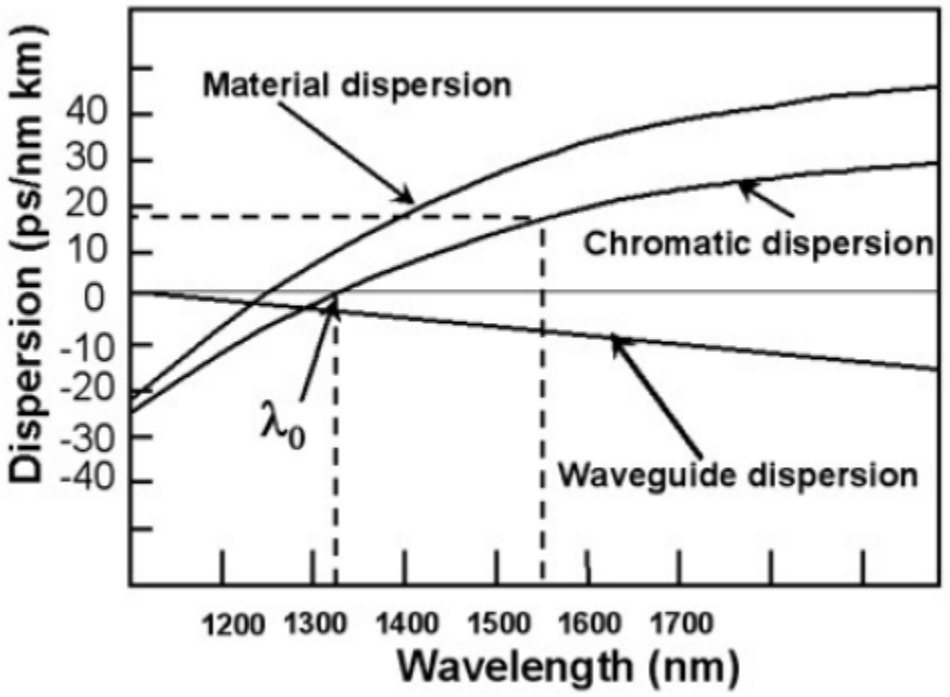

Fig. 2.7. Wavelength dependence of dispersion parameters in dispersion unshifted single mode fibers (ITU G.652) [5].

Chromatic dispersion of different wavelengths in standard single mode fiber is shown in figure 2.7. In figure 2.7, chromatic dispersion value is near zero at 1310 nm and 16 ps/(nm.km) at 1550 nm, which is the operational wavelength for most optical fiber communication systems today [5]. In traditional optical fiber transmission systems, CD is usually compensated by using dispersion compensation fibers. Fibers such as non-zero dispersion shifted fibers (NZDSF) are available for use in telecommunications. These fibers have near zero CD near 1550 nm. In coherent optical communication, equalization of this phenomenon is carried out in the digital domain either at the transmitter (pre-equalization) or at the receiver (post-equalization).

2.3.1.3 Polarization mode dispersion (PMD)

Single mode optical fiber (SMF) and components support one fundamental mode. This mode consists of two orthogonal polarization mode. Ideally, an SMF has perfect cylindrical symmetry over its full length. Both polarization modes have the same refractive index. These modes will thereby travel at the same speed and arrive at the same time at the receiver. However, due to the manufacturing process, imperfections in the geometry of the core of the fiber are introduced. These asymmetries introduce small index of refraction differences between the two polarization states. This is referred to as modal birefringence [11]. Birefringence generates differing optical axes and as such polarization modes will travel at different speeds when aligned to different polarization axes. This results in different propagation times between the two polarization modes known as differential group delay (DGD). DGD is the unit used to describe the degree of PMD and is typically measured in picoseconds per square kilometer (ps/√km) [5, 11]. Since PMD is random and follows the Maxwellian distribution, the mean DGD is used to express the degree of PMD in practical telecommunication systems. Figure 2.8 shows the effect of PMD on a polarized light wave propagating in optical fiber.

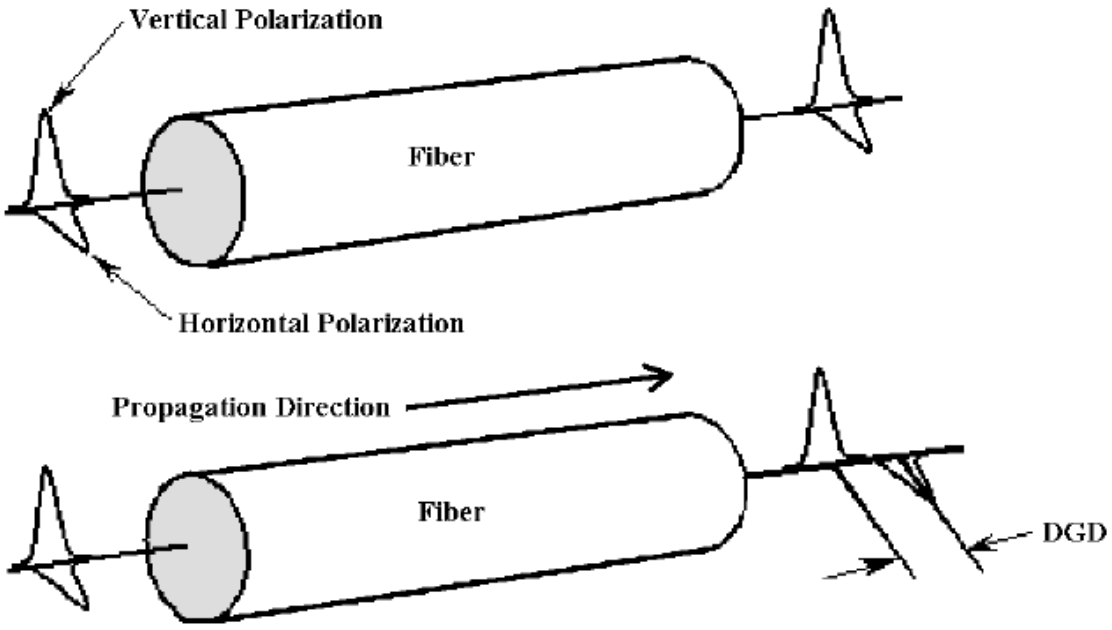

Fig. 2.8. Effect of PMD. Top: Perfect/theoretical fiber. Bottom: Real fiber [11].

In single mode fibers, the value of PMD is from 0.1 ps/√km to 1 ps/√km [5]. PMD effects are time varying therefore equalization can be archived by using a dynamic polarization controller to compensate for the differential group delay. However, such devices are both bulky and expensive. In coherent optical communication, equalization is archived in the digital domain by using adaptive filters.

2.3.1.4 Laser phase noise

Laser phase noise is one of the most significant transmission impairments in coherent optical communication. Phase noise influences synchronization between the transmitter and local oscillator. In systems which use intensity modulation direct detection (IM-DD), phase noise is not significant since information is in the amplitude of the carrier. For coherent communication, information is encoded in the phase of the carrier. Phase noise degrades the quality of the signal constellation. A signal constellation is a vector diagram depicting the position of symbols in the complex plane. These diagram are ideal in identifying the modulation format used in conveying information. The received constellation experiences rotation as well as scattering of symbols. Figure 2.9 shows this effect. In legacy coherent systems, phase noise equalization was achieved using an optical phase locked loop (OPLL) to track the phase of the incoming signal. In modern digital coherent systems, equalization is archived using DSP. Algorithms such as feed-forward and feed-back carrier phase estimation are used [5]. In feedback scheme, a digital phase locked loop is used. The digital loop comprises of a decision directed phase detector [12]. The error signal arising from the phase detector is then used to de-rotate the constellation points. In feedforward, data modulation is first removed from the signal. For M-PSK, raising the signal to the M^{th} power will remove data modulation. The estimated unwrapped phase is then averaged before being used to de-rotate constellation points.

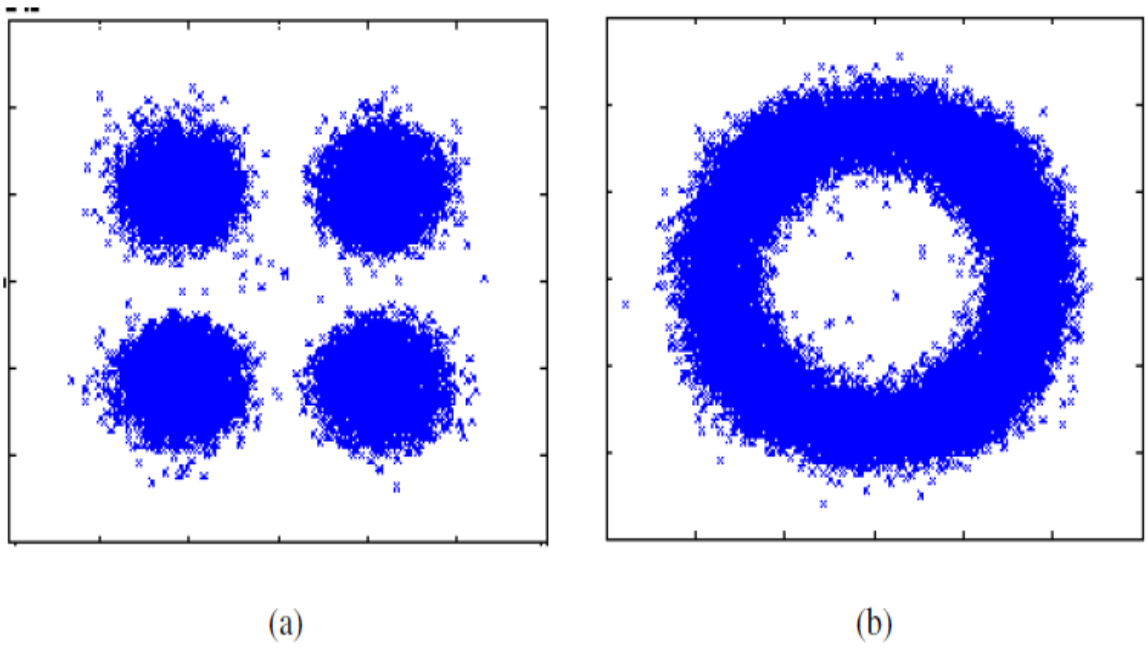

Fig. 2.9. Effect of Phase noise on QPSK constellation [5]. (a) With small phase noise, (b) with large phase noise value.

2.3.2 Nonlinear impairments

In the design of an optical fiber transmission link, it is assumed that the fiber acts as a linear medium. That is, properties of the fiber do not change with input optical power, wavelength remains the same and signals propagating in the fiber do not interact with one another. This assumption only holds for input power levels less than +3 dBm [13]. For high signals powers and high-power densities in the core, the fiber exhibits nonlinear properties. The signal propagating within the fiber alters properties of the fiber thereby affecting the signal itself. A fibers power density is given by

$$n = \frac{P_{sig}}{A_{eff}} \tag{2.14}$$

where A_{eff} is the fibers effective area. Nonlinear effects also depend on the fiber length. The longer the fiber, the more the signal can interact with the fiber. However, there is a tradeoff since a signal propagating in fiber experiences attenuation. The effect of nonlinear impairments gets diminished since they are dependent on signal strength. Therefore, most nonlinear impairments occur early in the fibers span, approximately in the first 21 km for fiber with 0.21 dB/km

attenuation at 1550 nm [13]. Moreover, dispersion in optical fiber helps reduce nonlinear effects. The pulses are spread in time hence reducing the peak power associated with the propagating signal. Nonlinear effects can be divided into two categories, Kerr effect and nonlinear stimulated scattering of photons.

2.3.2.1 Kerr effect

The refractive index of fiber is dependent on the power of the propagating signal. The refractive index is the sum of two components, the effective refractive index at low power and the nonlinear-index coefficient multiplied by power density.

$$M(\omega, E) = n_{eff-Low}(\omega) + n_2 \frac{P_{sig}}{A_{eff}} \tag{2.15}$$

At low signal power densities, the effect of the second term is minimal. However, at high power levels, the effect on refractive index becomes significant. A signal propagating in optical fiber in the presence of CD, attenuation and nonlinear effects follows the nonlinear Schrödinger equation (NLSE) given as

$$\frac{d\boldsymbol{E}(z,t)}{dz} + j\frac{\beta_2}{2}\frac{d^2\boldsymbol{E}(z,t)}{dt^2} + \frac{\alpha}{2}\boldsymbol{E}(z,t) = j\gamma|\boldsymbol{E}(z,t)|^2\boldsymbol{E}(z,t) \tag{2.16}$$

The Kerr effect is included by the terms proportional to the fiber nonlinear parameter defined as

$$\gamma = \frac{n_2\omega_c}{cA_{eff}} \tag{2.17}$$

where ω_c is the angular frequency of the optical carrier, and γ is the nonlinear coefficient. The nonlinear coefficient changes the propagation parameter [13]. This cause's nonlinear phase shift in the signal as it travels in the fiber. The main effects in this category are self-phase modulation (SPM), cross phase modulation (XPM) and four wave mixing (FWM). In FWM, three optical signals of different center frequencies propagating in the fiber interact to generate a fourth signal. The generated mixed signal creates both intra-channel and inter-channel interference on the original signals. For XPM, the phase of a signal in one channel is influenced by the phase of a wavelength in a different channel. XPM acts as noise like fluctuations in jitter and amplitude in co-propagating wavelengths. In WDM systems, nonlinear effects are classified into two, intra-channel interference and inter-channel interference. Figure 2.10 shows the classification of nonlinear interference in WDM systems. Intra-channel nonlinearities are dominant at high bit

rate transmission systems and inter-channel nonlinearities dominate at lower bit rates. Compensation of Kerr effects is difficult in traditional IM-DD transmission systems. In coherent optical communication, compensation is achieved in the digital domain by using backward propagation methods based on solving NLSE and Manakov equation [5]. This equalization method involves subjecting the received signal to propagation in virtual fiber with characteristics opposite, negative coefficients in NLSE or Manakov equations, to that of the physical fiber. Chapter 3 explains this technique further.

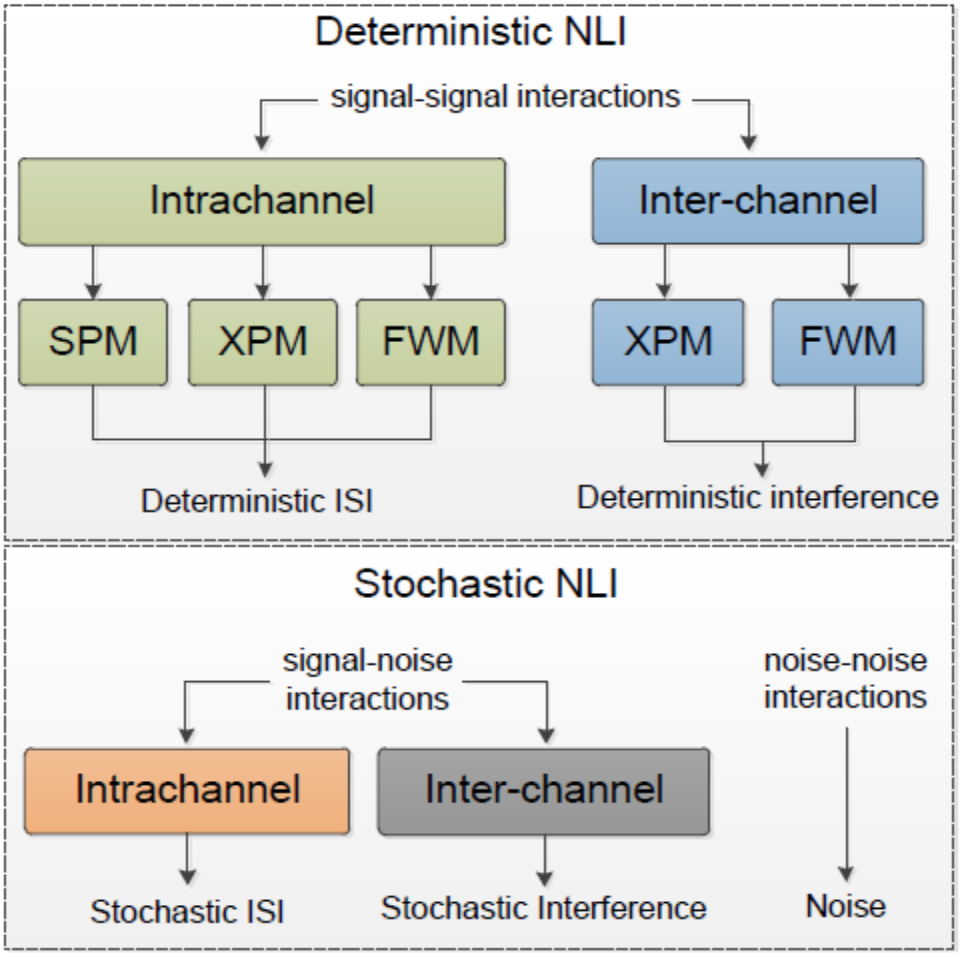

Fig. 2.10. Kerr effect on WDM communication systems [8].

2.3.2.2 Nonlinear stimulated scattering

Stimulated scattering is the nonlinear scattering of light of an incident wave to a lower power wave at a longer wavelength in the fiber. The effects are stimulated Raman scattering and stimulated Brillouin scattering. This reduces the signals power as it propagates through the fiber. In WDM systems, optical power is transferred between multiple signal causing cross talk and degrading system performance. Power transfer between signals spaced as much as 125nm can occur [13]. Power coupling occurs between channels occurs from signals with shorter wavelengths to signals with longer wavelengths. This results in increased level of noise for lower frequency (longer wavelength) signals thereby reducing the OSNR.

Summary

The purpose of this chapter was to provide a fundamental overview of optical fiber transmission technology. Description of light as an electromagnetic wave and how it propagates within the fiber was provided using Maxwell's equations. The fundamental design structure of fiber was also unpacked. As light travels through the fiber, it gets distorted. Theory associated with distortions/impairments such as PMD and CD was also discussed. This theory will be the fundamental basis for equalization of transmission impairments in the digital domain of which is discussed extensively in chapter 3.

References

[1] I.B. Djordjevic, "Propagation Effects in Optical and Wireless Communications Channels, Noise Sources, and Channel Impairments," in *Advanced Optical and Wireless Communications Systems*, Springer International Publishing, 2018, pp. 31-34.

[2] J.C. Whitaker and B. Benson, "Fiber Optic Devices and Systems," in *Standard Handbook of Video and Television Engineering*, 4th ed. McGraw-Hill, 2003. Available: https://0-www.accessengineeringlibrary.com.wam.seals.ac.za/content/book/9780071411806/chapter/chapter45

[3] J.L. Miller, "Optical Fibers," in *Optical Communications Rules of Thumb*, McGraw-Hill, 2003.
Available:https://0www.accessengineeringlibrary.com.wam.seals.ac.za/content/book/9780071387781/chapter/chapter9

[4] R.W. Waynant, and M.N. Ediger, "Optical Fibers" in *Electro-Optics Handbook*, 2nd ed. McGraw-Hill, 2000.

Available:https://0www.accessengineeringlibrary.com.wam.seals.ac.za/content/book/9780070687165/chapter/chapter12

[5] T. Xu, "DSP based Chromatic Dispersion Equalization and Carrier Phase Estimation in High Speed Coherent Optical Transmission Systems," Ph.D. dissertation, dept. of Optics and Photonics, Royal Institute of Technology, Stockholm, Sweden, 2012.

[6] Fosco, "Optical fiber loss and attenuation," Fosco, 2020. Accessed on July.10, 2020. [Online]. Available: https://www.fiberoptics4sale.com/blogs/archive-posts/95048006-optical-fiber-loss-and-attenuation

[7] J. Hecht, "Properties of Optical Fibers," in *Understanding Fiber Optics*, 3rd ed. Prentice-Hall, upper saddle river, New Jersey, 1999.

[8] E. Porto da Silva, "Linear and Nonlinear Impairment Compensation in Coherent Optical Transmission with Digital Signal Processing," Ph.D. dissertation, dept. of Photonics Engineering, Technical University of Denmark, Kongens Lyngby, Denmark, 2017.

[9] G. Li, “Recent advances in coherent optical communication” in Advances in Optics and Photonics, vol. 1, issue 2, pp. 279-307, 2009.

[10] “Chromatic Dispersion and Polarization Mode Dispersion,” 2001. Accessed on June.16, 2020. [Online].

Available: https://www.lightreading.com/chromatic-dispersion-and-polarization-mode-dispersion-(pmd)/d/d-id/575132

[11] Luna Technologies, “Introduction to Polarization Mode Dispersion,” Luna Technologies. Accessed on: May.12, 2020. [Online].

Available: https://lunainc.com/wp-content/uploads/2012/08/22pmdweb.pdf.

[12] K. Wu and H. Sun, "Techniques in carrier recovery for optical coherent systems," *OFC/NFOEC*, Los Angeles, CA, 2012, pp. 1-3.

[13] B. Chomycz, “Planning fiber optics networks: Fiber nonlinear impairments,” McGraw-Hill Companies, 2009.

Chapter 3

3.1 Introduction

Telecommunication technology has grown tremendously from the time the first telephone was invented in 1876 by Alexander Graham Bell. In 1884, the first copper telephone network was set up between Boston and New York with the first trans-Atlantic 36 channel telephone cable system (TAT-1) connecting north America and Europe being deployed in 1956 [1]. In the early 1970s, research and development related to fiber optic communication systems was initiated. The primary modulation format was intensity. The intensity modulated optical signal transmitted over optical fiber was detected using square law principle through a photodiode. This transmission reception method is referred to as IM-DD (intensity-modulation and direct-detection) scheme, which is still used in optical communications today. This communication systems scheme has an advantage in that the sensitivity of the receiver is independent of carrier phase and state of polarization (SOP) of the incoming signal, which vary randomly in real systems. However, there is polarization dependent loss (PDL). PDL is defined as the maximum peak-peak insertion loss variation caused by a component when stimulated by all polarization states [2]. PDL is mostly due to system components such as couplers, isolators, and wavelength division multiplexers in the transmission link especially at high bit rates.

A receiver in which a local oscillator is used to interfere with the incoming optical signal to extract phase information is referred to as a coherent receiver. In the 1980s, this receiver scheme was subject of intensive research because of its high sensitivity [3]. Table 3.1 gives a comparison of coherent and IM-DD schemes.

Table 3.1: Comparison between coherent detection and IM-DD

	Coherent detection	IM-DD
Modulation parameters	Amplitude and phase	Intensity
Detection method	Homodyne or heterodyne	Direct detection
Sensitivity to carrier phase	Yes	No
Sensitivity to polarization	Yes	No

In coherent optical communication, the message is stored onto the electrical field of the light wave. At the receiver, full information on the optical carrier, phase, amplitude, and SOP, can be restored [3]. Figure 3.1 shows the schematic configuration of a coherent receiver. To measure the full information of the light wave, the incoming data signal interferes with a local oscillator in a 90^o optical hybrid. The phase of one branch of the local oscillator signal fed into the hybrid is delayed by 90^o to enable measurement of the quadrature (Q) component of the input data signal. The non-delayed local oscillator signal measures the in-phase (I) component. For reliable measurement of the message signal, the local oscillator must be locked in phase and polarization. The oscillator must be stable enough with respect to the received signal. Therefore, these receivers are highly sensitive to fluctuations in phase and SOP of the data signal [3, 4].

Phase and SOP management turned out to be the main hindrance for implementation of coherent receivers. The SOP of the incoming data signal must match that of the local oscillator. When a light wave travels through the fiber, its SOP becomes scrambled. Therefore, dynamic control of this parameter is required. Each dynamic polarization controller is large and costly to manufacture. Phase locking is challenging as well. The optical signal modulated in the phase shift keying (PSK) format are usually carrier suppressed [3, 4]. In the case of BPSK, the optical power is constant. However, the optical field is shifted between 0 and pi thereby the average optical field being zero. Therefore, there is no distinct carrier component in the optical spectrum. Commonly used techniques such as injection locking and optical phase locked loop (OPLL) cannot be used directly to lock the phase of the local oscillator. Some form of non-linear signal processing is necessary. In the case of OPLL, the phase error between the recovered carrier phase and local oscillator phase is led to the frequency controlling terminal of the local oscillator so that the phase of the carrier can be tracked by the local oscillator. For example, in [2], the OPLL bandwidth was limited below 1MHz because of large loop delay and was difficult to maintain system stability when lasers used had large phase noise and frequency drift. For high data rates, the delays allowed in OPLL are so small that it becomes impractical.

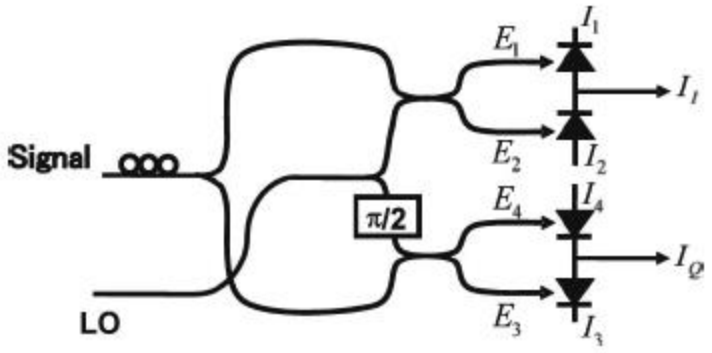

Fig. 3.1. Schematic configuration of a phase diversity coherent receiver [3].

In 1987, the first erbium doped fiber amplifier (EDFA) for optical fiber communication systems was demonstrated, with optical gains up to 26dB at 1530nm wavelength being shown [1]. An EDFA used as a low noise pre-amplifier reduced the need for a coherent receiver. Research and development on EDFA technology to amplify multiple wavelengths without crosstalk paved the way to wavelength division multiplexing systems (WDM) operating in the C-band (1530-1565 nm). The EDFA based and IM-DD system in conjunction with WDM increased the capacity of a single fiber. WDM networks were widely deployed due to their simplicity and low cost associated with optical repeater stations, where multiple WDM channels could be amplified simultaneously. In 1996, the first trans-Atlantic fiber network making use of EDFA-based, IM-DD, and WDM technology (TAT-12/13) was deployed initially carrying 2 channels at 5-Gbps [1].

Increased demand in data traffic, advances in analog to digital converters (ADC), digital to analog converters (DAC), application specific integrated circuits (ASIC's) and digital signal processing (DSP) renewed interest in coherent optical communication technology. Adaptation of this technology enabled use of higher order optical modulation formats which make use of all degrees of freedom, amplitude, phase, and polarization, to further increase the spectral efficiency beyond 1 b/s/Hz [3, 4]. Coherent detection has become the standard for long-haul optical fiber transmission networks. Coherent detection will prove vital for the SKA (Square kilometer array) telescope network project for aggregation of vast amounts of data from individual telescopes across Africa to a central computer where storage and processing is performed. Transoceanic

cables can carry up to 20Tbps with this technology [1]. Transoceanic optical fiber networks employing coherent detection have become the backbone of international communications network. Figure 3.2 shows the map of African optical submarine cables deployed.

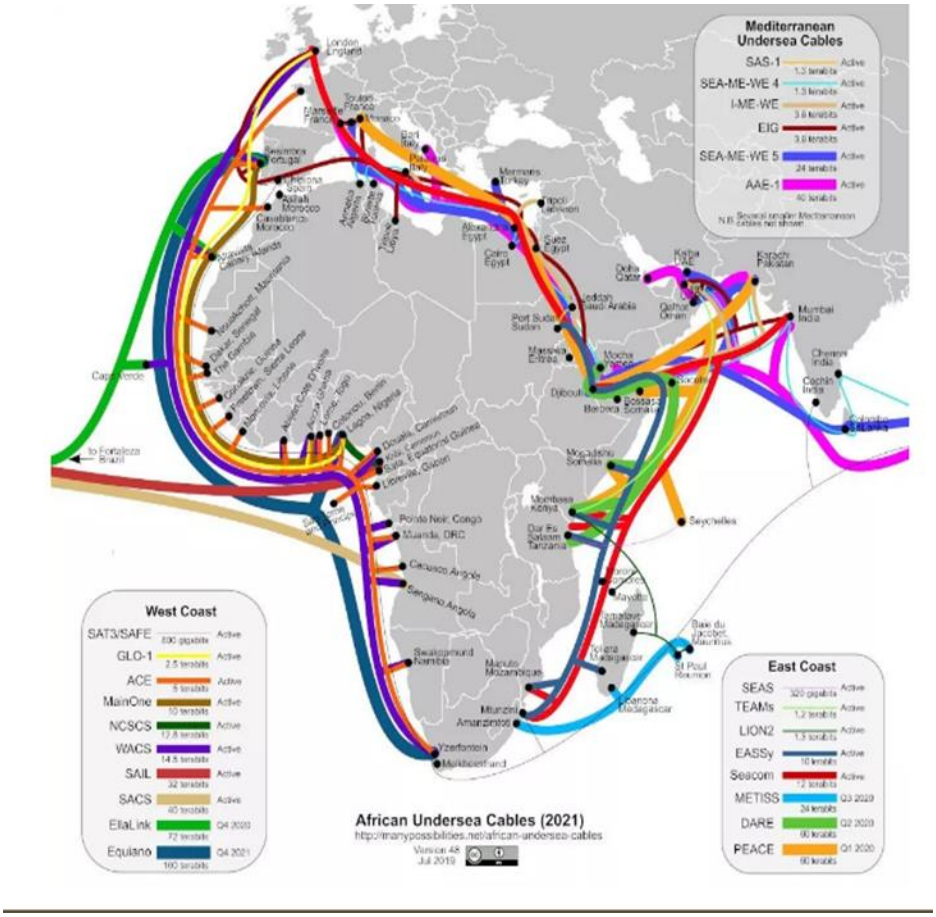

Fig. 3.2. Map of African undersea cables [5].

The speed of CMOS technology has greatly improved from sampling rates of 22-GSamples/s in 2006 to 100-GSamples/s in 2016 [1]. Information at high data rates can effectively be sampled by ADC's at sampling rates which meet or exceed Nyquist criterion. Therefore, phase and polarization management can be done in the electrical domain by using DSP [1, 4]. Linear optical fiber transmission impairments such as chromatic dispersion (CD) and polarization mode dispersion (PMD) can be easily compensated in the digital domain. Non-linear fiber optic effects limiting the performance of current fiber optic systems can also be compensated for using digital non-linear compensation techniques. Algorithms such as digital backpropagation have been used

in equalization of Kerr effects. However, hardware implementation of such algorithms is challenging because of their complexity and high computational resource requirement.

In this chapter, an overview of a fiber optic transmission system using coherent detection is presented. Section 3.2 explains the principle of operation of optical transmitters used in coherent communication. IQ modulator theory is unpacked here. Moreover, optical modulation formats used in communication systems are explained. In section 3.3, metrics used to quantify the quality of a recovered signal are unpacked. BER calculation for PSK signals is provided. In section 3.4, the principle of operation of a coherent receiver is discussed. Methods of detection with respect to configuration of the local oscillator are provided. Digital signal processing techniques such as carrier phase estimation and compensation of linear impairments are discussed here. Finally, a summary of the chapter is provided.

3.2 Optical transmitter

Digital optical fiber communication is the backbone of modern communication networks. A digital communication system is designed in a way that information is conveyed form source to the destination without errors irrespective of noise introduced in the transmission channel. Figure 3.3 shows the building blocks of a typical digital communication system. The processes of sending information, transmitter, can be described as follows.

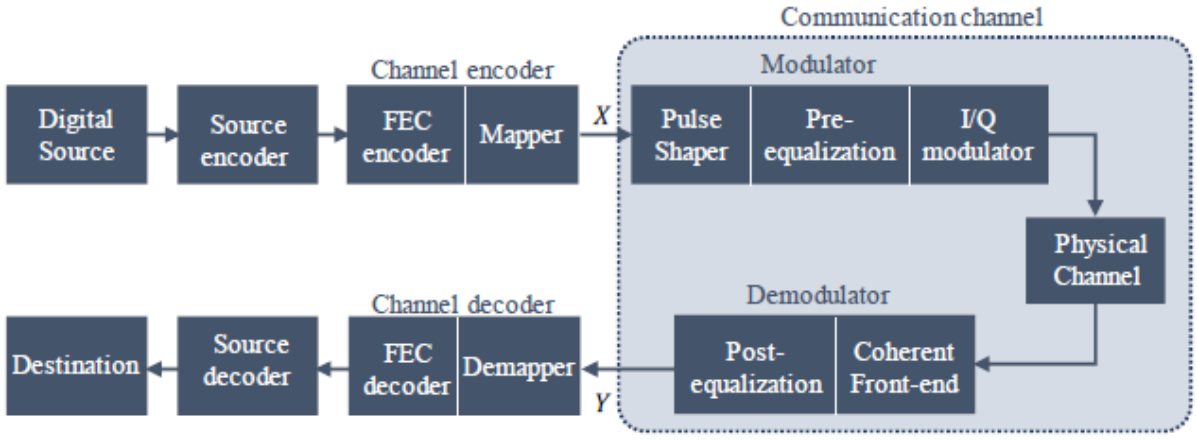

Fig. 3.3. Block diagram of a digital communication system [1].

An analog signal is Nyquist sampled, quantized, and converted to binary data by ADC's. The binary sequence representing the message signal is compressed by removing redundancies so that information is represented by the smallest number of bits as possible. At the channel encoder, forward error correction (FEC) codes are applied to the data to provide robustness to noise thereby reducing the bit error rate. For coherent optical communication, soft-decision FEC codes are applied enabling signals to travel longer distances while requiring fewer regenerator points [6]. The coded bits are then passed to a mapper which translates blocks of given bits to points in the constellation, each of which is a complex symbol. The necessary physical bandwidth is directly proportional to the symbol rate. The vector symbols at the output of the mapper are transformed to signal waveforms by a pulse shaper.

Pulse shaping determines the spectral width occupied by a signal. In-order to reduce inter symbol interference (ISI), pre-equalization is performed. For coherent optical communication, pre-compensation of linear impairments such as CD and PMD is performed using algorithms like those used in post-equalization such as least mean squares and constant modulus algorithm [7]. Explanation of these algorithms is provided in section 3.4.2. The resulting signal is then modulated into a carrier wave and transmitted through a physical channel. In the case of coherent optical fiber communication, the signal is modulated into the laser source by means of an IQ-modulator. To maximize spectral efficiency, information is encoded in all degrees of freedom of the light wave, i.e. polarization, amplitude, and phase. Multilevel modulation formats such as dual polarization quadrature amplitude modulation (DP-QAM) and dual polarization phase shift keying (DP-PSK) can be used. Figure 3.4 shows the schematic diagram of a dual polarization IQ modulator.

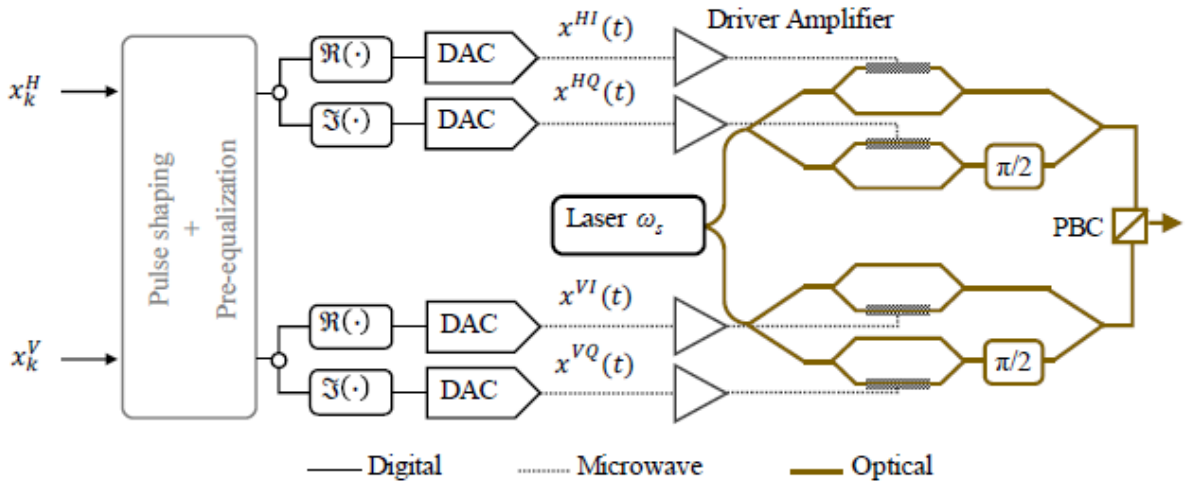

Fig. 3.4. Schematic diagram of dual polarization IQ modulator [1].

An optical carrier with central frequency ω_s is split into two orthogonal polarizations V and H using a polarization beam splitter. Each signal is fed into two nested Mach-Zehnder modulators with 90^o shift between their outputs. These Mach-Zehnder modulators are biased at the minimum transmission point -V_π hence creating an IQ modulator for each orthogonal polarization [8]. Each Mach-Zehnder modulator is driven by the pulse shaped electrical waveforms $x^{HI}(t)$, $x^{HQ}(t)$, $x^{VI}(t)$ and $x^{VQ}(t)$. A polarization beam combiner recombines the two signals at the output.

3.2.1 Optical modulation techniques

Light as a carrier constitutes too many benefits. It has three degrees of freedom, amplitude, phase (including frequency), and polarization. Therefore, information can be encoded in each of the degrees of freedom [9]. A modulated light wave can be expressed as

$$E(t) = \hat{e}Aexp^{j(\omega t+ \varphi)} \tag{3.1}$$

where ω represents the frequency of the carrier, A is the intensity of the carrier, φ is the phase and $\hat{e}$ is the polarization of the carrier. Classification of a modulation format is dependent on which variable is equation 3.1 is used to represent information.

3.2.1.1 Intensity Modulation

This is the oldest and one of the most widely used modulation formats in optical communication systems. Only one degree of freedom of the light carrier is used. In equation 3.1, all other parameters are kept constant with variable *A* being changed for implementation of this modulation format. Therefore,

$$E(t) = \hat{e}A_i exp^{j(\omega t + \varphi)} \ , i = 2, 4 \ldots 2^n \quad (3.2)$$

where *n* is an integer and *i* indicates the number of amplitude levels used for modulation. For *i* equivalent to 2 with $A_1 = A$ and $A_2 = 0$, we have unipolar modulation or on-off keying. There are two format techniques used in intensity modulation: Return-to-Zero (RZ) and Non-return-to-Zero (NRZ). For NRZ, bits '0' and '1' have specified power levels which are non-zero, usually with bit '1' being assigned positive voltage and '0' bit being assigned negative voltage. At 10Gbps bit rate and above, electro absorption modulators and directly modulated lasers are normally used in short reach optical communications with Mach-Zehnder modulators (MZMs) being the most widely used for long reach applications [10]. When using the MZM, the modulator is biased at the quadrature point for maximum voltage swing. In RZ format, a transition from bit '1' to bit '0' is forced to zero output level effectively representing every '0' bit with zero output. The optical intensity returns to zero within each bit slot. RZ can be implemented in two ways, electronically by generating RZ waveforms which modulate the optical carrier or by carving pulses out of an NRZ signal by using a pulse carver (additional modulator). RZ can further be implemented as chirped (CRZ) or Carrier-Suppressed (CSRZ). CSRZ is characterized by reversing the sign of the optical field at each bit transition. The MZM as a pulse carver is sinusoidally driven at half the data rate between its transmission maxima [10]. This causes phase inversions between neighboring bits to be produced. Therefore, zero mean optical field envelope is generated. The carrier at the optical center frequency varnishes hence suppressed carrier. In CRZ configuration, the phase of an RZ signal is sinusoidally modulated at the data rate, with typical amplitude around 1 radian [10]. The phase modulation property of this technique makes it robust to fiber nonlinearities and therefore used in ultra-long-haul optical communications.

3.2.1.2 Phase Modulation

Phase shift keying (PSK) is a modulation technique in which the phase of the optical carrier is used to convey information. The carrier exhibits constant amplitude for all bits. That is,

$$E(t) = \hat{e}Aexp^{j(\omega t + \varphi_i)}\ , i = 2, 4 \ldots 2^n \quad (3.3)$$

where *n* is an integer and *i* indicates the number of phases used for modulation. There are various phase modulation schemes, such as QPSK, 8PSK, depending on the number of phases used to encode information. For *i* equivalent 2, we have a BPSK signal. Binary '0' and '1' are represented by phase 0 and π, respectively. Furthermore, differential encoding is normally applied to PSK formats. Differential encoding is a method used to further improve robustness to noise by encoding the present bit basing on the previous bit. In the case of BPSK with differential encoding, DBPSK (differential binary phase shift keying), binary transition from '0-0' or '1-0' is encoded as a zero-phase (0 radians) change while transition from '1-1' or '1-0' is encoded as a π phase change. Differential encoding is archived by precoding the data before phase modulating the optical carrier [10]. Modulation of the carrier phase is commonly archived using external modulators such as the MZM and phase modulator. Phase modulation using an MZM is archived by biasing the modulator at the zero-transmission point which produces exact π jumps at the expense of residual optical intensity dips at phase transition locations. Therefore, practical DPSK transmitters are conveniently implemented using MZM as a phase modulator. Like OOK, DPSK signal can be transmitted as an RZ-DPSK. Inserting a pulse carver after phase modulation will convert the NRZ signal to RZ. Encoding information in the phase of the optical carrier constitutes too many benefits. The transmitted optical signal is robust against fiber transmission impairments. Also, there is 3-dB receiver sensitivity improvement due to improved symbol spacing at fixed optical power compared to OOK [10]. Therefore, PSK modulation formats are commonly used in long haul and ultra-long-haul optical communications.

3.2.1.3 Frequency shift keying

Frequency shift keying is a modulation technique in which the frequency of the carrier signal is tuned between multiple frequencies in-order to represent binary data. In this scheme, the amplitude of the light does not change therefore possible to combine FSK modulation with intensity modulation to transmit more information. In Binary frequency shift keying (BFSK),

only two carrier frequencies are used. One frequency is used to represent binary '1' with the other used to represent binary '0'. In order to avoid interference as well as for the receiver to be able to differentiate between the frequencies, the separation between the two carrier frequencies is typically set to $1/T_s$ (bit period) [11]. Implementation of an FSK transmitter can be archived using MZMs. [12] gives a detailed explanation of this method. The bandwidth occupied by the BFSK is $2\Delta f+2B$, with B the bandwidth of the baseband signal. FSK is essential for transmission of label information, which is destination information in optical packet switching systems, thereby alleviating bottlenecks caused by electrical processing in networks. The drawback with this modulation format is the complexity of the receiver required compared with intensity modulation formats.

3.2.1.4 Polarization shift keying

Polarization shift keying (PolSK) is a modulation format in which information is encoded in the Stokes parameter. Information is sent by switching the polarization of the transmitted light wave between two orthogonal linear states of polarization (SOP). In stokes space, two orthogonal SOP's map onto opposite points with respect to the origin [13]. Detection of information is archived by observing the sign of the scalar product of the received SOP vector in stokes space with a reference vector representing one of the SOP's in a noiseless channel [13]. PolSK is immune to phase noise. It has been shown that 8-PolSK can tolerate larger laser linewidths. PolSK results in increased channel data rate hence higher spectral efficiency. When light travels through fiber, its state of polarization becomes scrambled. Therefore, PolSK requires tracking of the polarization in-order to recover signal points.

3.2.1.5 Hybrid Modulation

Hybrid modulation formats are those that use the combination of two or more degrees of freedom to encode information. Currently, amplitude and phase are the most used degrees of freedom combination hence generating a modulation format referred to as quadrature amplitude modulation (QAM). QAM is a modulation format that combines two carriers whose amplitudes are modulated independently, whose phases are 90^o apart with the same optical frequency. These carriers are called the in-phase (I) and quadrature (Q). QAM can assign 2^N states (symbols) by using I and Q [14]. Therefore, QAM has the capability to encode more than 2 bits per symbol

thereby realizing N times spectral efficiency compared to OOK. The spectral efficiency of M-ary QAM increases with multiplicity of M thereby approaching Shannon's limit. However, a large SNR per bit is required to realize same BER value.

3.3 Modulation metrics

3.3.1 Signal to Noise Ratio

Quantifying the signal-to-noise ratio (SNR) of a transmission system is critical. This metric provides insight on the level of noise (degree of impairment) embedded which degrades overall system performance. SNR is defined as the ratio of signal power relative to the noise power normally expressed in decibels. The optical signal-to-noise (OSNR) is given by

$$OSNR = \frac{pR_s}{2B_{ref}}\, SNR \tag{3.4}$$

where SNR is the signal-to-noise ratio, p is the number of polarization states of the signal, R_s is the symbol rate and B_{ref} is the reference bandwidth approximately equal to 12.5GHz [15].

3.3.2 Bit error rate

Bit error rate is the most fundamental metric used in evaluation of performance of digital communication systems. BER is the ratio of incorrectly received bits to the total number of received bits. Figure 3.5 shows a typical theoretical BER curve for various modulation formats. In evaluating performance of digital modulation systems, error probability (BER) is not the only metric that should be considered but also bandwidth, spectral efficiency and hardware requirements. Tradeoffs exist between these parameters [14].

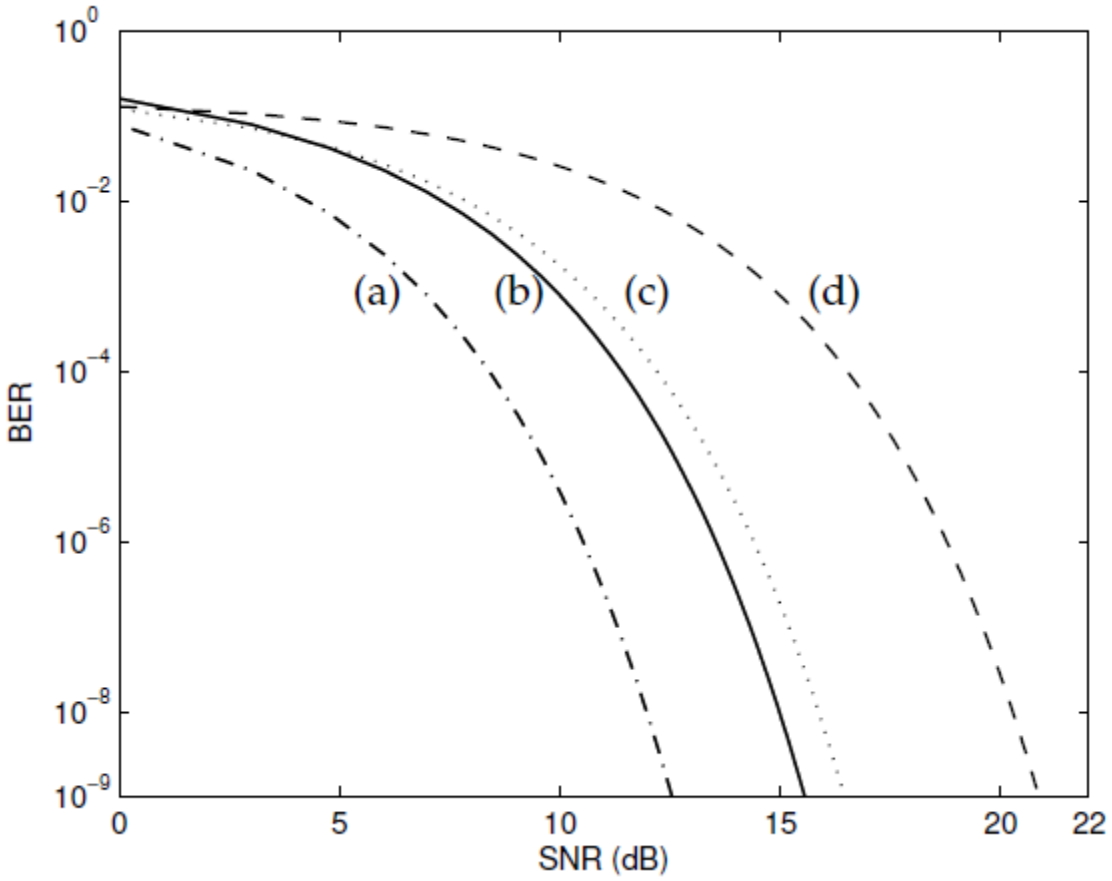

Fig. 3.5: BER theoretical performance of various modulation formats [14]. (a) BPSK and QPSK. (b) ASK and FSK. (c) 16QAM. (d) 64QAM.

In figure 3.5, if a BER of 10^{-9} is required, BPSK and QPSK attain this value with the lowest SNR with 64QAM having the highest required SNR. However, 64QAM allows the transmission of 8 bits per symbol thus having improved spectral efficiency compared with BPSK.

3.3.3 Error Vector magnitude

Error vector magnitude (EVM) is a performance metric for assessing quality of transmission. When monitoring performance using BER, the received signal constellation has to be demodulated first. With EVM, demodulation is unnecessary. EVM expresses the difference between the expected complex voltage of a demodulated symbol and the value of the received symbol [14, 16]. The root mean square (RMS) EVM is given by

$$EVM_{RMS} = \sqrt{\frac{\frac{1}{N}\sum_{j=1}^{N}(\delta I_j^2 + \delta Q_j^2)}{P_0}} \times 100\ [\%] \tag{3.5}$$

where δI and δQ are deviations of received data points form ideal locations of those points in the constellation. P_0 is the average power of the constellation. There exists a relationship between BER and EVM. This is given by

$$BER \approx \frac{2\left(1-\frac{1}{L}\right)}{log_2 L} Q\left[\sqrt{\left(\frac{3log_2 L}{L^2-1}\right)\frac{2}{EVM_{RMS}^2 log_2 M}}\right] \tag{3.6}$$

where Q is the Gaussian co-error function, L is the number of levels in M-ary modulation system.

3.4 Optical Coherent Receiver

3.4.1 Coherent receiver configuration

The schematic configuration of a polarization diversity coherent receiver is shown in figure 3.6. Two optical signals, local oscillator, and message signals mix in a 90^o optical hybrid to obtain the in-phase and quadrature components of the of the data signal.

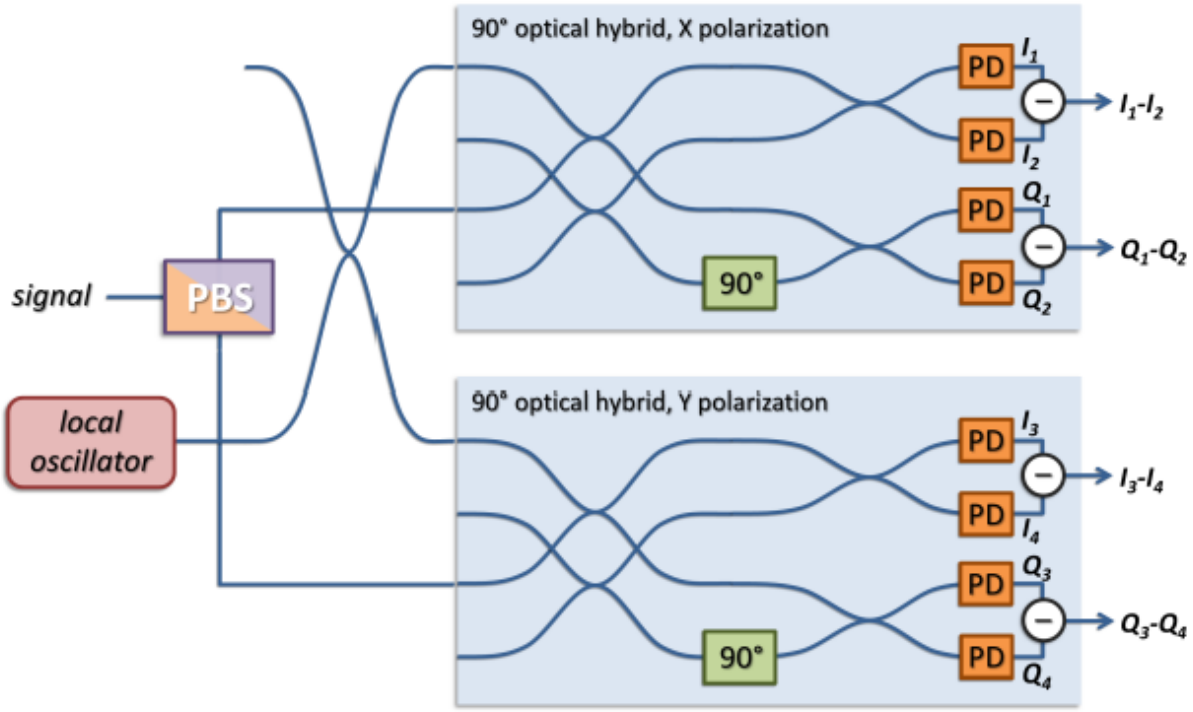

Fig. 3.6. Polarization diversity coherent receiver [8].

The electric field of the local oscillator, $E_{LO}(t)$ and transmitted signal $E_S(t)$ is given by

$$E_s(t) = \sqrt{P_s} exp^{j(\omega_s t + \varphi_s)} a(t) exp^{j\theta(t)} exp^{j\mu_{ns}(t)} \tag{3.7}$$

$$E_{LO}(t) = \sqrt{P_{LO}} exp^{j(\omega_{LO} t + \varphi_{LO})} exp^{j\mu_{nLO}(t)} \tag{3.8}$$

where P, ω, μ, and φ represent the power, angular frequency, phase noise, and phase of the optical local oscillator and carrier signals, respectively [3,8]. $a(t)exp^{j\theta(t)}$ is the phase modulated data. The 3-dB couplers used to feed the balanced photodiodes add 180^o phase shift to either signal field or local oscillator field at the output port. The output of mixing before detection by the balanced photodiodes is given by

$$\begin{bmatrix} E_1(t) \\ E_2(t) \\ E_3(t) \\ E_4(t) \end{bmatrix} = \frac{1}{2} \begin{bmatrix} E_S(t) + E_{LO}(t) \\ E_S(t) + jE_{LO}(t) \\ E_S(t) - E_{LO}(t) \\ E_S(t) - jE_{LO}(t) \end{bmatrix} \tag{3.9}$$

Each photodiode acts as a square law detector. Balanced detection is introduced to suppress the dc component and maximize the beat between local oscillator and message signal [3, 17]. Therefore, direct detection components are removed by subtracting the two photocurrents to obtain

$$I_1 - I_2 = R.E_1(t)E_1^*(t) - R.E_3(t)E_3^*(t) \tag{3.10}$$

$$Q_1 - Q_2 = R.E_2(t)E_2^*(t) - R.E_4(t)E_4^*(t) \tag{3.11}$$

where R is the responsivity of the photodiodes. The asterisk * indicates the conjugate. The photocurrents for the in-phase and quadrature are given by

$$I(t) = R\sqrt{(P_{LO}P_S)}.a(t)\cos(\Delta\omega t + \mu_n(t) + \theta(t) + \varphi) \tag{3.12}$$

$$Q(t) = R\sqrt{(P_{LO}P_S)}.a(t)\sin(\Delta\omega t + \mu_n(t) + \theta(t) + \varphi) \tag{3.13}$$

Δω is the beat frequency between the local oscillator laser and the optical carrier. Equation 3.12 and 3.13 show that the demodulated signal contains all information. The signal contains phase noise, μ_n, as well as the phases of the carrier and local oscillator φ. The data signal is a(t)exp{θ(t)}. Figure 3.7 illustrates the received constellation in a noiseless coherent receiver system.

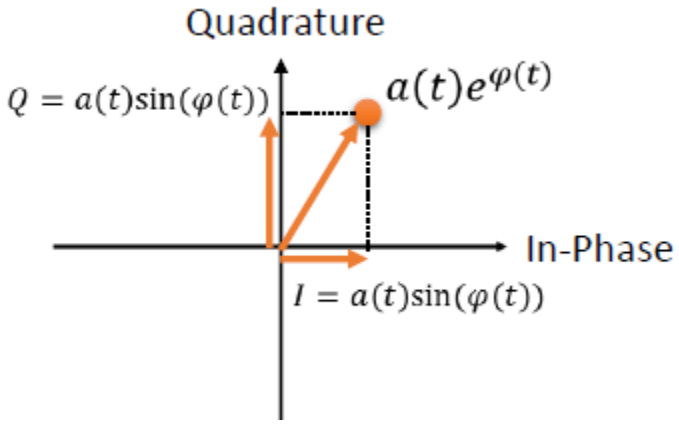

Fig. 3.7. Ideal signal constellation [8].

For a dual polarization coherent receiver shown in figure 3.6, the photocurrents are

$$I_h(t) \propto 2R\sqrt{(P_{LO}P_S^h)}.a(t)\cos(\Delta\omega t + \mu_n(t) + \theta(t) + \varphi)$$

$$Q_h(t) \propto 2R\sqrt{(P_{LO}P_S^h)}.a(t)\cos(\Delta\omega t + \mu_n(t) + \theta(t) + \varphi)$$

$$I_v(t) \propto 2R\sqrt{(P_{LO}P_S^v)}.a(t)\cos(\Delta\omega t + \mu_n(t) + \theta(t) + \varphi)$$

$$Q_v(t) \propto 2R\sqrt{(P_{LO}P_S^v)}.a(t)\cos(\Delta\omega t + \mu_n(t) + \theta(t) + \varphi)$$

There are two configuration techniques used in a coherent receiver, phase diversity-homodyne, and heterodyne detection.

a. Heterodyne detection

In this configuration, the frequency of the local oscillator and carrier are different thereby beating to generate an intermediate frequency ($\Delta\omega \neq 0$). The beat frequency must be such that $\Delta\omega >> 2\pi/T$, where T is the symbol rate [3]. The in-phase and quadrature photocurrents are given by

$$I(t) = R\sqrt{(P_{LO}P_S)}.a(t)\cos(\omega_{IF}t + \mu_n(t) + \theta(t) + \varphi) \quad (3.14)$$

$$Q(t) = R\sqrt{(P_{LO}P_S)}.a(t)\sin(\omega_{IF}t + \mu_n(t) + \theta(t) + \varphi) \quad (3.15)$$

The electrical field of the signal is down converted to the IF without spectral folding.

b. Phase-diversity homodyne detection

Homodyne detection refers to the case where the frequency of the carrier is the same as that of the local oscillator. The electrical field of the light is down converted to baseband without spectral folding. Output photocurrents from the balanced photodiodes are then given by

$$I(t) = R\sqrt{(P_{LO}P_S)}.a(t)\cos(\mu_n(t) + \theta(t) + \varphi) \quad (3.16)$$

$$Q(t) = R\sqrt{(P_{LO}P_S)}.a(t)\sin(\mu_n(t) + \theta(t) + \varphi) \quad (3.17)$$

3.4.2 Coherent communication digital signal processing

A coherent receiver can restore full information about the optical complex amplitude as shown by equations 3.12 and 3.13. Therefore, equalization of transmission impairments can be archived in the digital domain. Figure 3.8 shows the signal flow block diagram for compensation using DSP.

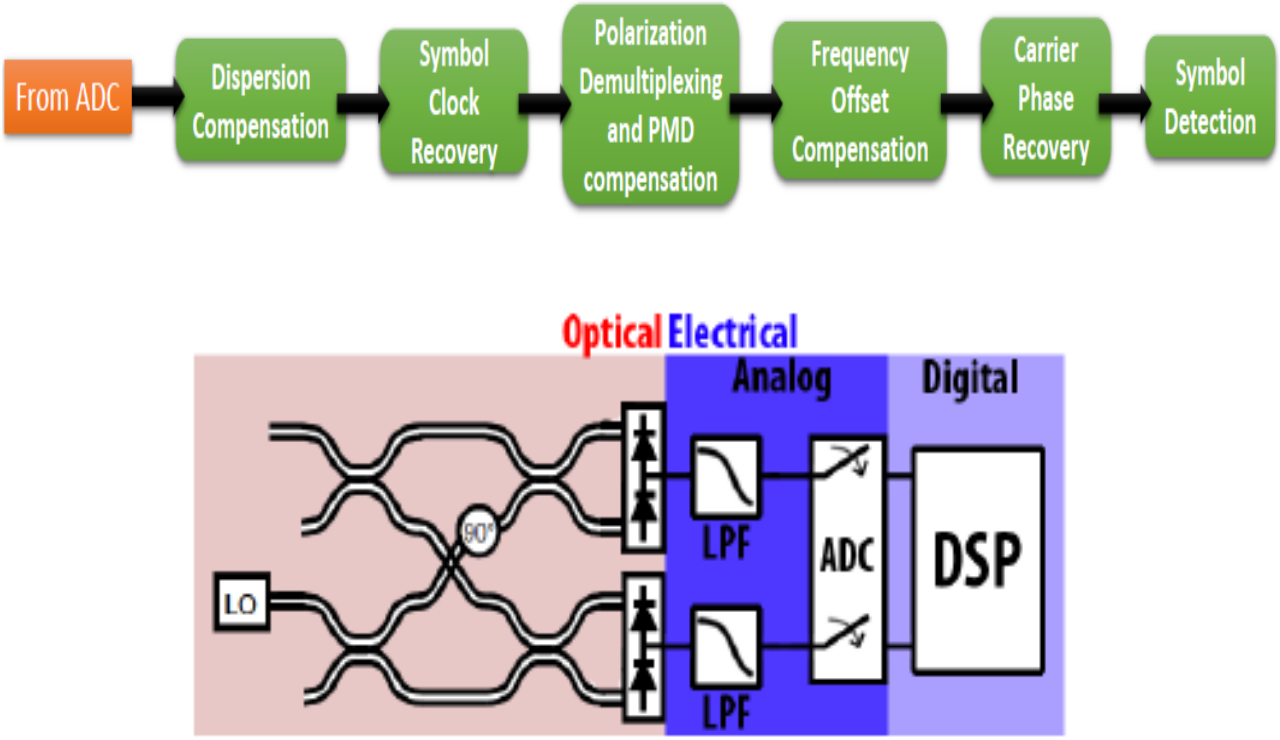

Fig. 3.8. Digital signal processing based coherent receiver [8]. Top: DSP signal flow block diagram. Bottom: Receiver configuration.

The received signals from the balanced photodiodes are converted to the digital domain by sampling at the Nyquist rate. For a 28Gbaud signal, we need a minimum sampling rate of 56GSamples/s (2 samples/symbol). The sampling rate clock at the receiver is asynchronous to the clock at the transmitter. Therefore, sampling is not at the optimum pulse height and the two clocks are not phase locked.

i. Chromatic dispersion compensation

Chromatic dispersion is an all pass filter in the electric field of light with complex transfer function in the frequency domain as shown by the equation in chapter 2 [4]. The effect of CD can be reversed by designing a filter with transfer function given by

$$H(\omega) = H(\omega)^{*} \tag{3.18}$$

The asterisk * represents the conjugate. Such a filter can be implemented by using a finite impulse response (FIR) filter with filter coefficients given by the discrete inverse Fourier transform

$$b_n = \frac{1}{N}\sum_{k=0}^{N-1} H(\omega)^* exp^{j\omega n} \quad (3.19)$$

Figure 3.9 shows the direct form-I structure of an FIR filter with filter coefficients b_n. The filter can also be realized as an infinite impulse response filter (IIR). This filter is more computationally efficient than its counterpart. However, implementation with this type of digital filter requires buffering.

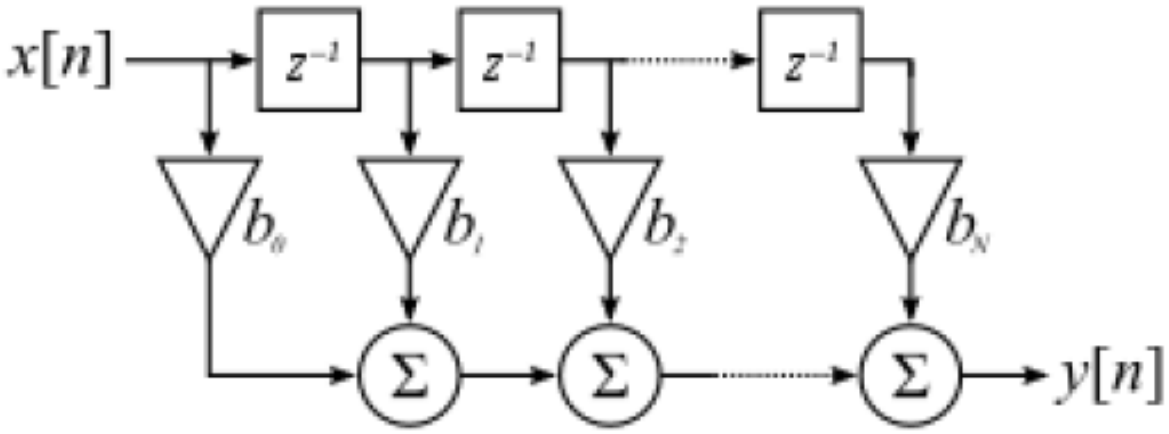

Fig. 3.9. Direct form-I structure of an FIR filter [8].

ii. Polarization mode dispersion equalization

Polarization rotation and PMD are random. Therefore, compensation of these transmission impairments is archived using adaptive filters [18]. Inherently, residual CD is also equalized by these filters. The general setup of an adaptive filter is shown in figure 3.10.

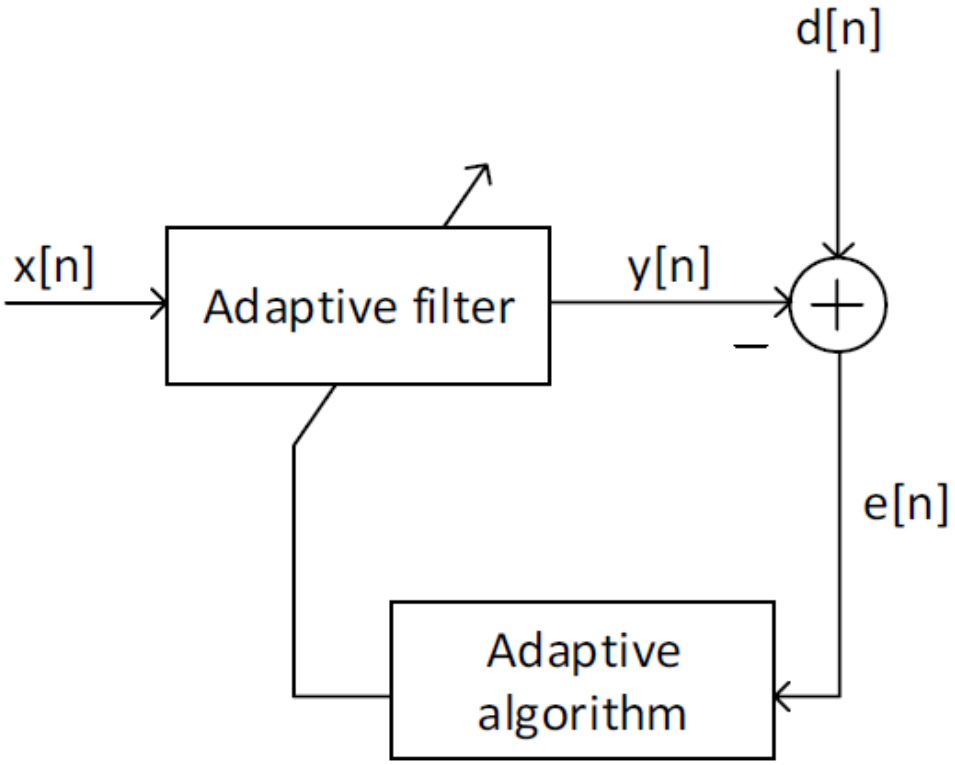

Fig. 3.10. General setup of an adaptive filter [20].

A discrete time signal is fed into a filter which outputs a signal corresponding to its impulse response. The filter may be designed as FIR or IIR. The output signal is then compared with the desired signal [3, 19]. For a QPSK modulated signal, the desired symbols will correspond to 1+j, 1-j, -1+j and -1-j. The difference between the desired response and the initial output response is used to drive an algorithm which modifies the coefficients of the filter such that the output y[n] at the filter is close to the desired response d[n] as possible. The filters coefficients are continuously updated at each time index. The following are the commonly used algorithms used to control the response of the filter:

a. Least mean squares algorithm

The LMS adaptive filter uses an iterative algorithm to find optimum tap weights which yield minimum mean square error. The following equations give the principal operation of the LMS filter

$$y(n) = w(n)^H x(n) \tag{3.20}$$

$$w(n+1) = w(n) + \varepsilon x(n) e(n)^* \tag{3.21}$$

$$e(n) = d(n) - y(n) \tag{3.22}$$

where *y(n)* is the output complex magnitude vector of the equalized signal, *x(n)* is the complex input magnitude vector of the sampled signal. *w(n)* represents the complex tap weight vector, $w(n)^H$ is the Hermitian transform of *w(n)*, *d(n)* is the desired symbol, *e(n)* is the error estimate between the desired symbol and the equalized output and ε is a real coefficient called the step size [19]. For convergence of the tap weight vector *w(n)*, the step size needs to be bounded between zero and the largest eigenvalue of the correlation matrix given by

$$R = x(n) x(n)^H \tag{3.23}$$

The polarization diversity LMS equalizer is expressed as the following equations:

$$\begin{bmatrix} x_{out}(n) \\ y_{out}(n) \end{bmatrix} = \begin{bmatrix} w_{xx}^H(n) & w_{xy}^H(n) \\ w_{yx}^H(n) & w_{yy}^H(n) \end{bmatrix} \begin{bmatrix} x_{in}(n) \\ y_{in}(n) \end{bmatrix} \tag{3.24}$$

$$w_{xx}(n+1) = w_{xx}(n) + \varepsilon e_x(n) x_{in}^*(n)$$

$$w_{yx}(n+1) = w_{yx}(n) + \varepsilon e_y(n) x_{in}^*(n)$$

$$w_{xy}(n+1) = w_{xy}(n) + \varepsilon e_x(n) y_{in}^*(n)$$

$$w_{yy}(n+1) = w_{yy}(n) + \varepsilon e_y(n) y_{in}^*(n) \tag{3.25}$$

$$e_x(n) = d_x(n) - x_{out}(n)$$

$$e_y(n) = d_y(n) - y_{out}(n) \tag{3.26}$$

There are two mode to realization of this filter, training mode and decision-directed mode. Initially, the filter is set to training mode. In this mode, training symbols are used to find the

optimum weights for the filter. In decision-directed mode, there is no training. The output of the filter is mapped to the ideal symbol according to the shortest Euclidean distance. Figure 3.11 illustrates the setup used for realization of a decision-directed adaptive filter.

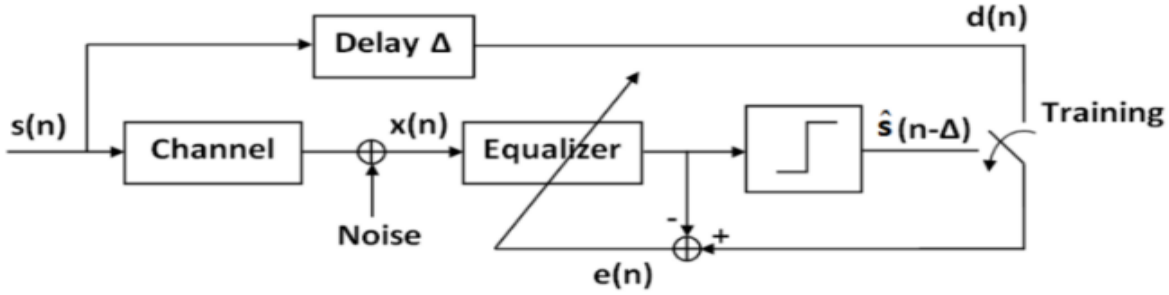

Fig. 3.11. Decision-directed compensator [20].

b. Constant modulus algorithm

The CMA algorithm can also be employed or compensation of PMD. The tap weights of the filter can be expressed as:

$$\begin{bmatrix} x_{out}(n) \\ y_{out}(n) \end{bmatrix} = \begin{bmatrix} v_{xx}^{H}(n) & v_{xy}^{H}(n) \\ v_{yx}^{H}(n) & v_{yy}^{H}(n) \end{bmatrix} \begin{bmatrix} x_{in}(n) \\ y_{in}(n) \end{bmatrix} \tag{3.27}$$

$$v_{xx}(n+1) = v_{xx}(n) + \varepsilon\mu_x(n)x_{in}^{*}(n)$$

$$v_{yx}(n+1) = v_{yx}(n) + \varepsilon\mu_y(n)x_{in}^{*}(n)$$

$$v_{xy}(n+1) = v_{xy}(n) + \varepsilon\mu_x(n)y_{in}^{*}(n)$$

$$v_{yy}(n+1) = v_{yy}(n) + \varepsilon\mu_y(n)y_{in}^{*}(n) \tag{3.28}$$

$$\mu_x(n) = 1 - |x_{out}(n)|^2$$

$$\mu_y(n) = 1 - |y_{out}(n)|^2 \tag{3.29}$$

The algorithm updates tap coefficients such that $|x_{out}(n)|^2$ and $|y_{out}(n)|^2$ approach unity. This algorithm does not require decision feedback process [19]. Therefore, its computational complexity is lower than the decision directed LMS algorithm.

iii. Frequency offset compensation and carrier phase recovery

Frequency offset estimation and carrier phase recovery rely on the same principle. The idea is to estimate the rate of rotation of the constellation and remove it. For frequency offset, the rotation is approximately constant while for phase noise it is much more rapid and needs to be tracked. The phase of the photocurrents from equation 3.12 and 3.13 contains PM and phase noise. This noise and frequency offset will translate to the samples along the processing blocks. The procedure for estimating frequency offset and carrier phase for M-ary PSK signal is shown in figure 3.12. In-order to estimate the phase of the complex amplitude, the M[th] power of the complex amplitude is taken to remove PM leaving a single rotating point in the IQ plane [3, 8]. For BPSK and QPSK, M is equivalent to 2 and 4, respectively.

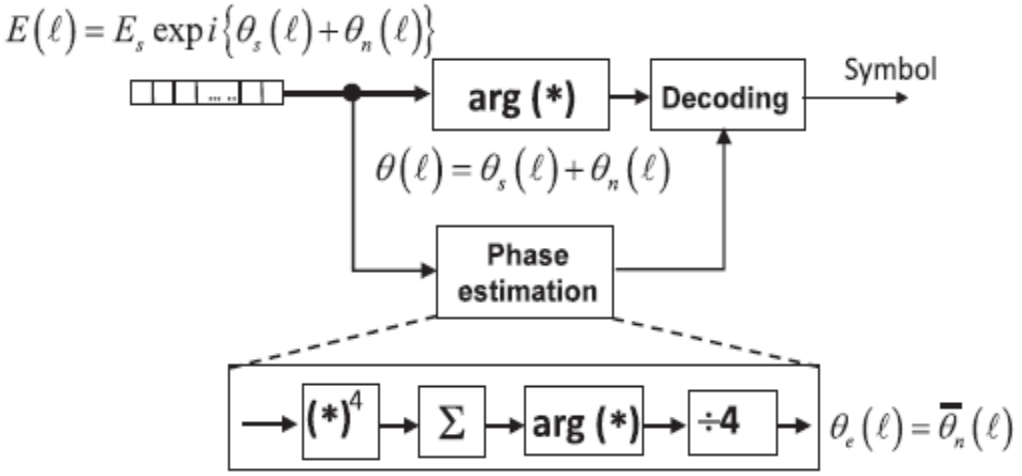

Fig. 3.12. M[th] power phase estimation DSP circuit [3].

The estimated phase is averaged over (2k+1) samples to improve the signal to noise ratio of the estimated phase reference. The estimated phase is given by

$$\vartheta_c(n) = \frac{1}{M} \arg\left(\sum_{j=-k}^{k} E(n+j)^M\right) \quad (3.30)$$

$\vartheta_c(n)$ is then subtracted from the original symbols *E(l)* to obtain the phase of the data in the constellation. The optimum averaging span depends on the linewidth of the laser [3]. When the linewidth is narrower, the optimum averaging span is longer giving better BER performance.

iv. Compensation of nonlinear impairments

Kerr effect in optical fiber introduces nonlinear waveform distortion and limits the maximum transmission distance. The adaptive filter algorithms used for equalization of PMD cannot compensate for nonlinear waveform distortions. However, these distortions can be pre-compensated or post-compensated by conducting backpropagation in the digital domain [3, 4]. In pre-compensation, the virtual fiber is placed between the input data stream and the IQ modulator so that the signal is pre-distorted by the virtual fiber while being equalized though the real fiber. For post equalization, virtual fibers and amplifiers are placed at the receiver. Figure 3.13 illustrates this concept. After coherent detection, the received signal is transmitted through virtual fibers and amplifiers.

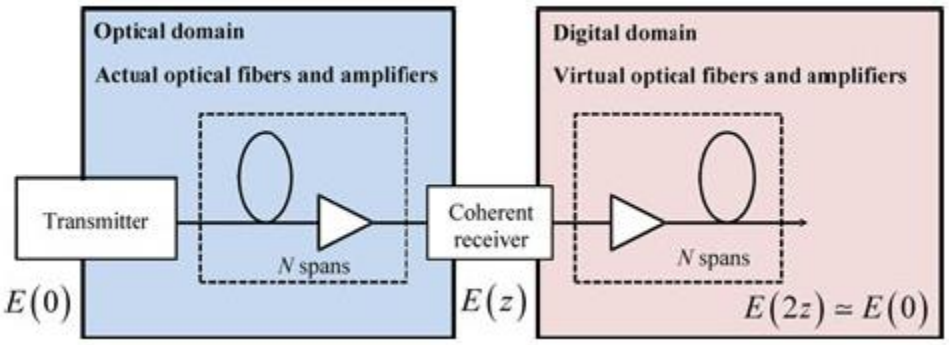

Fig. 3.13. Concept of digital backpropagation method [3].

The virtual fibers and amplifiers are emulated to have inverse characteristics of the real transmission link. Propagation of a signal through optical fiber is governed by Manakov equation. Therefore, by reversing the signs of that attenuation coefficient, nonlinear coefficient and second order dispersion parameter, virtual backpropagation process can be expressed as

$$\frac{dE_{x,y}}{dz} = \frac{\alpha}{2}E_{x,y} + j\frac{\beta_2}{2}\frac{d^2E_{x,y}}{dT^2} - j\frac{8}{9}\gamma(|E_x|^2 + |E_y|^2)E_{x,y} \quad (3.31)$$

With this method, all transmission impairments are equalized for simultaneously.

Summary

The main objective of this chapter was to provide a review on fundamentals of coherent optical communication. The concepts discussed include optical transmitters used in coherent communications, modulation format technologies currently being employed. Digital signal processing blocks used in coherent communication for recovery of transmitted information were also presented. Algorithms such as least mean squares used for equalization of transmission impairments where presented. All these introduced concepts serve as the basis for discussion for the remaining chapters of this thesis. In the next chapter, we will discuss optical clock generation techniques in application context of telescope networks.

References

[1] I. Fernandez de Jauregui Ruiz, “Advanced modulation formats and nonlinear mitigation for spectral efficient optical transmission systems,” Ph.D. dissertation, dept. of Electronic and Optical engineering, Telecom SudParis, Paris, France, April.12, 2018.

[2] Agilent Technologies, “Polarization Dependent Loss Measurement of Passive Optical Components,” Agilent Technologies, March.14, 2002. Accessed on: June.12, 2020. [Online]. Available: http://literature.cdn.keysight.com/litweb/pdf/5988-1232EN.pdf

[3] K. Kikuchi, “Fundamentals of Coherent Optical Fiber Communications,” in *Journal of Lightwave Technology*, vol. 34, no. 1, pp. 157-179, 1 Jan.1, 2016.

[4] G. Li, “Recent advances in coherent optical communication,” in Advances in Optics and Photonics, vol. 1, issue 2, pp. 279-307, 2009.

[5] “African undersea cables,” July 2019. Accessed on: May.12, 2020. [Online]. Available: https://manypossibilities.net/african-undersea-cables/.

[6] Ciena, “What is coherent optics,” Ciena, 2020. Accessed on: May.12, 2020. [Online]. Available: https://www.ciena.com/insights/what-is/What-Is-Coherent-Optics.html

[7] J. Zhang, J. Yu, N. Chi, and H.C. Chien, "Time-domain digital pre-equalization for band-limited signals based on receiver-side adaptive equalizers," in *Optics Express*, vol.22, no. 17, pp. 20515-20529, 2014.

[8] Photonics research communications laboratory, “Coherent optical systems,” Photonics research laboratory. Accessed on: May.12, 2020. [Online]. Available: https://www.photonics.ntua.gr/OptikaDiktyaEpikoinwnias/Lecture_4_CoherentOptical_DSP.pdf

[9] F. Feza Buyuksahin Oncel, “Modulation Format for Wavelength Division Multiplexing (WDM) Systems,” Ph.D. dissertation, dept. of Physics, Middle East Technical University, Ankara, Turkey, 2018.

[10] P. J. Winzer and R. -. Essiambre, "Advanced Optical Modulation Formats," in *Proceedings of the IEEE*, vol. 94, no. 5, pp. 952-985, May 2006, doi: 10.1109/JPROC.2006.873438.

[11] R.A. Thompson, D. Tipper, P. Krishnamurthy and J. Kabara, “Modulation,” in *The Physical Layer of Communications Systems*, chapter 14, pp. 690-714, 2006. Accessed on: June20, 2020. [Online] Available: http://www.sis.pitt.edu/prashk/inf1072/Fall16/modulation.pdf

[12] T. Kawanishi and M. Izutsu, “Optical Frequency Shift Keying Modulator,” in *journal of National Institute of Information and Communications Technology*, vol. 53, no. 3, 2006. Accessed on: June.12, 2020. [Online].

Available: http://www.nict.go.jp/publication/shuppan/kihou-journal/journal-vol53no3/tokkyo.pdf

[13] S. Benedetto and P. Poggiolini, "Theory of polarization shift keying modulation," in *IEEE Transactions on Communications*, vol. 40, no. 4, pp. 708-721, April 1992, doi: 10.1109/26.141426.

[14] R. Dionisio, “Advanced Optical Modulation and Format Conversion,” Ph.D. dissertation, dept. of Electronics, Telecommunications and Informatics, Aveiro University, Aveiro, Portugal, 2014.

[15] R. Essiambre, "Fiber capacity limits: Information theory meets optical communication and fiber physics," *35th Australian Conference on Optical Fibre Technology*, Melbourne, VIC, 2010, pp. 1-2, doi: 10.1109/ACOFT.2010.5929905.

[16] R. A. Shafik, M. S. Rahman, A. R. Islam and N. S. Ashraf, "On the error vector magnitude as a performance metric and comparative analysis," *2006 International Conference on Emerging Technologies*, Peshawar, 2006, pp. 27-31, doi: 10.1109/ICET.2006.335992

[17] F. Derr, "Coherent optical QPSK intradyne system: concept and digital receiver realization," in *Journal of Lightwave Technology*, vol. 10, no. 9, pp. 1290-1296, Sept. 1992, doi: 10.1109/50.156881.

[18] J. H. Winters, R. D. Gitlin and S. Kasturia, "Reducing the effects of transmission impairments in digital fiber optic systems," in *IEEE Communications Magazine*, vol. 31, no. 6, pp. 68-76, June 1993, doi: 10.1109/35.214895.

[19] T. Xu, “DSP based Chromatic Dispersion Equalization and Carrier Phase Estimation in High Speed Coherent Optical Transmission Systems,” Ph.D. dissertation, dept. of Optics and Photonics, Royal Institute of Technology, Stockholm, Sweden, 2012.

[20] D. Salminen, “Adaptive filters applied on radar signals”, MSc dissertation, Faculty of Science and Technology, Uppsala university, Uppsala, Sweden, 2013.

Chapter 4

4.1 Introduction

In today's technology, timing has become at the heart of communication. Clock signals are crucial for time stamping of data, i.e. voice packets, monitor and control functions (synchronization), digitization and use in big data projects such as the Square Kilometer Array (SKA). Timing is also the fundamental basis for digital communication networks in which time division multiplexing is used. Reference clocks used in such networks need to be highly stable. In ITU-Recommendation G.811, a network clock stability of 1 part in 10^{-11} for the primary reference source is required [1]. This is a standard which can only by far be reached by atomic sources such as, cesium and the hydrogen mazer [2, 3]. Stability requirements for various stratum levels of NTP are shown in figure 4.1.

Stratum	Accuracy/Adjust Range	Pull-In-Range	Stability	Time To First Frame Slip *
1	1×10^{-11}	N/A	N/A	72 Days
2	1.6×10^{-8}	Must be capable of synchronizing to clock with accuracy of $+/-1.6 \times 10^{-8}$	1×10^{-10}/day	7 Days
3E	1.0×10^{-6}	Must be capable of synchronizing to clock with accuracy of $+/-4.6 \times 10^{-6}$	1×10^{-8}/day	3.5 Hours
3	4.6×10^{-6}	Must be capable of synchronizing to clock with accuracy of $+/-4.6 \times 10^{-6}$	3.7×10^{-7}/day	6 Minutes (255 in 24 Hrs)
4E	32×10^{-6}	Must be capable of synchronizing to clock with accuracy of $+/-32 \times 10^{-6}$	Same as Accuracy	Not Yet Specified
4	32×10^{-6}	Must be capable of synchronizing to clock with accuracy of $+/-32 \times 10^{-6}$	Same as Accuracy	N/A

Fig. 4.1. Long term stability requirements for NTP [2].

Stratum 1 is defined as an independent source of timing which has no other reference source connected it. Clocks used in this level are required to be extremely stable as these clocks are used as primary reference sources in digital networks. The usual sources of stratum 1 timing are atomic standards such as Hydrogen maser (H-maser) or cesium (Cs). Stratum 2 clock tracks an input under normal conditions and holds it to the best estimate of input reference frequency. These clocks use stratum one clocks to act as their input reference. Typical stratum 2 clocks are Rubidium (Rb) standards and double oven cooled crystal oscillator (OCXO). Stratum 3 tracks an input as in stratum 2 over a wider range. Stratum 3 oscillators use stratum 2 clocks as the reference but can also be controlled by stratum 1 clock. Stratum 4 is defined as a clock system which tracks an input as in stratum 2 or 3. Stratum 3E is a new standard created as a result of

synchronous optical networking (SONET) equipment requirements and tracks input signals within 7.1 Hz of 1.544 MHz from a stratum 3 or better source while 4E is a proposed customer premises clock standard which allows a holdover characteristic that is not free running [2]. 4E is intended for use provided equipment in extending the local network is not yet standardized. Typical phase noise values for commonly used oscillators are shown in figure 4.2.

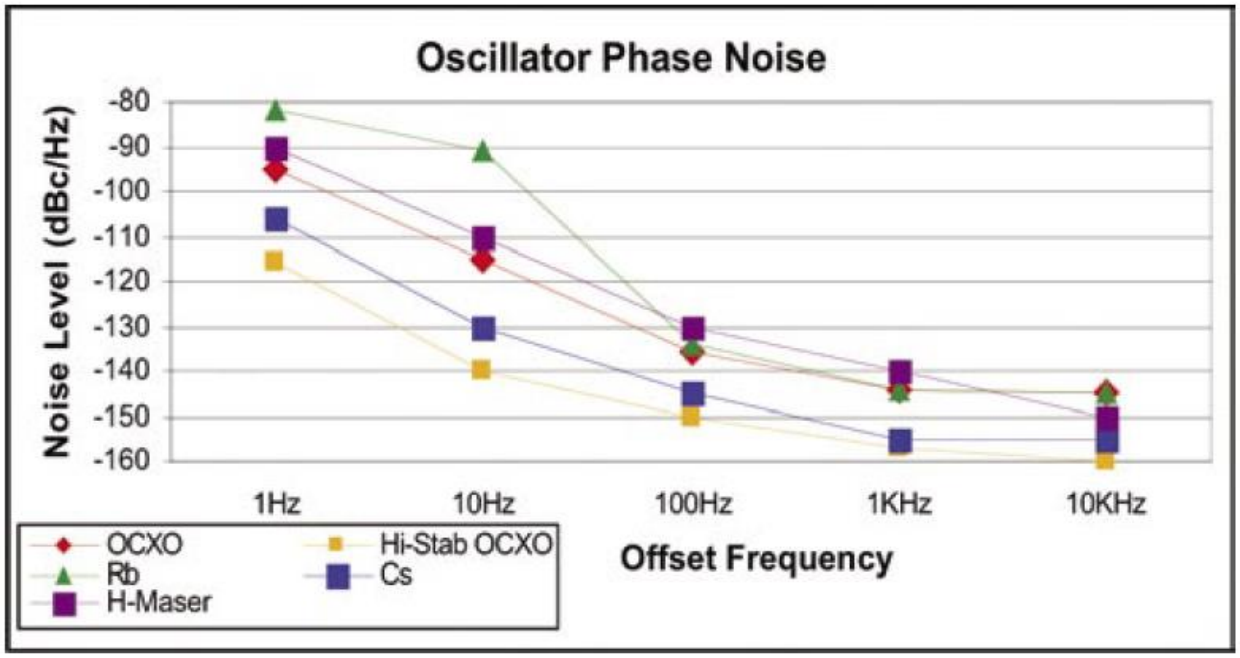

Fig. 4.2: Phase noise of commonly used oscillators in stratum 1 and 2 in NTP [3]. OCXO: oven cooled crystal oscillator. Rb: Rubidium. H-Maser: Hydrogen Maser. Hi-Stab OCXO: Hydrogen-stabilized oven cooled crystal oscillator. Cs: Cesium.

Due to the nature of the transmission channel and inherent physical properties of an oscillator, noise is added to the desired output signal. This degrades the overall quality of the generated and distributed clock by imposing power penalties and broadening the signal spectrum. As shown from figure 4.1, precision oscillators are not deployed at lower levels of the network. This is mainly because the cost of doing so would be extremely large. Also, different applications have different requirements. Therefore, cost effective, flexible, and highly stable clock systems are increasingly being required for deployment in today and future network systems. Various clock generation schemes have been extensively studied to try and meet the atomic standards. Some use multistage phase locked loop techniques to keep the frequency drift within an acceptable

level. In this chapter, we provide a short overview on some optical techniques used to generate radio and microwave signals in the optical domain.

4.2 Optical clock generation methods

A low phase noise and frequency tunable RF source is necessary for a wide range of applications. These signals are required in radar, wireless communication as well as telescope networks. Traditionally, the generation of an RF signal was archived in the electrical domain using multiple stages of frequency multipliers to achieve the desired RF signal. Distribution of RF signals in the electrical domain is tedious due to the high loss associated with coaxial cables. Due to the nature of optical fiber, low loss and tremendous bandwidth, optical fiber is the ideal candidate for dissemination. Therefore, the ability to generate RF signals in the optical domain is essential for easier system architecture (long reach to remote sites), reduced cost and increased flexibility in RF tunability. The following are the two techniques which can be used to generate RF signals in the electrical domain.

4.2.1 Frequency comb

A frequency comb consists of a series of evenly spaced distinct spectral lines. The general scheme of frequency comb generator is shown in figure 4.3. This technique consists of an opto-electronic comb generator, continuous wave (CW) laser source and radio frequency oscillator. A CW laser is sent to an optical system that constitutes of one or more modulators (opto-electronic comb generator) that are driven by an external radio frequency (RF) source [4]. At the output, a comb emerges with the central wavelength defined by the laser and fixed spacing dictated by the RF oscillator but limited by the bandwidth of the modulator.

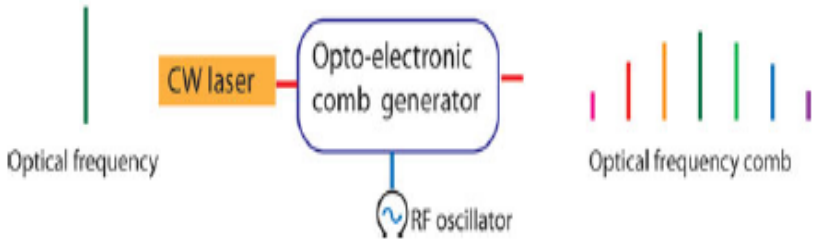

Fig. 4.3: Layout of an opto-electro comb generator [4].

The generated optical comb signals beat at the photodiode to generate RFs. However, considering the use of a state-of-the-art electro-optic phase modulator, it is worth noting that the power from the CW laser is not distributed uniformly which for some applications might be undesirable [4]. In order to attain a flat-top frequency comb, one solution would be to use cascaded intensity and phase modulators. The role of the intensity modulator is the produce a train of square pulses when biased appropriately.

4.2.2 Heterodyning

Optical heterodyning is the simplest, and less costly method of generating RF signals in the optical domain. Chapter 8 utilizes this technique to experimentally generate clock signals. The general scheme for this technique is shown in figure 4.4 below.

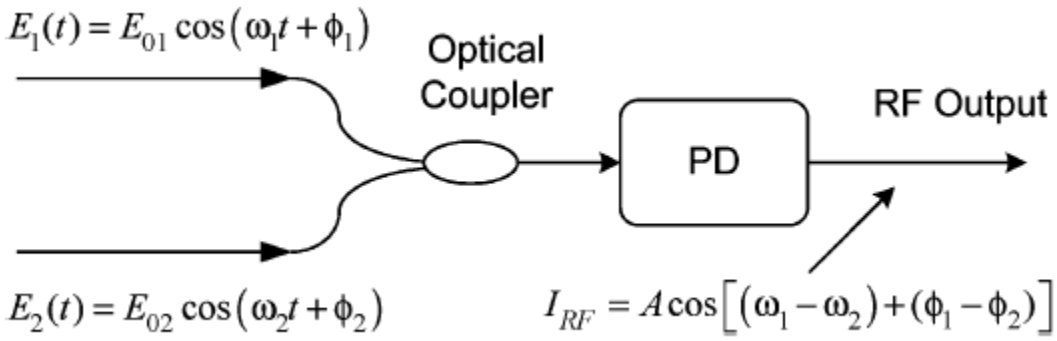

Fig. 4.4: Optical heterodyning technique. PD: Photo detector [5].

Heterodyning between two light waves can be destructive or constructive depending on the polarization states of each wave with respect to the other. For complete constructive interference, polarization of the incoming wave must match that of the traversing wave. This is achievable using of a polarization controller [5, 6]. The beat frequency associated with the mixing, equation 4.1, is detected by the photo detector.

$$E(t)^2 = [E_1 \sin(w_1 t)]^2 + [E_2 \sin(w_2 t)]^2 + A[\cos\{(w_2 - w_1)t + \varphi t\} - \cos\{(w_2 + w_1)t + \varphi t\}] \quad (4.1)$$

where w is the frequency of the laser, φ represents the phase after beating and A is a constant determined by E_1E_2 and the responsivity of the PD [5]. By changing the wavelength spacing between the two waves, higher frequencies are generated. However, higher frequency

components are limited by the bandwidth of the photodetector used. Moreover, beating two optical signals from free running lasers leads to an RF signal with high phase noise since the phases of the optical sources are not correlated. To solve this, techniques such as optical phase locked loops have been used to improve generated signal stability.

Summary

Generation of RF signals is important in today's digital networks. These signals are traditionally generated in the electrical domain before dissemination to remote sites. As in the electrical domain, stable RF signals can also be created in the optical domain by using techniques as simple as heterodyning to frequency combs method. In this chapter, we discussed two primary techniques which are used to create RF signals in the optical domain, heterodyning, and frequency combs. Generation of signals in the optical domain is hugely beneficial. Modern networks use optical fiber as the ideal transport medium hence inherent cost reduction and flexibility being provided by these all optical techniques. Furthermore, the dissemination network architecture becomes simplified. In the next chapter, we will briefly discuss major telescope network employing optical fiber technology as well as unpack the importance of timing in the context of these networks.

References

[1] ITU-T Recommendation G.811: "Timing characteristics of primary reference clocks"

[2] Raltron Electronics Corporation, “Technical notes: Stratum levels defined,” Raltron, Florida, USA.

[3] Symmetricom, “Fundamentals of Time and Frequency: Introduction to the technology and applications,” Symmetricom, San Jose, California, USA.

[4] V. Torres-Company and A.M. Weiner, “Optical frequency comb technology for ultra-broadband radio-frequency photonics,” in *Laser & Photonics Reviews*, vol. 8, no. 3, pp. 368-393, May 2014.

[5] J. Yao, "Microwave Photonics," in *Journal of Lightwave Technology*, vol. 27, no. 3, pp. 314-335, Feb.1, 2009, doi: 10.1109/JLT.2008.2009551.

[6] G. E. Keiser, D. H. Rice and S. W. Quinn, "A Review of Coherent Optical Communication," MILCOM 1985 - IEEE Military Communications Conference, Boston, MA, USA, pp. 65-69, 1985.

Chapter 5

5.1 Introduction

In many astronomical telescopes, very long baseline interferometry (VLBI) technique is used. This technique involves the transfer of signals from individual antennas to a central correlator where appropriate signals are extracted [1]. Furthermore, by using an array of antennas, the collecting area and sensitivity of the receiving is improved. Methods of signal transmission for telescopes originally used coaxial cables or microwave links. These methods have often been the main limiting factor in furthering the sensitivity of telescope networks. Therefore, the development of optical fiber technology has improved transfer of information from receiving antenna to the correlator due to its high-speed capability and available bandwidth. Moreover, timing and frequency reference signals from a central clock source such as the hydrogen maser are disseminated over optical fiber. Fiber optic technology enables individual antennas to be separated over several kilometers thereby improving the resolution of the telescope system. In this chapter, we provide a short overview on some telescope networks employing fiber optic technology. The significance of timing with regard to telescope networks is discussed with the main focus being on the state-of-the-art SKA telescope network.

5.2 Overview of existing and proposed fiber optic telescope networks

5.2.1 SKA

The SKA is the state-of-the-art radio telescope network which is being planned by an international group of astronomers and engineers. This telescope network will comprise of two array telescope networks located in two continents Africa (SKA1-mid) and Australia (SKA1-low). The SKA1-mid will be located in South Africa with some antennas being spread across Africa, 150 km maximum distance, so as to improve the collecting area hence sensitivity. The operational frequency range of this telescope array will be 350 MHz to 14 GHz [2]. Information from the antenna array, approximately 2 terabytes per seconds, will be aggregated to a central correlator for analysis. Optical fiber technology will serve as the backbone of the network architecture for aggregation of data to the correlator.

5.2.2 e-MERLIN (multi element radio linked interferometer network)

The e-MERLIN is the UK's national imaging facility for radio astronomers. It comprises of seven radio antennas with maximum baseline of 217 km. The long baseline means the telescope array can attain sub-arcseconds at centimeter radio wavelengths. The signals from each antenna

were returned to the Jodrell Bank Observatory for analysis over microwave links with a bandwidth of 30 MHz, a limitation to sensitivity [1]. The data transport network of the telescope network has now been upgraded to optical fiber. This has resulted in increase in instrument sensitivity whilst maintaining resolution.

5.2.3 Expanded very large array

The expanded very large array (EVLA) is consequence of the upgrade to the very large array (VLA) telescope network. This array network consists of 27 radio antennas connected in a 35 km diameter 'Y' shape architecture [1, 3]. Each antenna is 25 m in diameter and operates from 1 to 50 GHz. A key component of the EVLA is its new wideband digital correlator, proving improved processing power, and the use of WDM fiber links to provide better sensitivity.

5.2.4 Giant meter-wave telescope

The giant meter wave telescope (GMRT) is one of the largest and most sensitive low-frequency radio telescopes. The telescope array comprises of 30 antennas, each 45 m in diameter and span over 25 km in a 'Y' shape architecture [1, 4]. The network employs single mode optical fiber to transport information to the correlator. Direct intensity modulation is used to modulate the optical carrier using subcarrier-multiplexed signals. The use of analog fiber optic systems is beneficial since it simplifies the electronics required at the remote antennas.

5.3 Timing in telescope networks

5.3.1 Applications

Modern telescope networks comprise of multiple parabolic antennas situated in different locations so as to improve the collecting area. These standalone antennas can be separated by several hundreds to thousands of kilometers. Therefore, dissemination of stable clock signals is essential in these networks. Timing signals are crucial for driving the digitizers. A telescope receives an analog signal. Before transmission through the fiber, the analog signal is first converted to its digital counterpart through the use of ADC's. The ADC sample the received analog signal at the frequency of the clock signal. Instability in the distributed clock will manifest as signal distortions at the end receiver of the telescope network where signal reconstruction occurs.

Clock signals are used also used for timestamping of science and non-science data packets. Time stamping of data is these networks is essential for storage of received information for future reuse. Furthermore, clock signals are used for control, and monitoring functions. Antennas may require to be refocused to a particular direction for observatory. Clock signals control the position of the telescope in the azimuth and elevation plane by controlling the loop rate of the control system. In array telescope network, these clock signals need to be coherent.

5.3.2 SKA timing requirements

Timing is critical to the functionality of the SKA to work as a unified large telescope. The SKA timing and distribution system must be able to broadcast the reference clock to individual antennas over optical fiber with minor degradation in reference signal stability. The stringent timing requirements can only by far be met by atomic standards such as hydrogen maser, rubidium, and cesium clocks. The stability requirements of the frequency distributing system is summarized in table 5.1.

Table 5.1: Clock stability budget for MeerKAT and SKA telescope [5].

	Clock (GHz)	Clock Stability Budget (ps)	PMD penalty at 12km [MeerKAT] (ps)	PMD penalty at 100 km [SKA Phase1] (ps)	PMD penalty at 100 km [SKA Phase2] (ps)
MeerKAT L-band	1.712	18.6	0.2 (1.1% of budget)	0.58 (3.1% of budget)	1.84 (9.9% of budget)
MeerKAT X-band/SKA Phase1 mid	14.5	2.2	0.2 (9.2% of budget)	0.58 (26.5% of budget)	1.84 (83.8% of budget)
SKA Phase2	20	1.6	0.2 (12.7% of budget)	0.58 (36.6% of budget)	1.84 (115.6% of budget)

Distribution of reference clock signals over optical fiber inherently introduces noise in the recovered signal. For the SKA telescope network, active compensation of recovered reference

signals is performed at the client (dish) side so as to keep the phase noise and Allan variance specifications within the budget. However, the cost associated with such stabilization techniques is high. Since compensation at the client side, each individual antenna has to be equipped with a compensating device. In chapter 8, we experimentally demonstrate generation of clock signals in the optical domain. We further showed transmission of clock signals using phase and intensity modulation formats in chapter 9. The work in these two chapters present possible economical solutions to generation and dissemination of clock and frequency reference signals for the SKA and other telescope network projects.

It is apparent that telescope networks aggregate vast amounts of data to the correlator over long distances. Our work in chapter 7, experimentally demonstrates the use of a coherent receiver. The receiver is highly sensitive and supports complex modulation formats such as M-PSK and M-QAM. Therefore, larger amounts of information at high bit rates can be transmitted efficiently and over long distances without the need for a repeater station by employing such a receiver. This is an ideal solution for data transport network of telescope networks.

Summary

This chapter dealt with providing an overview of major telescope networks currently or scheduled to use fiber optic technology. The main focus was on the state-of-the-art telescope network, SKA. This provides the basis of understanding of the network architecture of these networks. The significance of timing signals with respect to these telescope networks was provided. Furthermore, timing and synchronization specifications of the SKA telescope network was provided. In the next chapter, we provide a description on the experimental techniques and various equipment which were employed for carrying out our work.

References

[1] R. McCool *et al*, "Enhancing the Sensitivity of Radio Telescopes Using Fiber-Optic Networks," in *The Radio Science Bulletin*, no. 317, June 2006.

[2] Square kilometer array, "SKA1 MID - the SKA's mid-frequency instrument," Square kilometer array. Accessed on July.15. [Online].

Available:https://www.skatelescope.org/wp-content/uploads/2015/04/SKA1-mid-Infographic.pdf

[3] R.A. Perley, C.J. Chandler, B.J. Butler and J.M. Wrobel, "The Expanded Very Large Array: A New Telescope for New Science," in *The Astrophysical journal letters*, vol. 739, no. 1, Aug. 29, 2011.

[4] Y. Gupta *et al*, "The upgraded GMRT: opening new windows on the radio Universe," in *Current Science*, vol. 113, no. 4, Aug. 15, 2017.

[5] P.P. Dlamini, "Optical Fiber Measurement for Clock Tones in Telescope Networks," MSc. dissertation, dept. of Physics, Nelson Mandela University, Port Elizabeth, South Africa, 2017.

Chapter 6

6.1 Introduction

The fundamental basis of this chapter is to provide an overview on the experimental techniques used. The spectrum analyzer method for quantifying the stability of an oscillator system is discussed. Furthermore, major optical equipment such as used lasers and optical modulators are discussed.

6.2 Frequency stability

Frequency instability of an oscillator system is defined using two parameters, Allan variance and phase noise. Allan variance describes long-term instability while phase noise is associated with short term instability. There are various techniques which can be used to measure frequency stability. The most widely used technique is the spectrum analyzer method of which was utilized in this work. A detailed explanation of this method, for both Allan variance and phase noise measurement, is provided below.

6.2.1 Measurement techniques

a. Phase noise measurement

Phase noise measurement using a spectrum analyzer is the most established and widely used method. It is also the simplest and cheapest. The electrical spectrum analyzer translates the time domain signal into the frequency domain by using the fast Fourier transform algorithm. The analyzer then computes single sideband phase noise values in logarithmic scale [1]. Figure 6.1 below shows the setup used in this method.

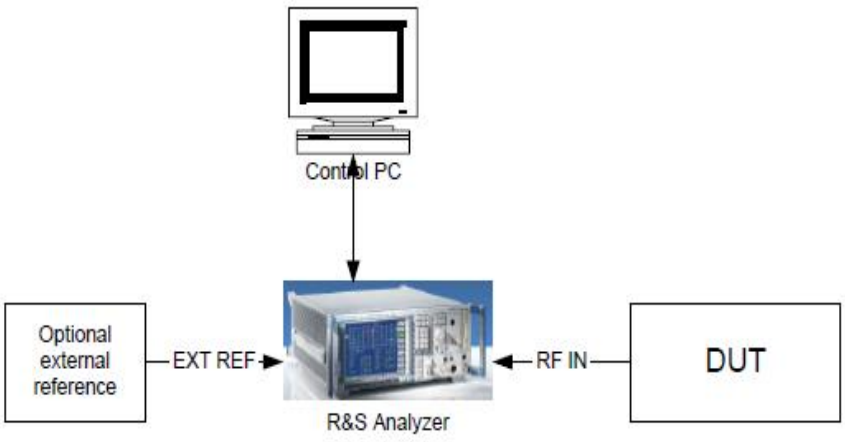

Fig. 6.1. Spectrum analyzer method for Allan variance and phase noise measurement [3].

The device under test (DUT) directly connected to the analyzer. For reliable phase noise measurement with this method, the following conditions must be met [2]:

- The frequency drift of the DUT must be small relative to the spectrum analyzer sweep time. This is necessary for correct calculation of the signal-to-noise ratio.
- The spectrum analyzers phase and amplitude noise must be low enough compared to the device under test. This is critical since the spectrum analyzer provides the sum of the source under test amplitude noise and phase noise with its own phase noise and amplitude noise.
- The device under test amplitude noise must be significantly lower than the phase noise.

b. Allan variance

The Allan variance is intended to estimate long term instability caused by noise processes and not that of systematic errors or imperfections such as frequency drift and temperature effects [4]. The mathematical equation for calculation of the Allan variance is given as

$$\sigma_y(\tau) = [\frac{1}{2(M-1)}\sum_{i=1}^{M-1}(y_{i+1} - y_i)^2]^{1/2} \quad (6.1)$$

Where τ represents the sample time, y_i are discrete frequency averages. M is the number of samples over the sample time.

The beat frequency counter method is one way of directly measuring frequency variations. The spectrum analyzers internal counter is utilized in this method. Figure 6.1 shows the setup required for this measurement technique. This method provides high precision depending on the accuracy of the frequency counter [3, 4]. Also, AM noise is not considered. Signals from two independent oscillators, DUT and reference, are fed into the two ports of the double balanced mixer. The difference frequency is obtained as the output of the low pass filter. This frequency is

$$f_b = f_{DUT} - f_{ref} \quad (6.2)$$

with fractional frequency corresponding to

$$y(t) = \frac{f_{DUT} - f_{ref}}{f_{ref}} \quad (6.3)$$

Frequency measurements involve some sample time. The frequency counter is triggered either by the rising or falling edge of the zero crossings of the beat signal. The output at counter is a value which has been captured over some specific gate time. After this time has expired, the counter latches out this value so as it can be either stored or printed [4]. Therefore, the average fractional frequency between two-time differences is given by

$$y_{ave}(t) = \frac{x(t+\tau)-x(t)}{\tau} \tag{6.4}$$

Through a computer interfaced with a spectrum analyzer, the Allan variance can be computed using equation 6.1.

Modern electrical spectrum analyzers such as the Rohde & Schwarz provide capability measurement of Allan variance through frequency counter method using a computer running the Allan variance application software or through domain conversion. In domain conversion, these analyzers measure the phase noise of the DUT before converting the data into corresponding Allan variance data. The Allan variance is derived numerically using

$$\sigma_y{}^2(\tau) = 2\int_0^f S_y \frac{[\sin(\pi\tau f)]^4}{(\pi\tau f)^2} df \tag{6.5}$$

where f is the offset frequency in Hz and Sy is the spectral density of frequency fluctuations. This method is recommended for small τ as the uncertainty for frequency counter measurements with regards to τ become dominant for $\tau < 0.1$ seconds [3].

6.3 Optical fiber communication system

6.3.1 Optical sources

Optical sources are fundamental in optical communication. They are sources of the optical field for which information is encoded. For this work, two types of lasers where used.

6.3.1.1 Distributed feedback lasers

The distributed feedback (DFB) is the most stable single-frequency tunable laser configuration. The DFB laser has high SNR, low temperature sensitivity, inherent fiber compatibility, single mode operation, and is easy to manufacture for predefined wavelengths. This makes it the most attractive optical source for direct detection and WDM schemes [5]. For this work, DFB lasers in the C-band where used.

6.3.1.2 Fiber lasers: Koheras BASIK

The Koheras BASIK is a single frequency distributed feedback fiber laser system with passive vibration reduction. This laser features ultra-narrow linewidth in the Hertz range and exceptionally low frequency and intensity noise [6]. The ultra-narrow linewidth, low frequency and intensity noise make this laser ideal for coherent sensor applications and coherent optical communication. A computer application is used for monitoring and control of the laser modules. The operational wavelength for this laser is from 900 nm to 2100 nm [6]. This laser is manufactured by NKT photonics.

6.3.2 Optical Modulators

Optical modulators are essential in communication. They manipulate the property of the optical source thereby encoding information on the optical carrier. The following two modulator technologies were utilized for this work.

6.3.2.1 Mach-Zehnder modulator

Mach Zehnder modulators (MZM) work by principle of inference, controlled by modulating the optical phase [7]. Figure 6.2 shows the structure of an MZM. Light is split into two paths at the input coupler. One path is equipped with a phase modulator thereby generating a relative phase difference between the two optical fields. The two fields interfere at the output of the coupler. The degree of interference, constructive or destructive, is determined by the applied electrical voltages (biasing), thereby producing intensity modulation.

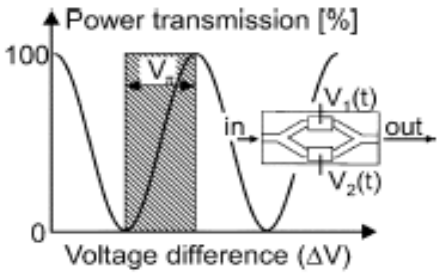

Fig. 6.2. Structure and transmission function of MZM [7].

6.3.2.2 Phase Modulator

A phase modulator (PM) modulates the phase of the light wave along the unit circle in the complex plane, leaving constant intensity of the phase modulated light. These modulators use an

electro optic crystal, sandwiched between a pair of electrode, and an input polarizer [8]. A voltage applied across the electrodes causes rotation of the principal axes of the crystal cross section. When light passes through the crystal, it experiences a phase shift proportional to the applied voltage. However, since the optical phase follows the electrical drive signal, the speed of phase transitions is limited by the combined bandwidth of the driver amplifier and phase modulator. Moreover, any overshoots in the drive waveform manifest itself in phase distortions [7]. The PM utilized for this work supported bit rates between 100 Mbps to 40 Gbps.

6.3.3 Optical Receivers

The significance of optical receivers is to demodulate the received optical information into its equivalent electrical. The optical receiver must therefore have the necessary bandwidth to demodulate the data carrying signal to baseband. For this work, the following receivers where used.

6.3.3.1 PIN photodiode

A PIN (positive intrinsic negative) photodiode translates an optical signal to electrical by acting as a square law detector (envelope detection). Therefore, only intensity modulated carrier signals can be demodulated by the photodiode. A PIN photodiode comprises of three layers, p-type layer, n-type layer, and intrinsic layer. The diode is electrically operated in reverse bias mode. The intrinsic region has no free charges and has high resistance. Most of the reverse biased voltage is applied to this region. This region is usually made wide such that incoming photons have a greater probability of absorption in this layer compared to p or n layers [9]. When light is introduced into the intrinsic layer, a hole-electron pair is generated. The hole and electron will migrate in opposite directions under the action of the electric field across the intrinsic region thereby current flowing. The amount of current flowing is proportional to the light entering he intrinsic layer. The more the light, the greater the number of electron-hole pairs generated and more current flowing thereby detecting the intensity of a modulated light wave. For this work, a 10 GHz bandwidth PIN photodiode was utilized.

6.3.3.2 Coherent receiver: Lab Buddy

A coherent receiver, lab buddy, comprises of four matched balanced PIN photodiodes. This device is a dual polarization receiver which supports both intradyne and homodyne detection technologies in the C band. Bit rates up to 100 Gbps are supported by this receiver [10]. This

device supports modulation formats such as BPSK, QPSK and QAM. Lab buddy configuration circuit is shown is chapter 3. The lab buddy has two modes of operation, manual gain, and automatic gain. In automatic mode, a constant differential output voltage swing of approximately 500 mV peak-peak is maintained. In manual gain, the transimpedance gain varies from 50 to 4600 ohms through the use of a ten-turn potentiometer [10]. The lab buddy employed for this work is manufactured by Discovery Semiconductors.

Summary

The main objective of this chapter was to provide an overview of techniques and equipment utilized in carrying out experiments for our research. The use of a spectrum analyzer as a frequency stability measurement technique was discussed. Furthermore, the fundamental theory behind the functional working principle of major optical components employed was unpacked. The next chapter is the first of which represent our experimental work. We experimentally compare performance of coherent BPSK with that of intensity modulation. Furthermore, we demonstrate the use of the LMS filter for equalization of PMD.

References

[1] K. Gheen, “Phase noise measurement methods and techniques,” Agilent technologies, California, USA, 2012.

[2] Rohde & Schwarz, “Measuring with modern spectrum analyzers,” Rohde & Schwarz, Munich, Germany, Feb. 2013.

[3] Rohde & Schwarz, “Time domain oscillator stability measurement Allan variance,” Rohde & Schwarz, Munich, Germany, April. 2015.

[4] D.A. Howe, “Frequency stability,” in *Encyclopedia of RF and Microwave Engineering*, pp. 1706-1720, Jan.1, 2005.

[5] L. B. Fu, M. Ibsen, D. J. Richardson, and D. N. Payne, "977-nm all-fiber DFB laser," in *IEEE Photonics Technology Letters*, vol. 16, no. 11, pp. 2442-2444, Nov. 2004, doi: 10.1109/LPT.2004.835619.

[6] NKT photonics, ‘Koheras BASIK Low noise single frequency laser module - Instructions Manual,’ *NKT photonics*, April. 2016.

[7] P. J. Winzer and R. -. Essiambre, "Advanced Optical Modulation Formats," in *Proceedings of the IEEE*, vol. 94, no. 5, pp. 952-985, May 2006, doi: 10.1109/JPROC.2006.873438.

[8] M. Bass, “ELECTRO-OPTIC MODULATORS” in *Handbook of Optics: Volume V – Atmospheric Optics, Modulators, Fiber Optics, X-Ray and Neutron Optics*, 3rd ed. McGraw-Hill Professional, 2010.

Available:https://0www.accessengineeringlibrary.com.wam.seals.ac.za/content/book/9780071633130/chapter/chapter7

[9] G. Keiser, “Photodiodes and Receivers,” in *Optical Communications Essentials*, McGraw-Hill, 2003.

Available:https://0www.accessengineeringlibrary.com.wam.seals.ac.za/content/book/9780071412049/chapter/chapter7

[10] Discovery semiconductor Inc., “DP-QPSK 100 Gb/400 Gb Coherent Optical Receiver Lab Buddy,” Discovery semiconductor Inc., 2013.

Available: https://www.discoverysemi.com/Product_Pages/DSCR413.php

Chapter 7

7.1 Introduction

In modern telecommunication networks, modulation formats which are immune to distortions and can be used in long distance communication at high bit rates with few repeater stations are attractive. The use of such modulation formats in conjunction with highly sensitive receiver systems is also a conducive aspect of desired overall communication system especially in today's high data demanding networks such as the SKA and 5G. In this chapter, we perform a comparative study between intensity modulation (OOK) and coherent phase modulation (BPSK). In the first part of this chapter, we experimentally demonstrate transmission of OOK and BPSK signals at 10 Gbps. In section 7.4, the two modulation systems are compared in terms of receiver sensitivity, and bit error rate. Moreover, offline equalization of PMD through the use of the least mean square (LMS) algorithm is presented for the received BPSK data.

7.2 Intensity modulation

7.2.1 Experimental procedure

The setup for optical transmission of intensity modulated OOK carrier is shown in figure 7.1.

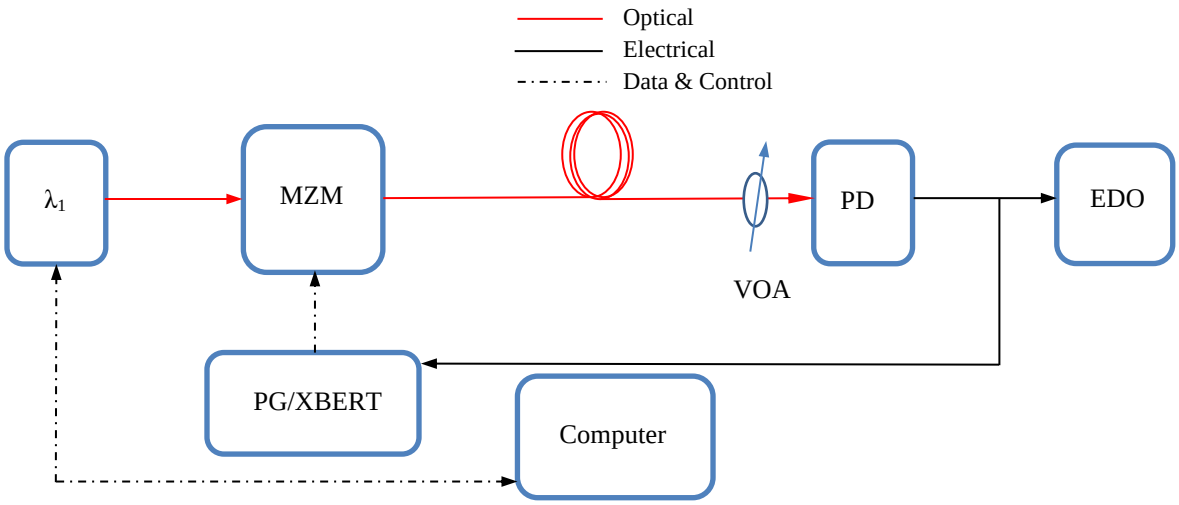

Fig. 7.1. Set-up scheme for OOK at 10 Gbps. MZM: Mach-Zehnder modulator. VOA: Variable attenuator. PD: Photodiode. EDO: Electrical digital oscilloscope. PG: Pattern generator. XBERT: Bit error rate tester

Non-return to zero pseudo random binary sequence with word length equivalent to 7 bits from the pattern generator at 10 Gbps bit rate was used as input to the March-Zehnder modulator. The wavelength of the carrier, λ_1, was set to 1550.1206 nm using a computer as a control module.

The OOK signal was transmitted in an NZDF fiber with length and attenuation coefficient corresponding to 26.6 km and 0.210 dB/km, respectively. The intensity modulated optical signal was directly detected using a 10 GHz bandwidth PIN photodiode. The VOA was used to control the optical power into the photodiode to keep it within the diodes power specifications. Bit error rate measurements were conducted in real time by using the detected electrical signal as input to the XBERT. The gating time of the XBERT was set to 10 seconds.

7.3 Phase Modulation

7.3.1 Experimental procedure

The setup for optical transmission of phase modulated BPSK carrier is shown in figure 7.2. Non-return to zero pseudo random binary sequence with word length equivalent to 7 bits from the pattern generator at 10 Gbps bit rate was used as input to the phase modulator.

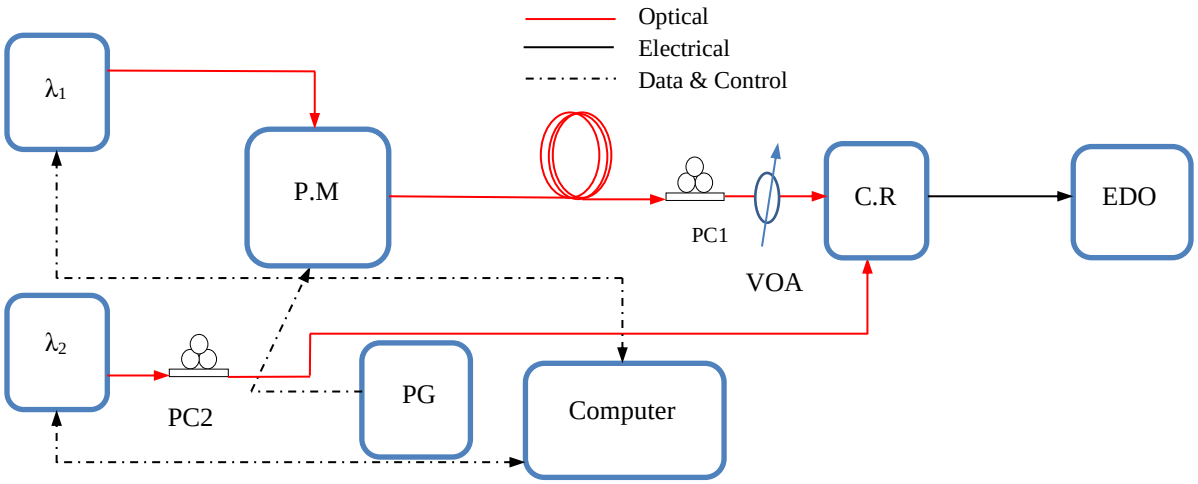

Fig. 7.2. 10 Gbps BPSK transceiver configuration. PG: Pattern generator. PM: Phase Modulator. PC: Polarization controller. CR: Coherent receiver

Wavelength of the carrier, λ_1, was set to 1550.1207 nm at +13.14 dBm. Heterodyne reception was used. Therefore, the local oscillator wavelength input to the coherent receiver, λ_2, was set at 1550.1204 nm at +13.14 dBm. Wavelength control of both laser modules was archived through a computer aided graphic user interface using USB communication. A variable optical attenuator was used to reduce power from the two laser modules to within coherent receiver power input specifications. The BPSK signal was transmitted in an NZDF fiber with length and attenuation coefficient corresponding to 26.6 km and 0.210 dB/km, respectively. Polarization controllers,

PC1 and PC2, were used to maximally align the polarization states of the carrier and local oscillator signals. The coherent receiver was set to both automatic gain and bandwidth. Signals of the in phase and quadrature channels of the coherent receiver were viewed on the digital oscilloscope. Digital signal processing techniques for equalization of transmission impairments were performed offline using MATLAB software.

7.4 Results and analysis

The optical spectrum of the two modulation formats used in transmission of the data are shown in figure 7.3 below.

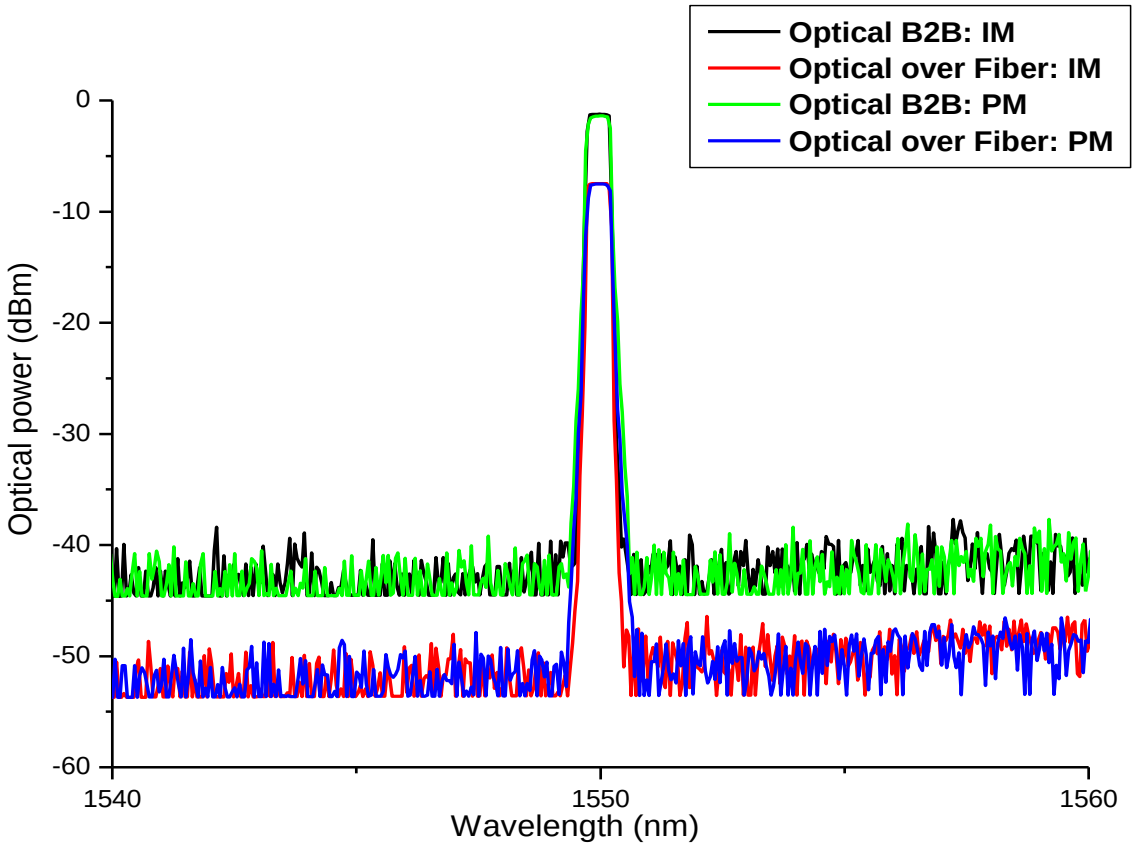

Fig 7.3. Optical spectrum of modulation techniques. IM: Intensity modulation. PM: Phase modulation.

The two modulation formats, IM, and PM occupy the same bandwidth for both back-to-back and transmission over optical fiber. The measured optical spectrum validates the theoretical spectral

occupation and efficiency of both the two modulation formats being identical for the same bit rate. Both modulation formats have a spectral efficiency of 1 bit per second per hertz since a single bit corresponds to one symbol. The attenuation associated with transmission over fiber is approximately the same for both modulation formats, 6.29 dB. Figure 7.4 and 7.5 present the electrical eye diagrams for the intensity modulated and phase modulated signals, respectively. For the intensity modulated signal, the extinction ratio for the back-back recovered data at -6.32 dBm optical power is 6.02 dB. At -16.11 dBm, the extinction ratio is 4.68 dB. This represents a degradation of 1.34 dB which constitutes to increased error probability in the received signal.

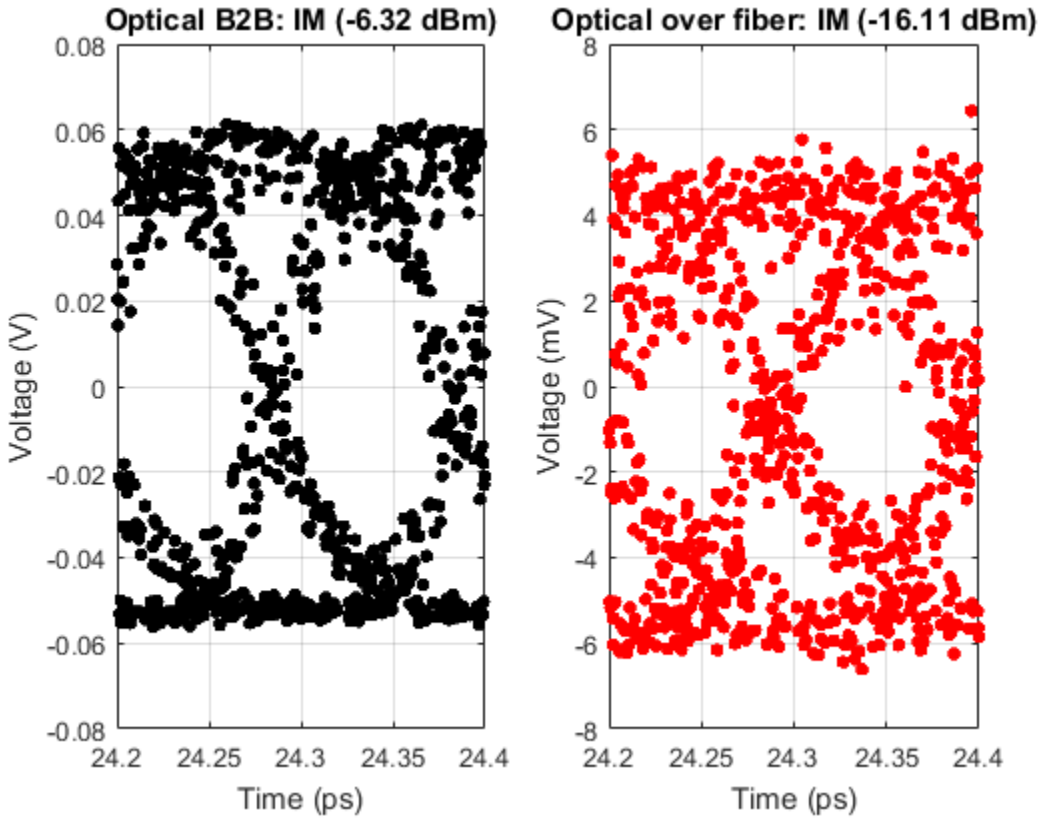

Fig. 7.4. Electrical eye diagram plots for intensity modulated data.

For the phase modulated signal, the eye diagram for both the in-phase and quadrature components are open for back-to-back case with a mean voltage swing of 0.1 v. Therefore, error probability is low for this signal. As with intensity modulation, introduction of the fiber degraded the quality of the signal. This is depicted by the eye diagrams at -17.86 dBm. Compared with the

back-to-back signal, the mean voltage swing is greatly reduced by a factor of 10 to 0.01 v. However, the eye is still open, therefore less error probability.

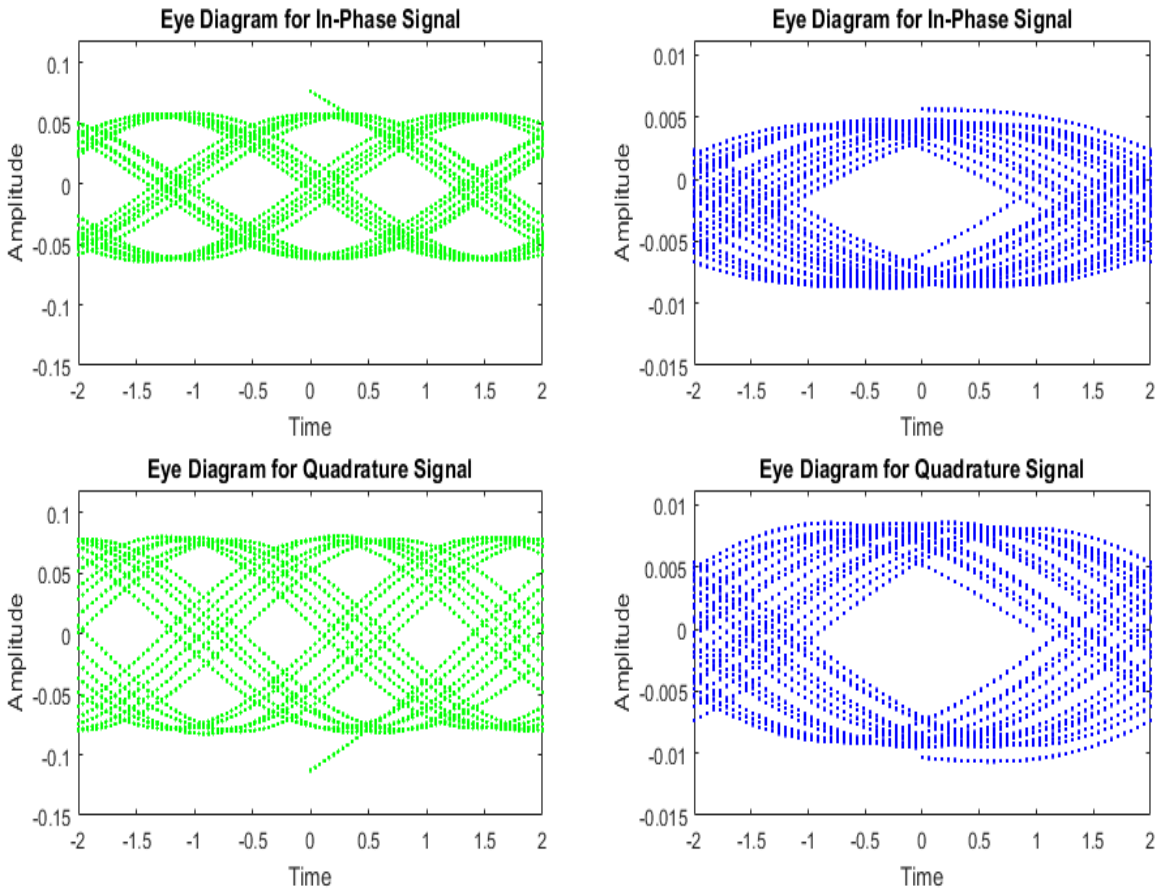

Fig. 7.5. Electrical eye diagram plots for phase modulated data. Left: Optical back-back (-4.37 dBm). Right: Optical over fiber (-17.86 dBm).

The constellation diagram for back-back and transmission over fiber for the BPSK signal is shown in figure 7.6. The constellation diagram here, represents the unsampled continuous time signals of I and Q which were visualized thorough an electrical oscilloscope. From the constellation diagram, it is apparent that transmission over fiber degrades the signals quality. The signal strength of I and Q signals for transmission over fiber are considerably small hence increase error probability.

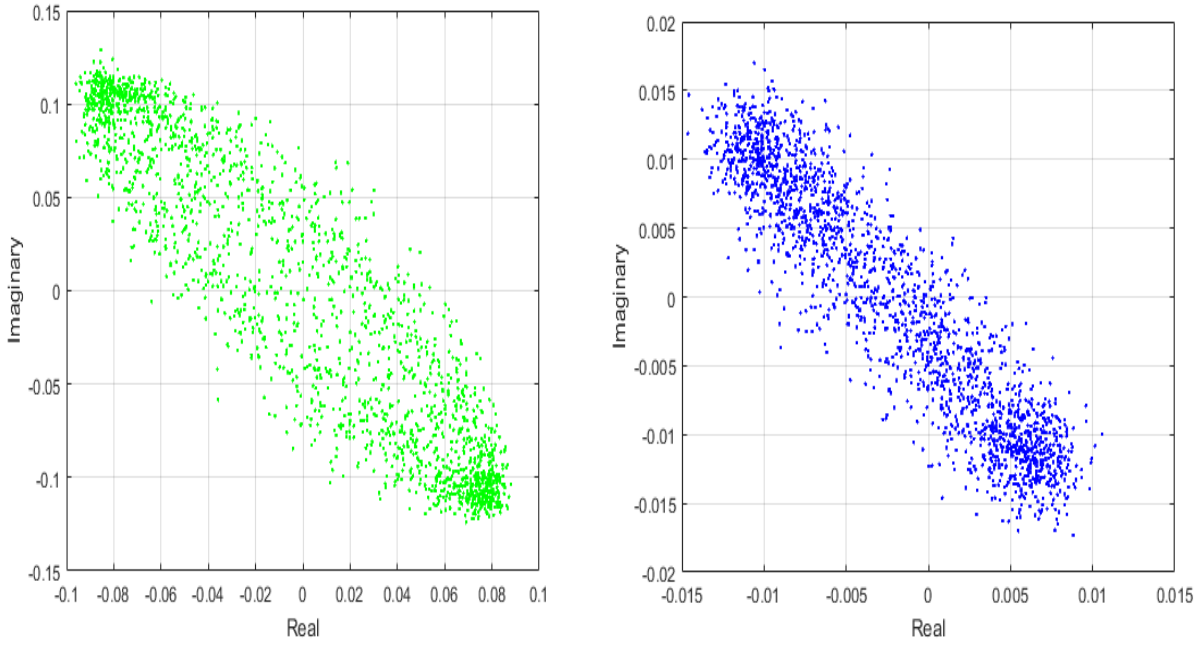

Fig. 7.6. Constellation diagrams of phase modulated data. Left: Optical back-back (-4.37 dBm). Right: Optical over fiber (-17.86 dBm).

Bit error rate performance for the two-modulation systems is presented in figure 7.7. In the case of intensity modulation, bit error rate of 5.72×10^{-11} was attained at -11.95 dBm input optical power for back-back transmission. For transmission through the optical fiber, an input power of -9.92 dBm is required to attain the same bit error rate as for the back-to-back intensity modulated signal. This represents 2 dB degradation of in receiver sensitivity. Coherent BPSK has superior receiver sensitivity compared to intensity modulation for both back-to-back and transmission through the fiber. At received optical powers as low as -15 dBm, bit error rates in the range of 10^{-13} where attained for the back-back condition. In our developed algorithm, bit error rate computation is carried out through calculation of error vector magnitude (signal not demodulated) from the sample sequence obtained from the continuous time IQ signals (refer to MATLAB code in appendix section for computation of bit error rate). However, as is the case for intensity modulation, introduction of optical fiber in the transmission system degraded receiver sensitivity. Bit error rate of 1.86×10^{-15} was attained at -10.00 dBm optical input power for back-to-back while for transmission through the fiber, optical power of -5.79 dBm is required to

maintain the aforementioned bit error rate. This represents 4.79 dB degradation in receiver sensitivity.

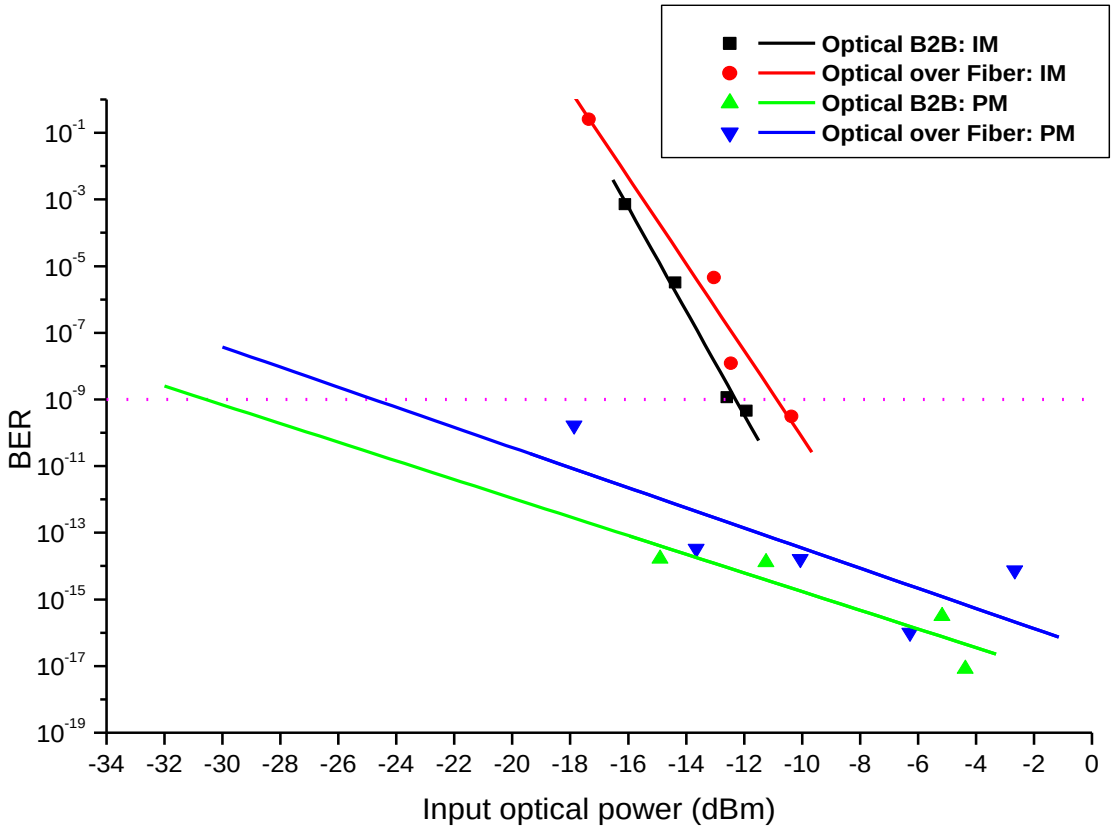

Fig. 7.7. Bit error rate of intensity and phase modulated data.

Receiver sensitivities for both modulation systems at maximum telecommunications bit error rate of 10^{-9} is summarized in table 7.1 below.

Table 7.1: Receiver sensitivity at 10^{-9}.

Transmission system	Receiver sensitivity (dBm)
Optical B2B: IM	-12.30
Optical over Fiber: IM	-10.90
Optical B2B: PM	-30.67
Optical over Fiber: PM	-24.79

Even though the sensitivity of coherent BPSK is degraded more compared to intensity modulation, bit error rate performance for transmission through optical fiber is far superior compared to intensity modulation for both back-to-back and transmission through optical fiber. Moreover, equalization of transmission impairments is easily achievable. MATLAB script code for equalization of PMD and residual CD by employing LMS filter can be found in the appendix 1. Figure 7.8 shows received constellation at –4.37 dBm optical input power for 31 symbols before and after equalization.

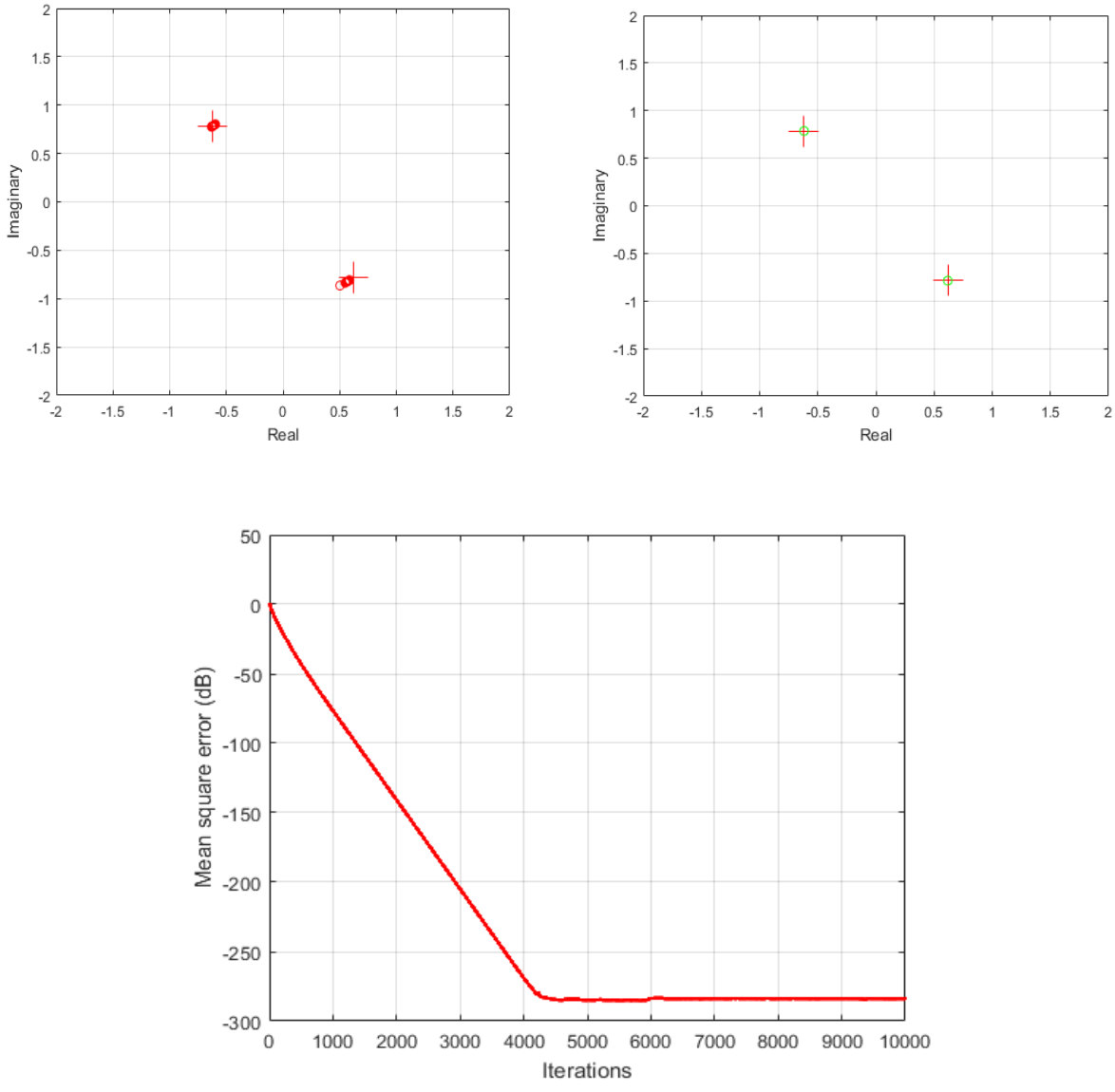

Fig. 7.8. Constellation diagrams (top) and LMS filter cost function (bottom). Top left: Received constellation. Top right: Equalized symbols.

The ‘+’ signs in the constellation represent the desired response while the circular points are the symbols which correspond to one bit for BPSK modulation. Analysis of this equalization method is in the appendix 1.

Coherent detection offers high sensitivity compared to IM-DD. From table 7.1, receiver sensitivity is improved by 13.89 dB for transmission over optical fiber. The use of modulation formats such as M-QAM and M-PSK with such as receiver improves the spectral efficiency beyond 1 bit/s/Hz. Therefore, the application of such a receiver system is ideal for high speed big data applications and projects such as telescope networks, i.e. SKA, 5G and IoT. Moreover, due to high receiver sensitivity, ultra-long-haul transmission is easily feasible.

Summary

Highly sensitive receiver systems coupled with the ability to support advanced complex modulation formats are attractive. In this chapter, we provided a comparative study between two modulation formats, IM-DD and coherent BPSK. The results showed that coherent BPSK has superior sensitivity and is immune to errors compared to IM-DD. Coherent BPSK archived bit error rates in the range of 10^{-13} with input optical powers as low as -14 dBm. Compared to intensity modulation, coherent BPSK attained receiver sensitivity improvements of 18.37 and 13.89 dB for the back-back and transmission over fiber, respectively. Moreover, this system allows for equalization of all transmission impairments in the digital domain hence improving performance of the system further. In the next chapter, we experimentally demonstrate generation of clock signals in the optical domain through heterodyning technique.

Chapter 8

8.1 Introduction

Generation of stable clock signals is essential in today's digital communication technologies. Timing signals are embedded in applications as small as smart watches to larger systems such as smart grid. As technology evolves, more stringent timing stability requirements are required for high end technologies and projects such as 5G and SKA. The purpose of this chapter is to experimentally generate a clock signal optically using heterodyning technique. The frequency instability of the generated clock signal is then measured using spectrum analyzer method. Measurement of both long term and short-term stability is essential. These measurements provide insight into the types of noise processes predominant on the designed oscillator system/clock generation scheme. In the case of an oscillator which is dominated by random-walk FM, the effect of this noise process can be reduced significantly by operating the oscillator in a temperature-controlled environment.

This chapter is organized as follows: The setup used in the experiment is explained in section 8.2. Section 8.3 presents the performance of the system and detailed analysis of the clock generation scheme. Finally, suitable applications of the scheme are identified in section 8.4.

8.2 Experimental set-up

The experimental set-up is shown in figure 8.1. The following two experimental schemes where used:

a. Fiber laser scheme

A computer was used to control the wavelengths of the two lasers depicted in figure 8.1. Wavelength of laser 1, λ_1, was kept at 1550.1209 nm while that of the second laser, λ_2, was tuned to 1550.1860 nm. The output power from each of the two lasers was +13.14 dBm. The two lasers where allowed to interfere constructively at the photodiode to generate a 4 GHz RF signal. Lasers used are commercial manufactured by NKT photonics.

b. DFB laser scheme

Wavelength of laser 1, λ_1, was tuned to 1549.867 nm while that of the second laser, λ_2, was set to 1549.836 nm. The output power form each of the two lasers was +10 dBm. The two lasers where

allowed to interfere constructively at the photodiode to generate a 4 GHz RF signal. Lasers used are commercial manufactured by ThorLabs.

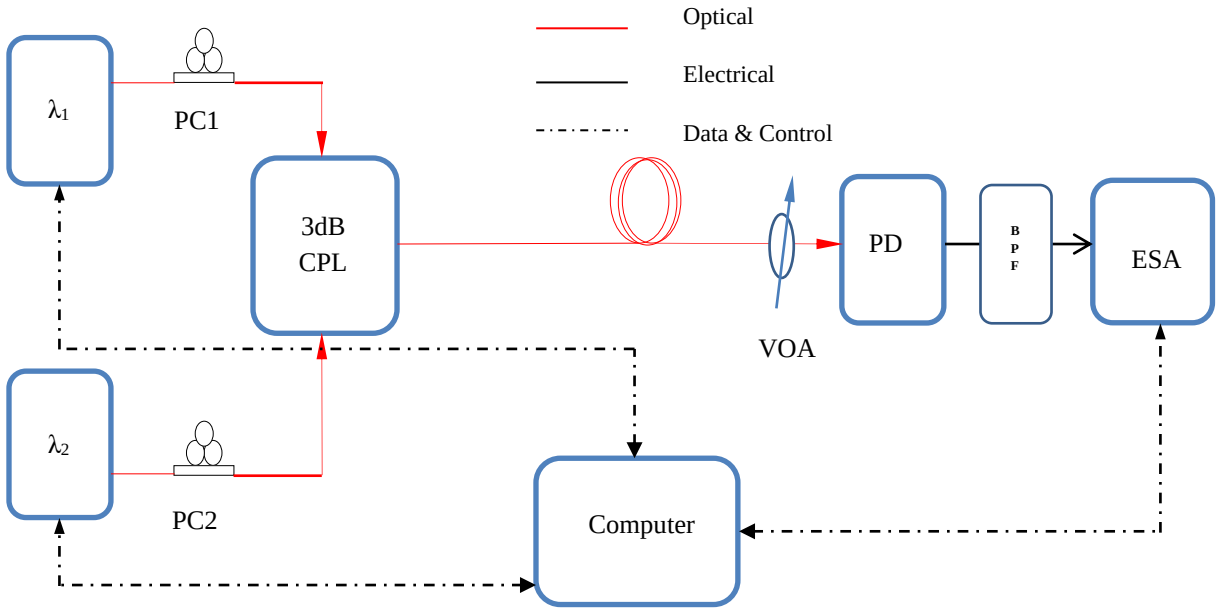

Fig. 8.1. Set-up scheme for optical generation of a 4 GHz clock. ESA: Electrical spectrum analyzer. BPF: Band pass filter. PD: Photodiode. PC: Polarization controller. CPL: Coupler.

For both the two experimental schemes, polarization controllers were used just before the coupler for both channels. This is necessary for alignment of polarization states of both lasers so as to enable maximum constructive interference at the photodiode. The two wavelengths were then coupled into the optical fiber through a 3dB coupler. The optical fiber used here is Non-Zero-Dispersion-Shifted-Fiber (NZDSF) fiber with length and power loss corresponding to 26.6 km and 0.2 dB/km, respectively. A variable optical attenuator was used to control the received optical power. After the VOA, the optical signal was directly detected by a 10 GHz bandwidth PIN-type photodiode. A 3.5-4.5 GHz band pass filter was used to suppress harmonics generated by beating of the two lasers. An electrical spectrum analyzer was then used to directly measure both phase noise and Allan variance of the generated RF signal. For phase noise measurement, offset frequency range set on the analyzer was from 1 Hz to 100 MHz. On the analyzer, AM rejection mode was turned on for reliable measurement of phase noise. In measurement of Allan variance, the computer was interfaced to the analyzer. The Allan variance application from R&S

was run on the interfaced computer. The frequency counter method was used. The measurement window was set to 5.5 hours.

8.3 System Performance

The optical spectrum profile of the two types of lasers used for the experiments is shown in figure 8.2 below. The NKT lasers have the same spectral shape and linewidth. Furthermore, the two lasers are able to produce the same optical power. However, the spectral linewidth measured by our optical spectrum analyzer does not coincide with that of the manufacture. The linewidth of NKT fiber lasers is in the Hertz range. The resolution of our optical spectrum analyzer is large and therefore cannot measure such ultra-narrow linewidths.

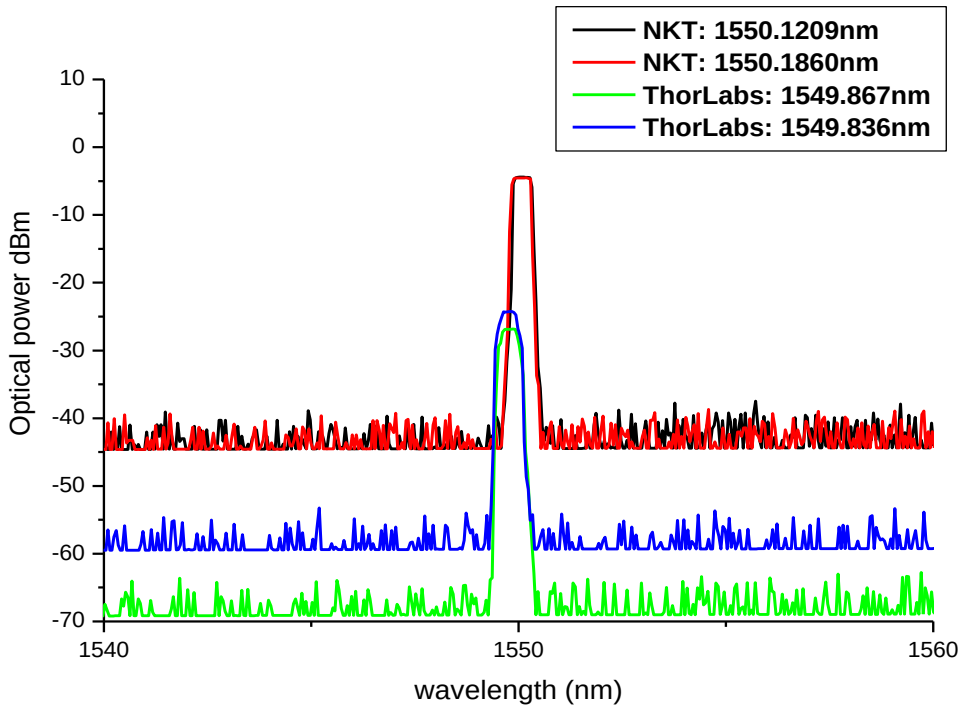

Fig. 8.2. Optical spectrum of the DFB lasers used.

ThorLabs lasers exhibit the same spectral linewidth and produce nearly the same output power. However, the spectral shape of the two DFB lasers are different. The noise floor of laser 1 (1542.867 nm) is considerably lower than that of laser 2 (1549.836 nm). Noise floor for laser 1 is 10 dB lower compared with that of laser 2. The electrical spectrum profile of the heterodyne 4

GHz clock generation schemes is shown in figure 8.3. The spectral shape of the NKT heterodyne laser scheme matches that of the reference, electrical signal generator (SMB 100A), for both the back-to-back and transmission over fiber cases. This is due to the narrow linewidth of the fiber lasers. The coherence time is large thereby enabling constructive interference since the two waves are highly correlated. ThorLabs lasers exhibit broad heterodyne spectral linewidth which degrades performance. This degradation in performance is shown more clearly in figure 8.4.

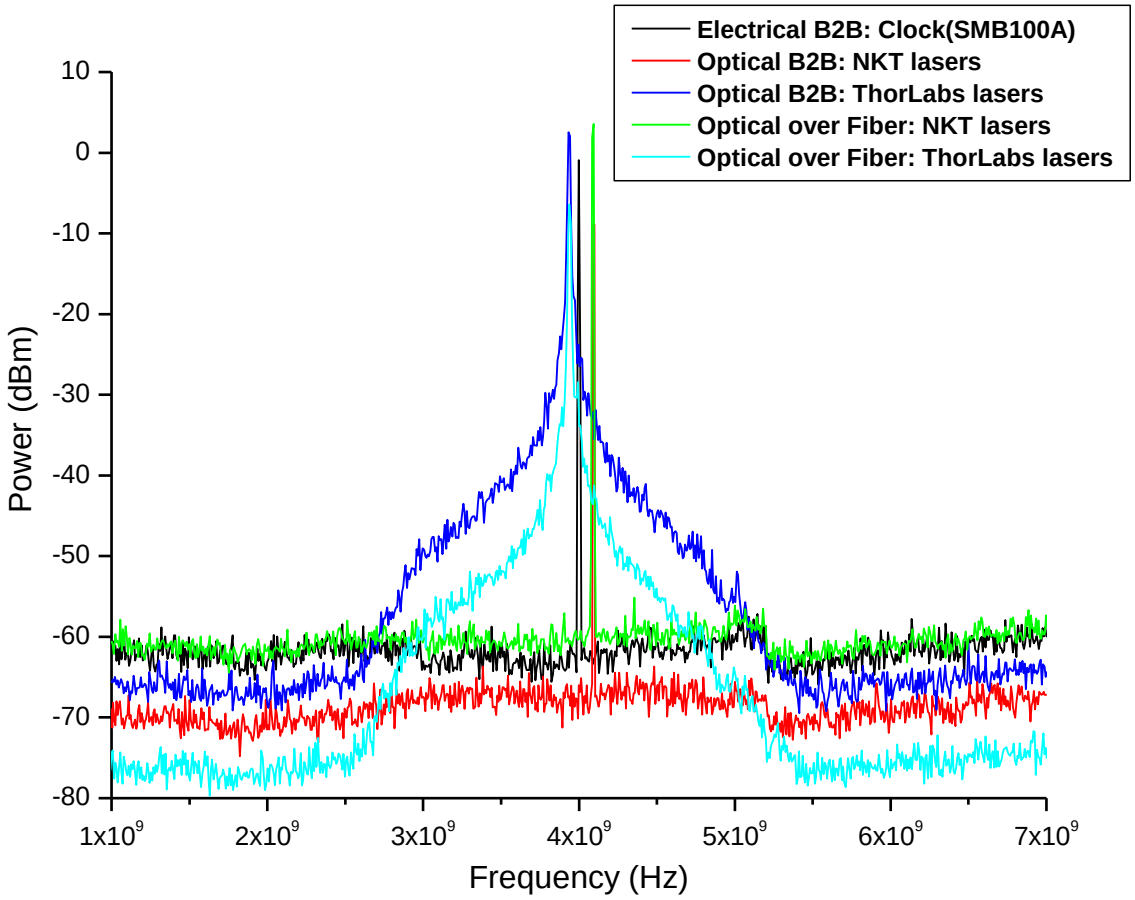

Fig. 8.3. Electrical spectrum of the heterodyne clock. B2B, back-to-back.

The heterodyne system using ThorLabs lasers exhibits a lot of amplitude noise for both the back-to-back and transmission over fiber cases. This large amount of noise is attributed to the by spectral shape of the heterodyne system. Considerable amount of electrical power is distributed across frequencies close to the fundamental (4 GHz). Most of these frequencies are within the

band of the filter used to suppress generated harmonics and therefore significantly contributing to the overall degradation in performance as illustrated by the waveform in figure 8.4. In order to significantly improve performance, a narrow band filter may be employed.

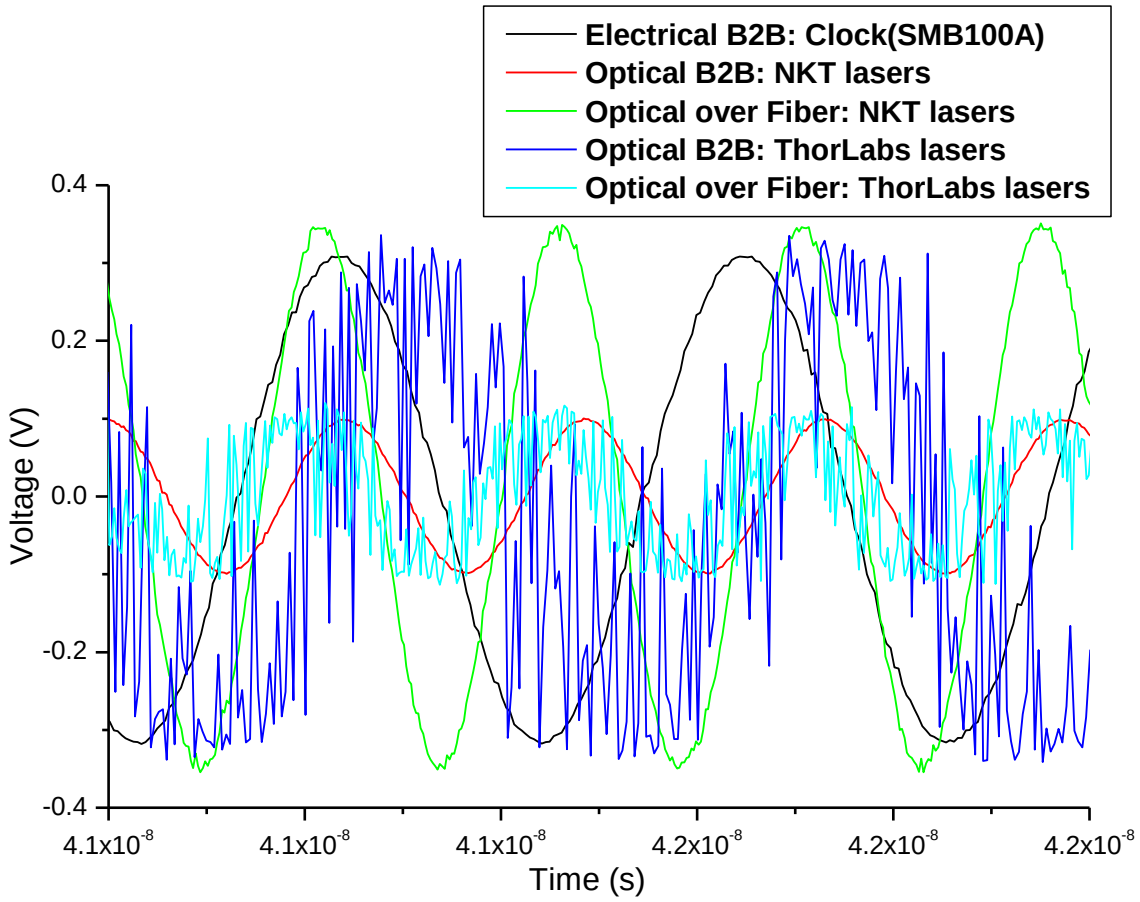

Fig. 8.4. Generated heterodyne electrical waveforms.

The electrical waveforms of the NKT heterodyne configuration is comparable to that of the reference, SMB 100A, signal. The electrical signal generator achieved an average peak-peak voltage of 0.6 V while the heterodyne system over fiber using NKT lasers attained an average peak-peak of 0.7 V. Furthermore, the NKT heterodyne systems for the back-to-back and transmission over fiber cases exhibits better phase noise performance for offset frequencies less than 10 Hz compared to the SMB 100A signal generator employing a rubidium clock as reference. This is depicted in figure 8.5. At 1 Hz offset, phase noise for the SMB 100A is -41.63

dBc/Hz while that of the back-to-back heterodyne ThorLabs and NKT laser systems is -67.33 dBc/Hz and -123.50 dBc/Hz, respectively. However, beyond 10 Hz frequency offsets, SMB 100A exhibits better performance reaching noise floor as low as -153.91 dBc/Hz.

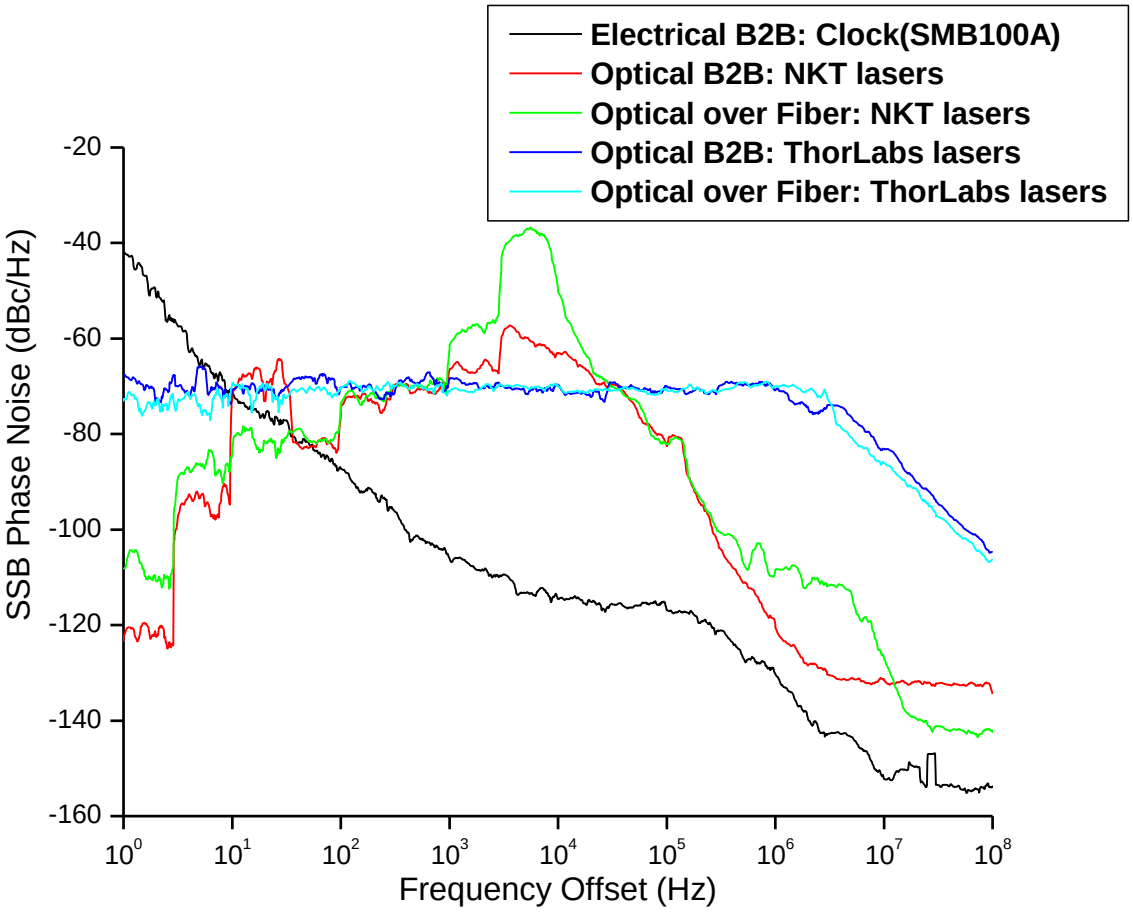

Fig. 8.5. Phase noise of a 4 GHz optical heterodyne clock.

The heterodyne system employing ThorLabs lasers is hugely dominated by white phase modulation noise (broadband noise) with an average floor figure of -73.16 dBc/Hz between 1 Hz and 1 MHz offset frequencies for both transmission cases. Since broadband noise is due to mixing of frequencies up to the oscillation frequency reduction of this mechanism can be archived by narrow band filtering the heterodyne spectrum. It is worth noting that the phase noise of this configuration does not change considerably for both the back-to-back and transmission over fiber. Even though the DFB ThorLabs laser system exhibits poor phase noise

performance compared to the NKT heterodyne laser system, its long-term stability is better compared to the latter. Figure 8.6 shows the statistical performance (Allan variance) of the clock generation schemes. The SMB 100A, reference signal, has superior long-term performance with an Allan variance of 1.88×10^{-11} at 1s averaging times. Although it possesses superior long-term stability, it exhibits random walk frequency noise for averaging times beyond 1000 s, a noise process which laser heterodyning does not possess.

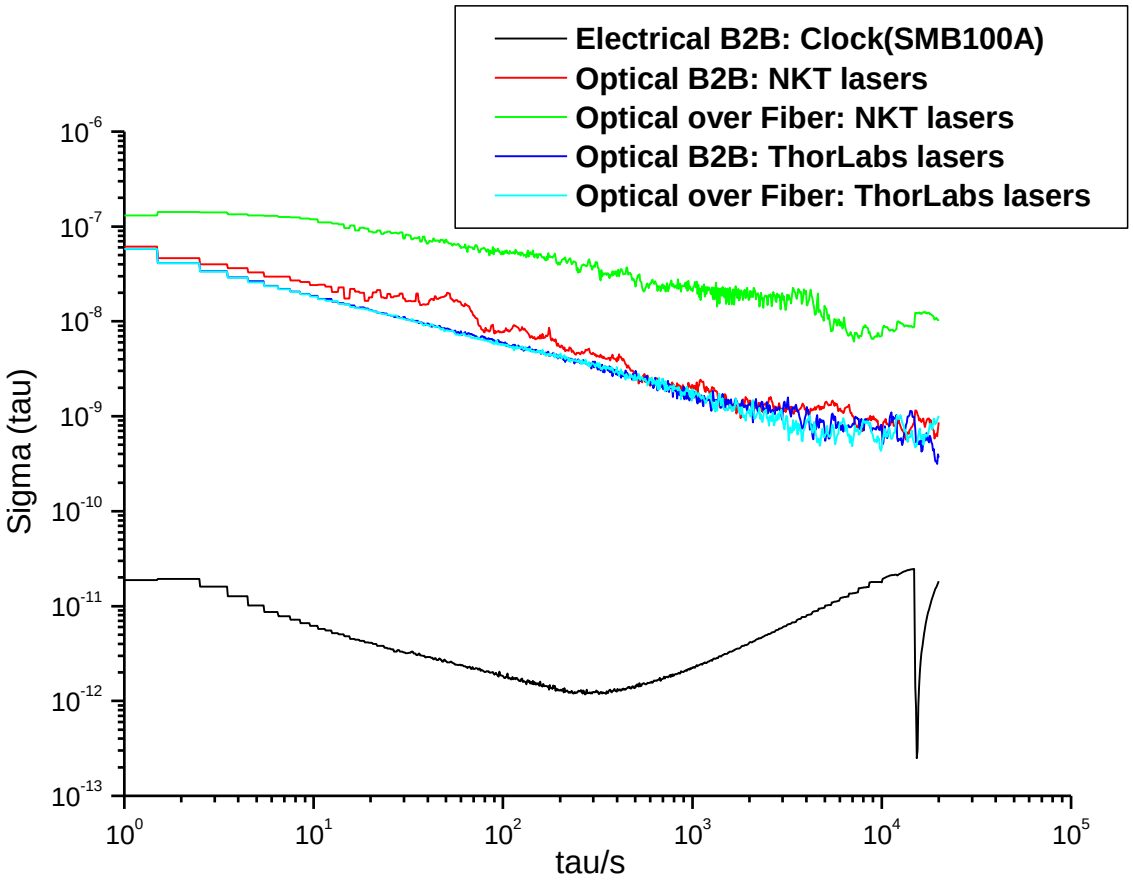

Fig. 8.6. Allan variance of a 4 GHz optical heterodyne clock.

Allan variance values of 5.83×10^{-8} and 5.82×10^{-8} for the back-to-back and transmission over fiber cases were attained at 1s averaging times, respectively for ThorLabs heterodyne configuration. For the heterodyne clock generation scheme using NKT fiber lasers, Allan variance values of 6.12×10^{-8} and 1.31×10^{-7} were attained for the back-back and transmission

over fiber cases, respectively at 1s averaging times. Introduction of the fiber in the clock generation scheme degraded long-term performance. The inherent nature of the fiber introduce noise which impacted on stability. However, the performance does not change significantly for the ThorLabs DFB lasers for all averaging times. In order to compare to the SMB 100A signal generator, the heterodyne systems need to be kept within acceptable frequency drift. This stabilization can be archived by using optical phase locked loops as well as using narrow band electrical filters to suppress generated harmonics.

8.4 Applications

Generation and dissemination of highly stable clock signals is important. However, different applications have different requirements. Clock stability requirements for the SKA telescope network are not the same as for a data center internal to an organization. Furthermore, some applications require a clock with low phase noise while others require high long-term stability. A radio detection and ranging (RADAR) and satellite tracking system (data, and control circuitry) are one of the applications which require low phase noise. In this case, the heterodyning scheme using NKT fiber lasers would be the ideal choice.

In NTP, the primary reference network clock requires a highly stable source in the 10^{-11} accuracy range while stratum 3 requires a clock stability of 3.7×10^{-7} /day (refer to figure 4.1 in chapter 4). Both the heterodyne methods are within stratum 3, 4 and 4E standards. Therefore, the heterodyne clocks can be used to drive digital switches, DAC's and SONET network elements (stratum 3 applications). In stratum 4, the clock is distributed in facilities and end user switching equipment like private branch automatic exchange (PBAX). Moreover, the clock is generated in the optical domain. Optical fiber is intensively being deployed to connect to organizational remote areas. Therefore, applications at stratum levels, 3-4E, located in remote areas can be driven easily by the heterodyne clock economically.

Summary

Generation of stable clock signals is wholly critical in today's digital era. In this chapter, we optically generated a 4 GHz clock signal using heterodyning technique. The frequency instability of the generated signal was determined using spectrum analyzer method. Furthermore, the instability of the system was compared with that of the electrical signal generator employing a rubidium oscillator as its input reference. The heterodyne system archived free running phase noise values of -123.50 dBc/Hz at 1 Hz with long term stability of 6.12×10^{-8} at 1s averaging times. The all optical system is compliant with stratum 3, 4 and 4E of NTP. Therefore, it can be used by networking devices requiring clocks meeting these stratum standards. In the next chapter, we experimentally demonstrate phase modulation and transmission of a 4 GHz electrical clock signal over optical fiber with the aim of recovering the signal with frequency stabilities near the non-transmitted clock.

Chapter 9

9.1 Introduction

Stable timing signals are increasingly becoming an integral part of the functionality of networks and applications. Requirements for such timing sources, oscillators, are also becoming more stringent as new technologies are being developed and deployed. 5G and the SKA project are examples of key technologies with such stringent requirements such that the timing standards set can only be met by atomic standards. In-order to reduce organizational cost, reference timing signals must be distributed from a local point to the end application with few penalties being encountered. Fiber optic technology offers the best possible medium for distribution of timing signals cheaply, especially to remote areas, with less penalties. Therefore, the same analogy for data transmission can be made for clock generation and distribution. In this chapter, we demonstrate two clock generation and dissemination techniques: intensity and phase modulation. The performance of these two systems is evaluated through determination of the frequency instability of the recovered clock signal.

9.2 Intensity modulation

9.2.1 Experimental procedure

Figure 9.1 depicts the set-up that was used to carry out the experiment. A 4 GHz sine wave was used to drive the Mach Zehnder modulator (MZM). The optical carrier from the fiber laser was set at 1550.1206 nm with output power corresponding to +13.14 dBm. The optical modulated signal was transmitted through NZDSF fiber with length and power loss corresponding to 26.6 km and 0.210 dB/km, respectively. The intensity modulated signal was directly detected using a 10 GHz bandwidth PIN photodiode. An electrical spectrum analyzer was then used to directly measure both phase noise and Allan variance of the generated recovered signal. For phase noise measurement, offset frequency range set on the analyzer was from 1 Hz to 100 MHz. On the analyzer, AM rejection mode was turned on for reliable measurement of phase noise. In measurement of Allan variance, the computer was interfaced to the spectrum analyzer. The Allan variance application from R&S was run on the interfaced computer. The frequency counter method was used. The measurement window was set to 5.5 hours.

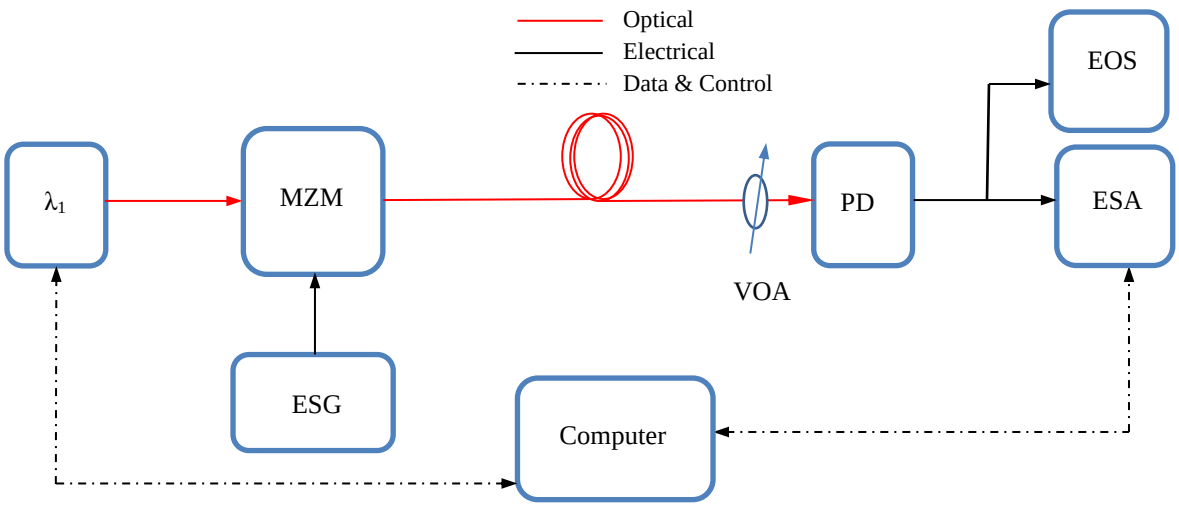

Fig. 9.1. Set-up scheme of a 4 GHz IM-DD signal. ESG: Electrical signal generator, MZM: Mach Zehnder modulator, VOA: Variable optical attenuator, PD: Photodiode, EOS: Electrical oscilloscope, ESA: Electrical spectrum analyzer.

9.3 Phase modulation

9.3.1 Experimental procedure

Figure 9.2 depicts the set-up that was used to carry out the experiment. A 4 GHz sine wave was used to drive the phase modulator (PM). The optical carrier from the fiber laser, λ_1, was set at 1550.1206 nm with output power corresponding to +13.14 dBm.

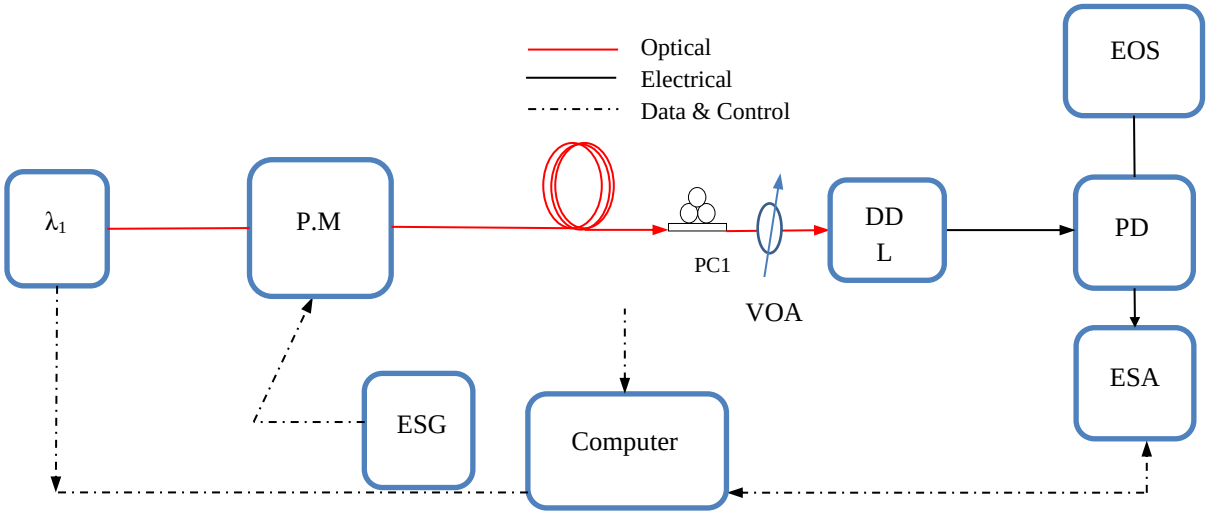

Fig. 9.2. Experimental set-up of a phase modulated 4 GHz clock signal. PC: Polarization controller, PM: Phase modulator, DDL: Differential delay line.

The optical modulated signal was transmitted through NZDSF fiber with length and power loss corresponding to 26.6 km and 0.210 dB/km, respectively. An interferometric technique was used for recovery of the phase modulated signal. An optical differential delay line was used, with interference between the two internal arms effecting phase to intensity conversion. The differential delay time was set to 74.6 ps. For best performance, a polarization controller, PC1, was installed just before the differential delay line to align the random states of polarization from the fiber midway between the polarization axes of the differential delay line. This maximizes interference at the output of the delay line for optimum phase to intensity conversion. For frequency stability measurements, the same specifications used for determining the stability of the intensity modulated signal where employed.

9.4 Results and analyses

The optical spectrum of the two modulation formats used in transmission of the clock are shown in figure 9.3 below.

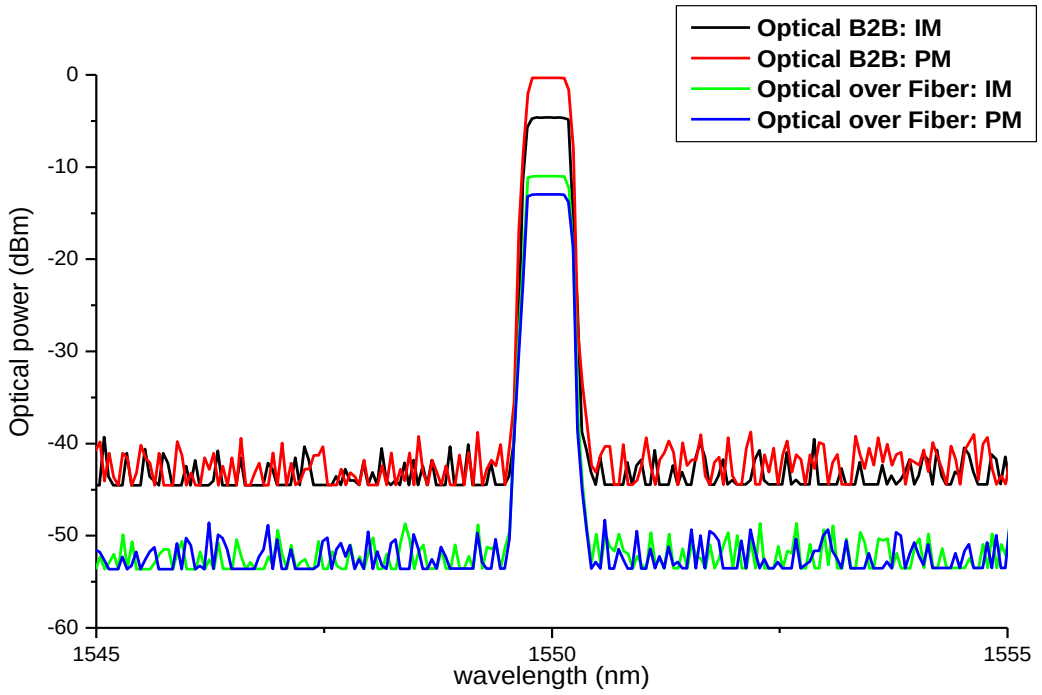

Fig. 9.3. Optical spectrum of modulation techniques. IM: Intensity modulation. PM: Phase modulation.

The two modulation formats, IM, and PM occupy the same bandwidth for both back-to-back and transmission over optical fiber. However, both modulation formats incurred optical power drops during transmission over fiber with the phase modulated signal experiencing significant 12.44 dB attenuation compared to 6.81 dB loss for the intensity modulated clock. The detected electrical clock spectrum is depicted in figure 9.4. The recovered electrical signals have the same spectral linewidth relative to the electrical signal generator (SMB 100A). The intensity modulated signal exhibits higher electrical power, 2.19 dBm for the back-to-back case compared to -9.95 dBm of the electrical signal generator. Moreover, the detected intensity modulated signal over fiber has an electrical power, -10.72 dBm, approximately equivalent to the SMB 100A. The phase modulated signals illustrated least electrical powers of -27.87 dBm back-to-back and -43.22 dBm for transmission over fiber.

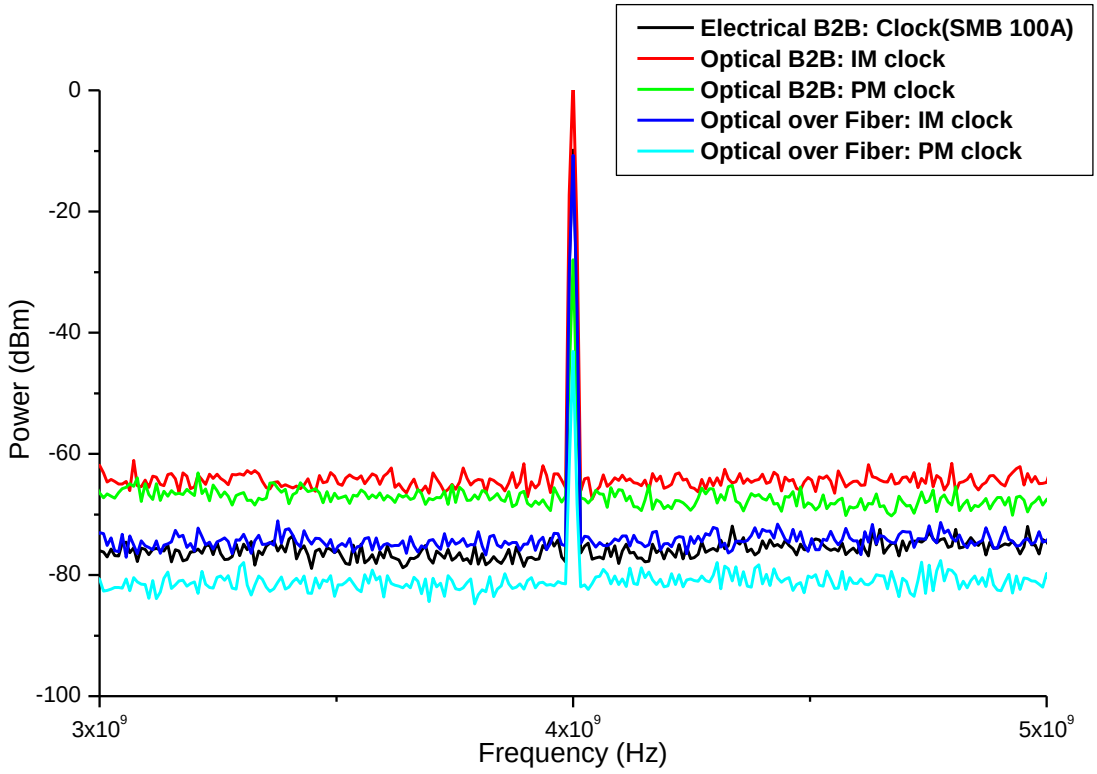

Fig. 9.4. Electrical spectrum of recovered 4 GHz clock signals.

The low electrical power and high noise floor of the recovered phase modulated signals significantly degrades performance. This is evident in the detected electrical wave as shown in figure 9.5. The signals contain significant amplitude noise especially for transmission over fiber. This is mainly due to the insufficient delay time when translating the signal from phase to intensity using the differential delay line (DDL).

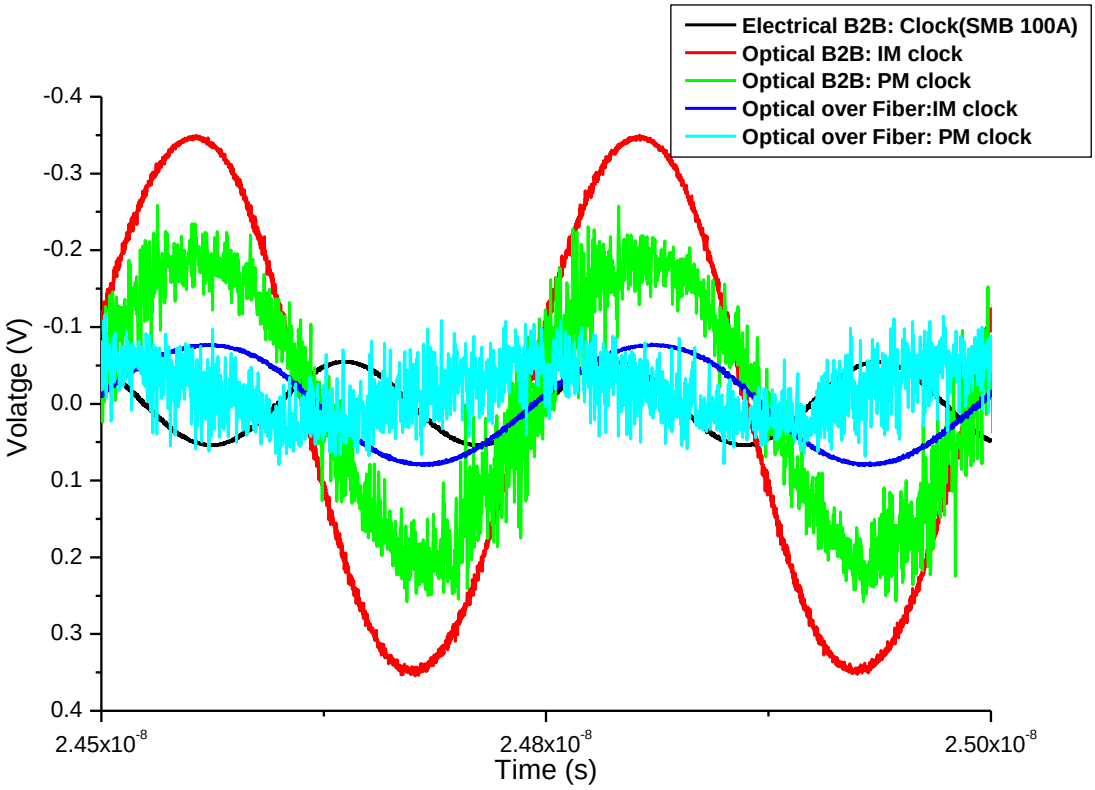

Fig. 9.5. Electrical waves of recovered 4 GHz clock signals.

At 4 GHz, the period is 250 ps. The deferential delay time set on the delay line was 74.6 ps, the maximum delay time for the instrument. Therefore, interference at the output of the DDL was not optimum for phase to intensity translation. Figure 9.6 shows the short-term stability of the recovered clock for the two modulation formats. The intensity modulated clock exhibits a phase noise trend which follows that of the reference, SMB 100A, for both back-to-back and transmission over fiber. Single sideband (SSB) phase noise values of -42.83 and -106.17 dBc/Hz were attained for the recovered back-to-back intensity modulated clock at 1 Hz and 1 kHz

frequency offsets, respectively. These values are approximately the same for the electrical signal generator. Transmission over fiber using this modulated format introduced a penalty of 2.12 and 2.57 dBc/Hz at 1 Hz and 1 kHz frequency offsets, respectively. The recovered back-to-back phase modulated clock indicates good phase noise performance which follows that of the signal generator for frequency offsets less than 100 kHz. SSB phase noise values of -42.59 and -104.40 dBc/Hz were attained at 1 Hz and 1 kHz frequency offsets, respectively.

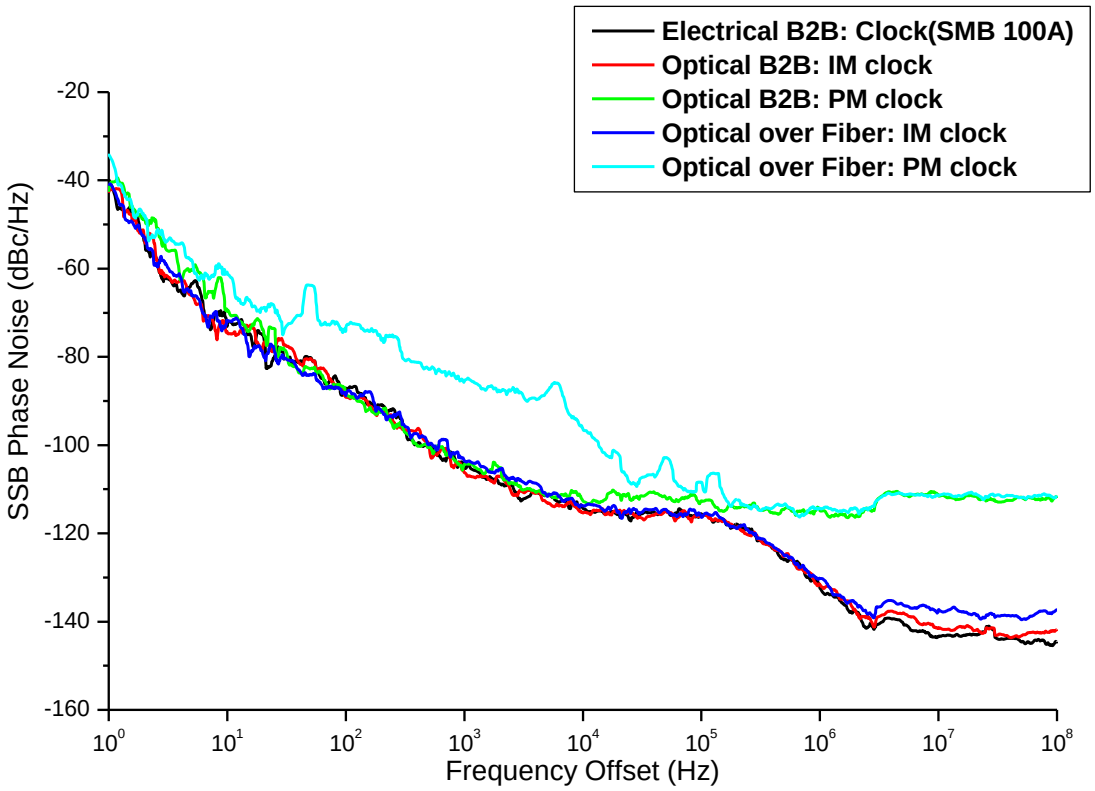

Fig. 9.6. Phase Noise of recovered modulated 4 GHz clock signals.

Transmission of the phase modulated clock over optical fiber introduced a penalty of 8.64 and 18.97 dBc/Hz at 1 Hz and 1 kHz frequency offsets, respectively. Moreover, the recovered phase modulated clock exhibits a lot of broadband noise for both back-to-back and transmission over fiber. Noise floor in the vicinity of -116 dBc/Hz was attained for the PM clock compared to -143 dBc/Hz of the signal generator. The high broadband noise degrades the long-term performance as shown in figure 9.7. The back-to-back intensity modulated clock has superior long-term

performance with Allan variances of 1.87×10^{-11} and 1.77×10^{-12} at 1 and 100 second averaging times, respectively. The SMB 100A clock attained variances of 1.89×10^{-11} and 1.89×10^{-12} at 1 and 100 second averaging time, respectively. Introduction of optical fiber for the phase modulated clock degraded stability. Stability penalties, with respect to back-to-back IM, of 0.21×10^{-11} and 0.11×10^{-12} were attained for 1 and 100 second averaging times, respectively.

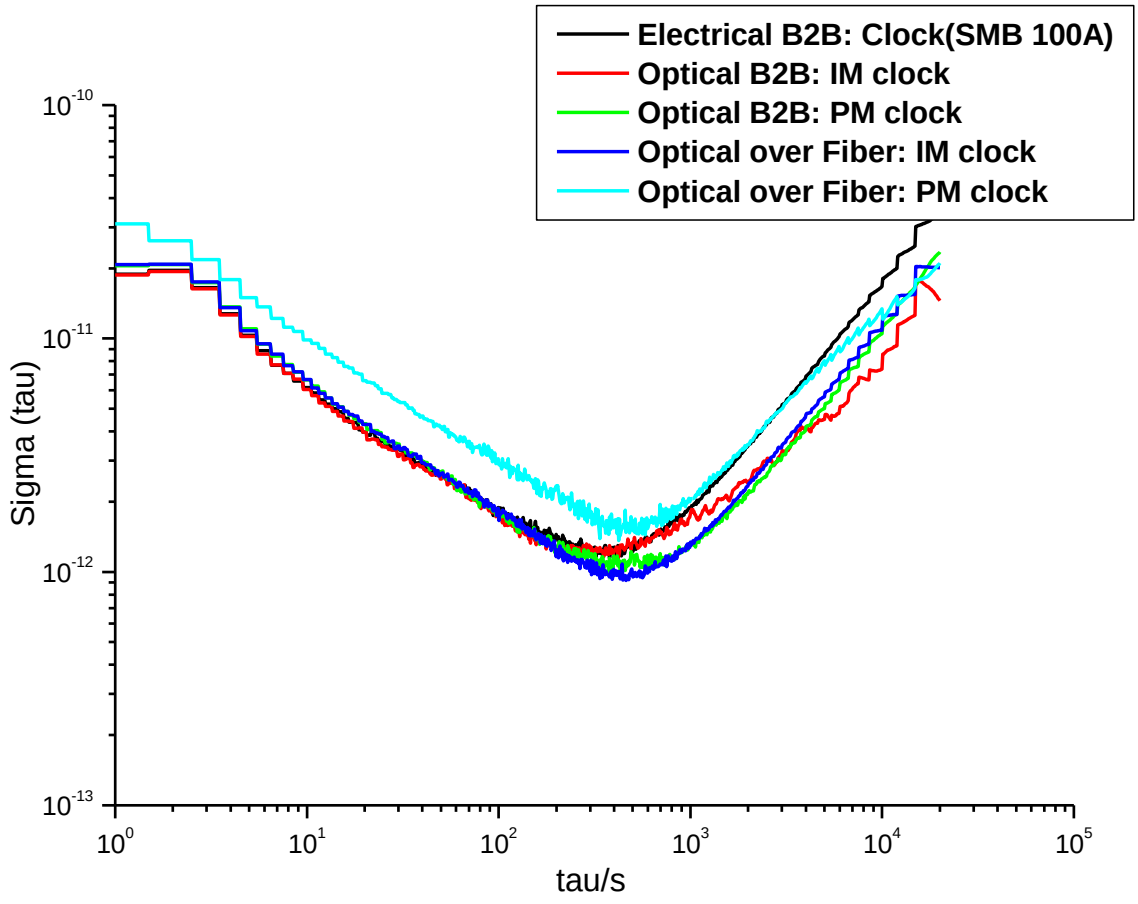

Fig. 9.7. Allan variance of recovered clock signals.

The recovered back-to-back phase modulated clock attained Allan variance values of 2.05×10^{-11} and 1.86×10^{-12} at 1 and 100 second averaging times, respectively. The stability of the recovered transmitted clock over optical fiber is significantly was significantly degraded for this scheme. Allan variance values of 3.09×10^{-11} and 3.06×10^{-12} were attained at 1 and 100 second averaging times, respectively. Recovered clock signals for both modulation formats portray random walk

frequency noise for averaging times greater than 1 ks. This noise is translated as a consequence of the electrical signal generator. Significant reduction of this noise process can be archived by operating the source (SMB 100A) in a temperature-controlled environment.

The clock generation and distribution schemes of intensity and phase modulation achieved phase noise and Allan variance performances in the vicinity of the reference clock (SMB 100A) for both back-to-back and transmission over optical fiber. Allan variance values in the range of 10^{-11} were attained. These values are within the boundaries of stratum 3, 3E, 4E and 4 (refer to figure 4.1 in chapter 4). Therefore, applications in these levels can readily be provided with generated intensity or phase clock signals. Furthermore, it is worth noting that the generated clocks follow the stability trend of the electrical signal generator (SMB 100A). Therefore, for applications and networks with stringent requirements such as 5G, operational costs would be greatly reduced by employing these techniques especially in local organizational networks such as learning in learning institutions.

Summary

Stable clock tones are important in digital communications. Therefore, when clock signals are distributed to end devices, they must have stability performance close to that of the source. In this chapter, we experimentally demonstrated optical transmission of a 4 GHz clock signal. Two modulation techniques where used: intensity and phase. The frequency stability of the recovered clock signals was measured. Single sideband phase noise values of -42.83 and -106.17 dBc/Hz were attained for the recovered back-to-back intensity modulated clock at 1 Hz and 1 kHz frequency offsets, respectively. Furthermore, Allan variance values in the vicinity of 10^{-11} were attained for 1 second averaging times for both modulation schemes. These attained values are close to those of the electrical signal generator (SMB 100A) hence representing few encountered transmission penalties for recovered clock signals.

Chapter 10

10.1 Introduction

Deployed fiber networks carry millions of organizational data across the world. As it has been the case before, legacy communication technologies have been subject to hacking and manipulation and fiber optics bears no exception. Despite fiber optic networks inherently being more secure than copper and radio wireless networks, it is vulnerable to hackers using easily obtained commercial hardware and software [1-5]. The purpose of this chapter is to experimentally implement optical fiber tapper technique in-order to determine the best C-band wavelength for implementation of continuous optical physical layer security. Currently, security in the form of encryption is implemented on layer 3 or above in the OSI (Open system interconnection) model. There are two forms of encryption, link layer and end-end encryption. Link layer encryption is applied at layers 1 and 2 while implementation of end-end encryption is at or above layer 3 of the OSI model [2]. At the receiver, an encryption key is used for decryption of the encrypted information. In optical networking, the physical layer is normally disregarded as being an area for data theft and service disruption. Transmitted data is encoded and therefore gaining access to this information is regarded as non-threatening since the data appears to be unreadable. However, information can be stored and with time the encryption key determined by using commercially available software. Therefore, hackers need only access to the fiber to obtain information for processing on or offline. This can be archived using different eavesdropping methods such as optical splitting, bending and evanescent coupling. Figure 10.1 shows these techniques.

Optical splitting involves installing an optical splitter to direct some percentage of the signal to the intruder's end point [1-3]. The target fiber is cut, and both ends are spliced to the splitter. Therefore, there is a brief interruption of service hence making this type of attack detectable by most systems. However, when the downtime is very short, many network operators will attribute this disturbance as a network glitch hence continue data transit. A much more effective eavesdropping method which does not impose network downtime is the use of a fiber tapper. This technique involves stripping the fiber down to the gladding and bending it to compromise its total internal reflection [1, 2]. A small fraction of the optical signal is coupled out of the fiber. The total power tapped depends on the bend radius. The strength of the tapped optical signal can be adjusted such that the received signal power at the legitimate receiver is within the transmission power budget thus making this method difficult to detect.

Evanescent coupling is similar to optical splitting technique although it does not require the target fiber to be cut. The target and capture fiber claddings are polished very close to the core there reducing the reflectivity of the core cladding boundary allowing for a portion of light to be captured by the tap fiber. While this approach seems to have a significant advantage over splitting method, it is difficult to implement and results in noticeable optical loss, approximately 1-2 dB [1].

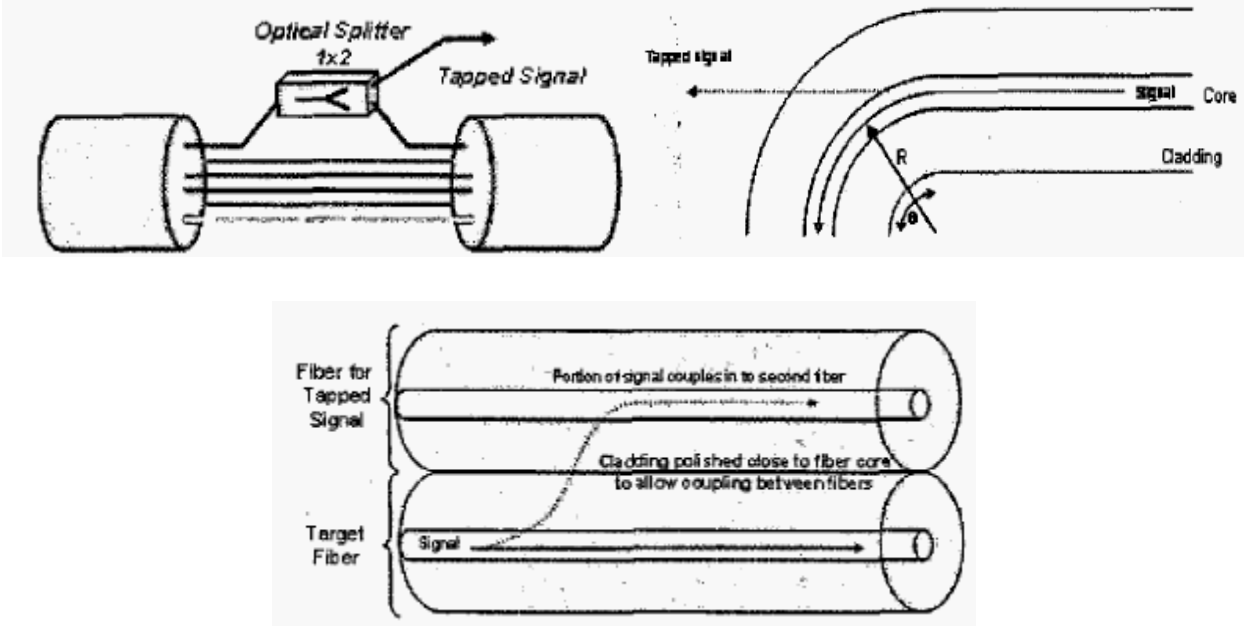

Fig. 10.1. Fiber eavesdropping techniques [1]. Top right: Optical splitter method. Top left: Bending technique. Bottom: Evanescent coupling.

Continuous monitoring of the physical layer for attacks is critical more especially in networks which carry sensitive information. Monitoring enables the intelligent network to reroute data to a safe link.

This chapter is organized as follows: The setup used in the experiment is explained in section 10.2. Section 10.3 presents the wavelength performance of the system and detailed analysis of the tapping scheme. The suitable wavelength which shows greater response is identified for fiber optic physical layer monitoring applications.

10.2 Experimental procedure

The set up used for the experiment is shown figure 10.2 below. The wavelength of the DFB laser source, $\lambda_{0\text{-}n,}$ was tuned to frequencies in the C-band at +10 dBm. The C-band was chosen since this is the most used band in optical telecommunication networks. A 1.65 km long bare NZDSF fiber with 0.20dB/km loss was used to emulate the tapped transmission medium.

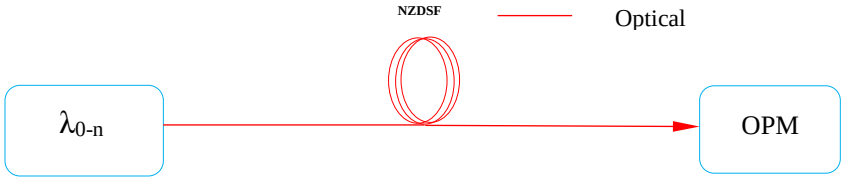

Fig. 10.2. Fiber tapping through bending. OPM: Optical power meter.

The optical fiber was bent such that it creates a circle with some distinct radius. An optical power meter was used to measure the power loss endured for corresponding set wavelength. This procedure was repeated for various wavelengths and circle radiuses.

10.3 Results and Analysis

The effect of fiber tapping on the received optical power for various wavelengths is presented in figure 10.3. The results show that different wavelengths experience different attenuation for the same bend radius. 1551.524 nm experiences more attenuation compared to the other wavelengths at 80 mm to 30 mm bend radiuses. 1551.918 nm wavelength is the least attenuated for radiuses greater than 30 mm. However, this wavelength experiences exponential 2.28 dB drop in optical power between 30 mm and 10 mm bend radiuses. Therefore, when information is transmitted at this wavelength, data can easily be accumulated by an intruder. However, for the service provider, this wavelength serves as an ideal channel candidate for continuous monitoring of tapping since it experiences significant and rapid power loss at bend radiuses associated with information being coupled out of the fiber. Moreover, tapping of information can be detected by monitoring the power ratio between the least and greatly attenuated wavelengths. When the power ratio between two wavelengths drops below an expected threshold, the network management system can be triggered to shut down the fiber optic link or re-direct traffic to a different safe link hence mitigating against information theft. In this case, these two wavelengths are 1551.524 nm and 1551.918 nm with an average power ratio of 1.20 between 30 mm and 80

mm bend radiuses. The power ratio of these wavelengths greatly changes for the 10 mm and 30 mm window.

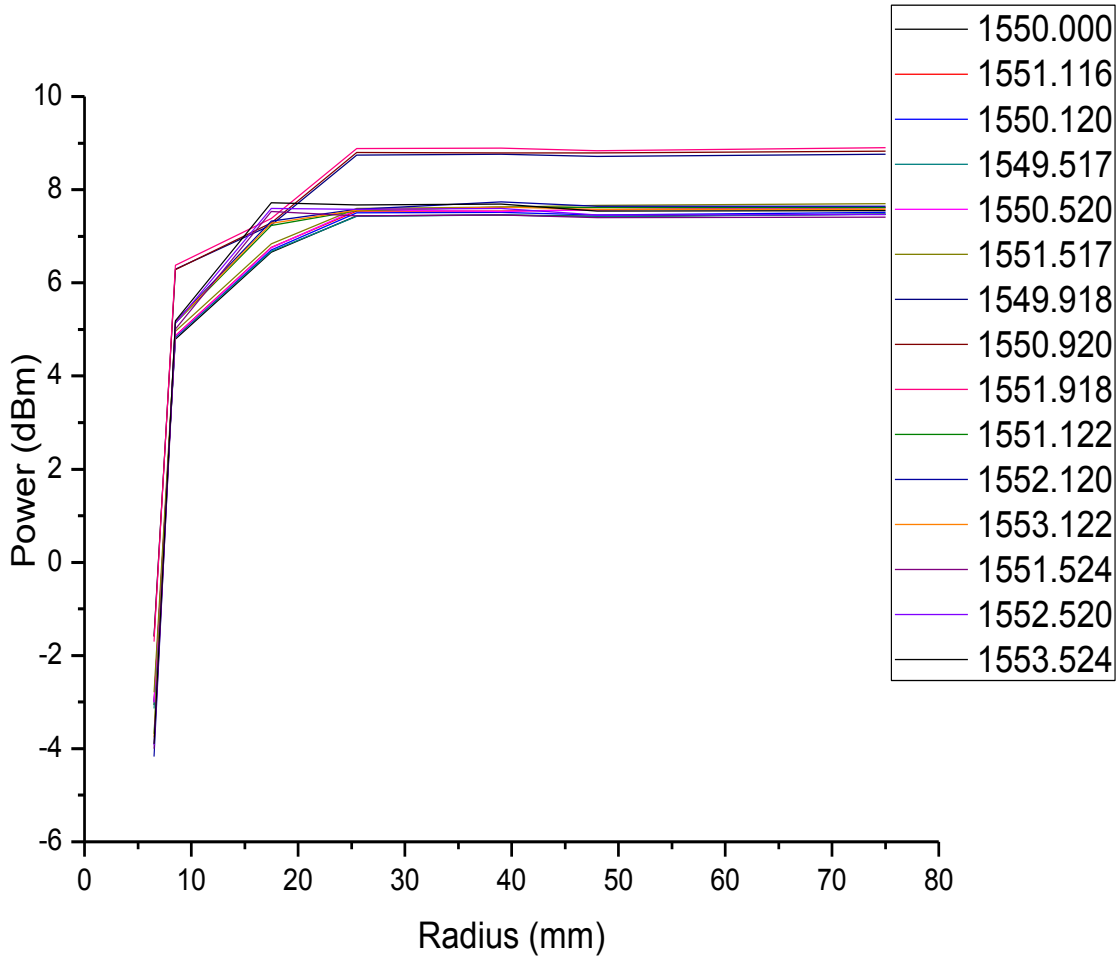

Fig. 10.3. Bend radius against received power for C-band frequencies.

Even though encryption of information is significant in networks, the encryption key and network protocol can be determined with time by intruders by using commercially available software and hardware. Encryption as a security measure does not prevent a hacker from gathering information transmitted in the network. Therefore, continuous automated monitoring of the network is essential to detect and prevent unauthorized access of client information. By demonstrating the fiber tapping scheme, we have shown that physical optical hacking can be detected by simply monitoring receiver end power for channels which are greatly affected by tapping using a power ratio. In our case, for the C-band, these wavelengths are at 1551.918 nm

and 1551.524 nm. For an automated intelligent system, these channels need not carry client information but can be dedicated for the network monitoring system.

Summary

Implementation of security is essential in all layers of the OSI model. Physical layer security has not received much attention due to the use of data encryption and misconception that optical fiber is inherently safe from being tapped as compared to copper. In this chapter, we have successfully demonstrated tapping principle as well as the wavelength dependence of the system. The most suitable wavelengths for physical layer security monitoring purposes with regards to the C-band where identified. These wavelengths are 1551.918 nm and 1551.524 nm.

References

[1] K. Shaneman and S. Gray, "Optical network security: technical analysis of fiber tapping mechanisms and methods for detection & prevention," *IEEE MILCOM 2004. Military Communications Conference, 2004.*, Monterey, CA, USA, 2004, pp. 711-716 Vol. 2, doi: 10.1109/MILCOM.2004.1494884.

[2] Z. Banjac, V. Orlic, M. Peric and S. Milićević, "Securing data on fiber optic transmission lines," *2012 20th Telecommunications Forum (TELFOR)*, Belgrade, 2012, pp. 935-938, doi: 10.1109/TELFOR.2012.6419362.

[3] H. Si, H. Liu and H. Ma, "Optical Fiber Communication Network Eavesdropping and Defensive Measures," in *Advances in Social Science, Education and Humanities Research*, vol. 130, 2018.

[4] B. Wu and E. Narimanov, "Secure communications over a public fiber-optical network," *2006 Conference on Lasers and Electro-Optics and 2006 Quantum Electronics and Laser Science Conference*, Long Beach, CA, 2006, pp. 1-2, doi: 10.1109/CLEO.2006.4628537.

[5] F. Qian, Y. Ye, Y. Zhuang and Y. Shi, "Research on Security Threats and Protection Strategies of Optical Fiber Communication," *2019 International Conference on Robots & Intelligent System (ICRIS)*, Haikou, China, 2019, pp. 168-170, doi: 10.1109/ICRIS.2019.00051.

Chapter 11

11.1 Introduction

Fifth generation technology (5G) is the pinnacle of the impact communication change can bear on innovation. With its expected high data rate, low network energy consumption, tremendous bandwidth, and low round trip time (RTT) latency, the scope of application of this technology broadens from mobile communication to other implementations [1]. End user applications such as autonomous vehicles, augmented and virtual reality, IoT, robotics & artificial intelligence, remote patient monitoring etc. can now be fully supported. For realization of these communication-based technologies through 5G, fiber optics serves as the backbone of the network architecture providing high speed node to node connectivity to the application edge router. 4G has a data rate of 100-200 Mbps while the expected data rate for 5G is 10-50 Gbps [2]. Typically, a bit error rate of 10^{-9} is acceptable for telecommunication applications [3]. The acceptable BER when forward error correction (FEC) is applied is typically between 10^{-3} to 10^{-2} when overheads of 7% to 21.5% are used [4]. In modern networks, keeping latency as low as possible is desirable. Low latency in the path taken by packets implies shortest path therefore high-end user experience. For optical fiber, the latency is 5 μsec per kilometer [5]. For LTE, the average latency is around 50 ms [1]. Keeping latency below one millisecond is one of the key features of 5G systems. This is crucial for applications such as online gaming, self-driving cars as well as industrial automation which require split second response. In this chapter, we present a new affordable way of continuous tracking of data latency for 5G specifications. The method used is all-optical, can accurately track latency of <1 ms and is spectrally efficient. Furthermore, our approach is far more efficient and ubiquitous than traditional ping method since it is directly and transparently implemented in the physical layer. The experiment and results presented in this chapter are part of the journal publication made in Optical society of America (OSA) [6].

The organization of this chapter is as follows: Section 11.2 explains the setup which was used for the experiment. The main results with corresponding discussions are presented in section 11.3.

11.2 Experimental set-up

Figure 11.1 depicts the system design which was used to conduct the experiment. Pseudo random binary sequence with word length equivalent to 7 bits from the pattern generator at 10 Gbps bit rate and a 20 MHz sine wave form the electrical signal generator were used as electrical inputs to the Mach-Zehnder and phase modulators, respectively. The 20 MHz sine wave is the clock signal introduced for monitoring latency in a 5G network. By recovering the phase of the clock at the receiver, system latency can be tracked. A clock frequency of 20 MHz was chosen for high resolution latency monitoring. The corresponding period of the clock is 50 ns with 20 000 cycles in a 1ms latency window. This is suitable for monitoring latency down to the nanosecond timescale.

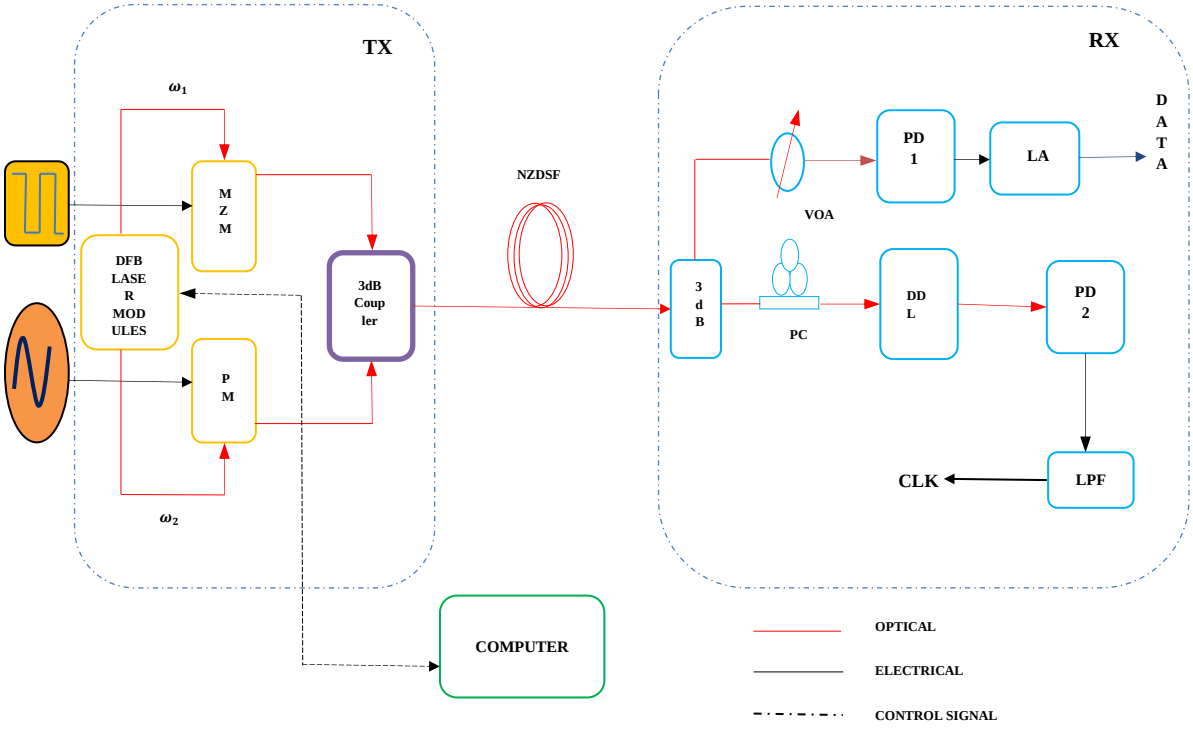

Fig. 11.1. Proposed flexible intensity/phase data latency tracking transmitter. PD: Photodiode. DDL: Differential delay line. PC: Polarization controller. LPF: Low pass filter. LA: Linear amplifier.

The wavelength spacing between the two optical carriers, ω_1 and ω_2, was kept at 0.0987 nm, with each having power corresponding to +13.14 dBm. The wavelength for the intensity modulated channel was 1550.2207 nm while that of the phase modulated channel was 1550.1220

nm. The two modulated signals were coupled into the Non-Zero-Dispersion-Shifted-Fiber (NZDSF) with length and power loss corresponding to 26.6 km and 0.210 dB/km, respectively. The operating wavelength is around 1550 nm, so NZDSF is used to manage chromatic dispersion. Heterodyne beating of the two wavelengths creates a 5G carrier of 12.3 GHz. The clock is included in a spectrally efficient manner since both wavelengths are required to create the 5G data carrier.

The intensity modulated signal was directly detected by a 10 GHz bandwidth PIN photodiode. Due to the bandwidth of the photodiode, the generated heterodyne 5G carrier is effectively filtered. For quantification of quality and integrity of received data, bit error rate and eye diagram measurements were conducted for various optical output powers. This was achieved by using variable optical attenuator, VOA.

An interferometric technique was used for recovery of the phase modulated signal. An optical differential delay line was used, with interference between the two internal arms effecting phase to intensity conversion. The differential delay time was set to 74.6 ps. For best performance, a polarization controller was installed just before the differential delay line to align the random states of polarization from the fiber midway between the polarization axes of the differential delay line. This maximizes interference at the output of the delay line for optimum phase to intensity conversion. The short-term instability of the recovered 20 MHz radio frequency clock signal was then analyzed directly using an electrical spectrum analyzer.

11.3 Results and analysis

The electrical spectrum profile of the recovered clock signals is presented in figure 11.2. The spectral shape of the recovered phase modulated clock co-propagating with intensity modulated data matches that of the reference signal (SMB 100A) for both back-to-back and transmission over optical fiber. However, for the back-to-back phase modulated clock with intensity modulated data, harmonics with maximum power of -52 dBm are generated. These are a result of beating of the two carrier wavelengths at the photodiode. For transmission through fiber, the PM clock with IM data signal experiences attenuation. Power associated with the fundamental frequency was -32.24 dBm, which is a 29.08 dBm penalty relative to the SMB 100A signal generator.

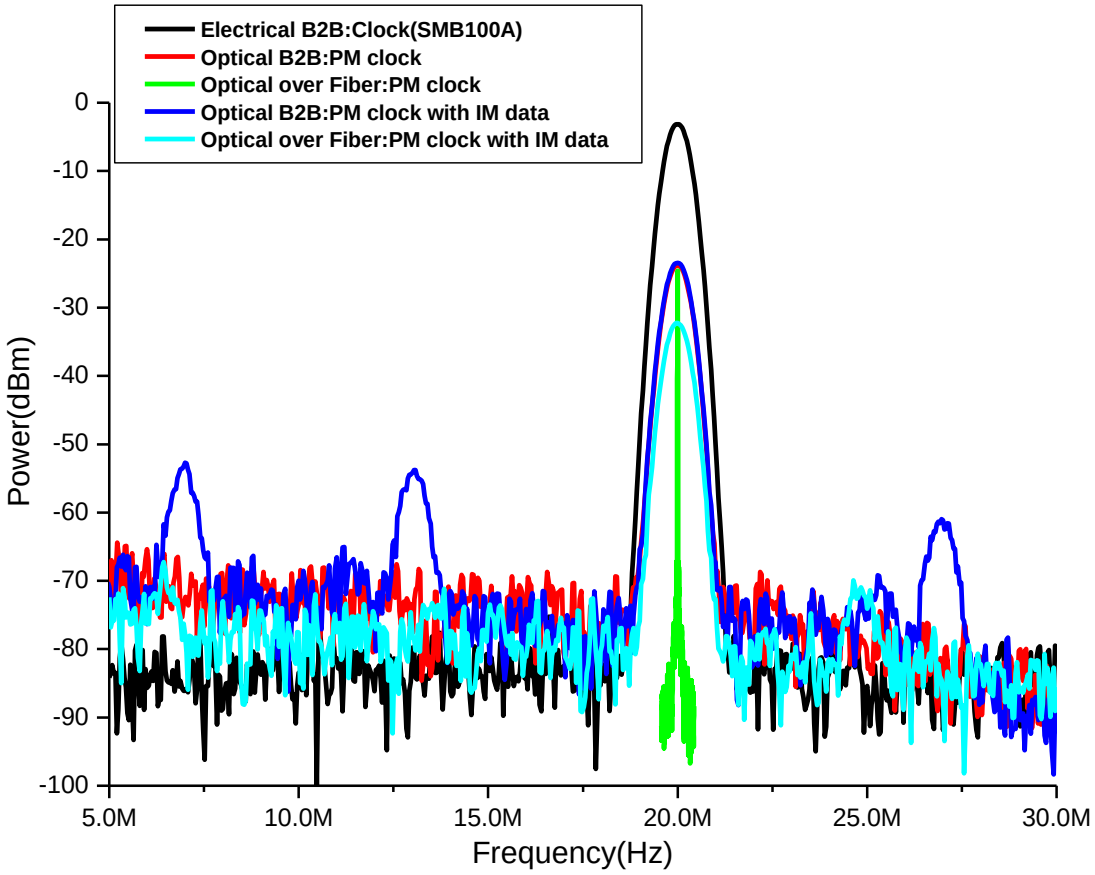

Fig. 11.2. Electrical spectrum of recovered 20 MHz sine wave. IM: Intensity-modulated. PM: Phase-modulated.

However, the noise floor of the phase modulated clock with intensity modulated data is higher compared to that of the signal generator for both back-to-back and transmission through fiber. The high noise floor figure translates to a lower signal to noise ratio hence degraded performance of the recovered clock. The recovered electrical waves of the phase modulated signal are shown in figure 11.3. The back-to-back phase modulated clock achieved peak-peak voltage of 60 mV. Introduction of the data carrying channel resulted in attenuation of the electrical signal. Peak-peak voltages of 24 mV and 17 mV where attained for phase modulated clock with intensity modulated data for back-to-back and transmission over fiber, respectively.

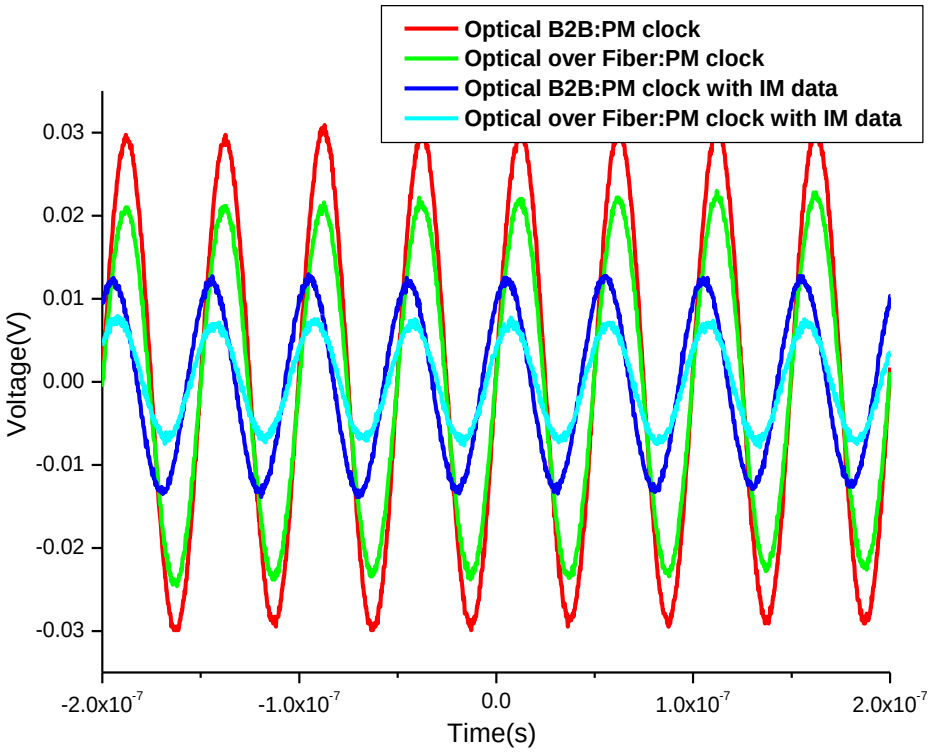

Fig. 11.3. Electrical waves of recovered 20 MHz sine wave.

The phase noise performance of the recovered clock signals is depicted in figure 11.4. The reference signal, SMB 100A clock, has the best performance. Phase noise values of -89.84 and -134.95 dBc/Hz where measured at 1 Hz and 1 kHz frequency offsets, respectively. For the back-to-back phase modulated clock, phase noise values of -57.74 and -112.99 dBc/Hz where attained at 1 Hz and 1 kHz frequency offsets, respectively. The phase noise performance of the PM clock with IM data is considerably degraded relative to the back-back phase modulated sine wave. This is due to interference from the data carrying channel as well as noise introduced by the fiber optic link. Single side band phase noise values of -40.55 and -77.84 dBc/Hz where attained for the recovered clock signal at 1 Hz and 1 kHz frequency offsets, respectively. These specifications are within stratum 3 oscillators used in network time protocol (NTP). Furthermore, for an offset frequency of 1 Hz, the corresponding phase noise value is only 20 dBc/Hz greater than that of an oven-controlled crystal oscillator.

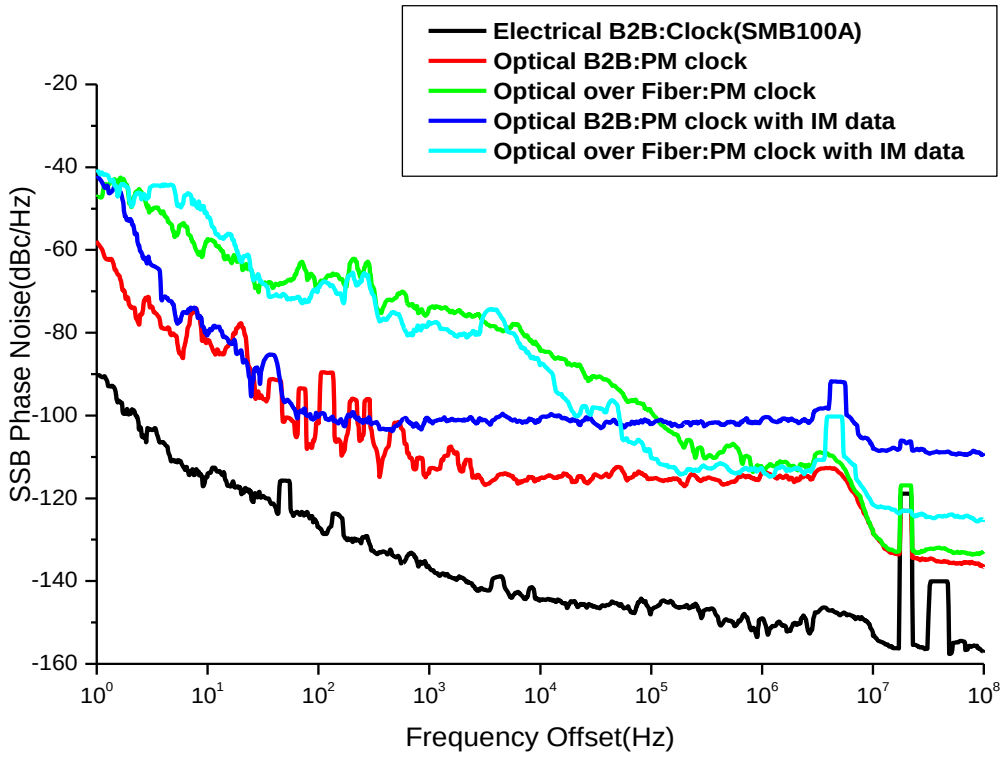

Fig. 11.4. Phase Noise of recovered 20 MHz clock signals.

The phase noise values at 1 Hz and 1 kHz frequency offsets corresponded to a penalty of 17.19 and 35.15 dBc/Hz respectively for back-back case. The recovered clock is stable since its phase noise reduces considerably with frequency offset. Figure 11.5 and 11.6 present the eye diagrams and BER measurements for the 10 Gbps intensity modulated signal, both with and without the 20 MHz clock along the fiber. The extinction ratio for the recovered bits is 4.86 dB. The signal quality is only degraded by 1.55 dB when the phase modulated channel is introduced. For transmission over 26.6 km of single mode fiber, the performance is somewhat more degraded, but within the acceptable 10^{-2} FEC limit. This is due to cross talk triggered by narrow spacing between the two co-propagating channels. However, the output peak-peak voltage is greatly improved by a factor of 10 when the phase modulated channel is introduced in the transmission system. This is caused by beating between the two signals at the photodiode.

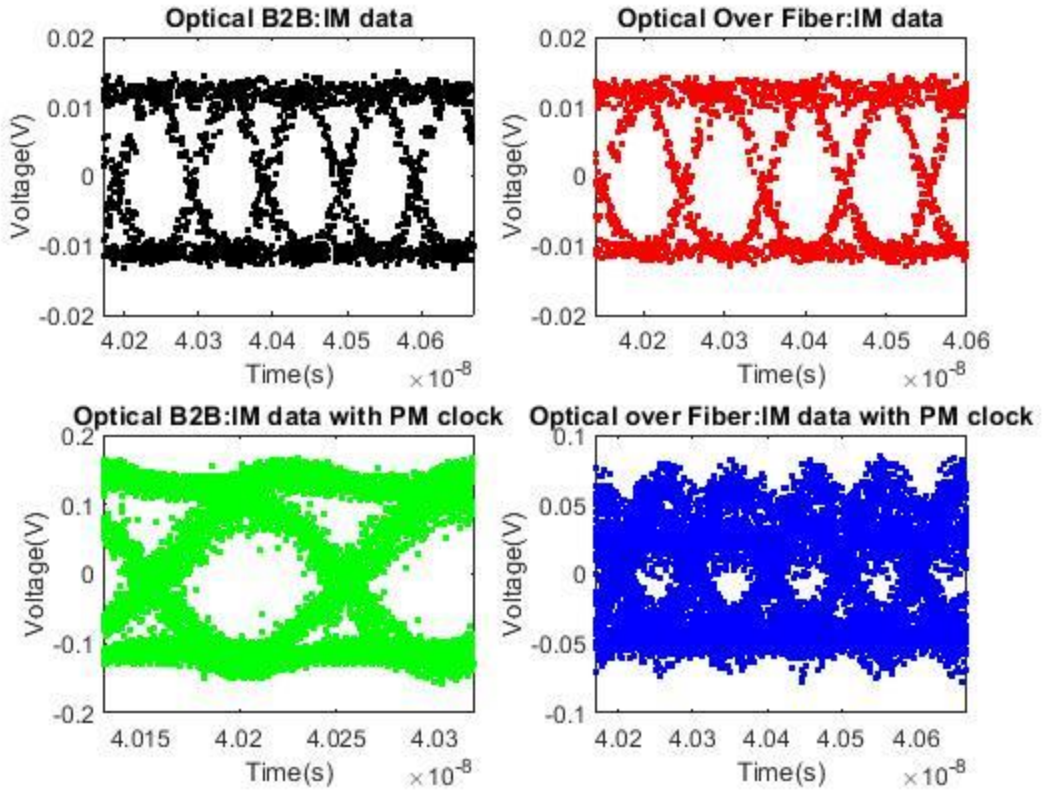

Fig. 11.5. Eye diagrams of received data.

For bit error rate of 10^{-9}, back-back intensity modulated data required optical input power of -17.67 dBm. To achieve the same bit error rate for 'Optical B2B: IM data with PM clock' transmission system, an optical power of -16.12 dBm is required. This represents a power penalty of 1.55 dB. Receiver sensitivity associated with co-propagation of the two channels through fiber for bit error rate of 10^{-1} is notably degraded, compared with the back-back case. The power penalty is 12.05 dB. The eye for 'Optical over Fiber: IM data with PM clock' is not completely closed with BER around 10^{-2} achievable. Therefore, 5G data transmission at 10 Gbps over fiber, including the 20 MHz clock is successfully realized through FEC. Moreover, bit error rate performance of the 'Optical over Fiber: IM data with PM clock' system can be greatly improved by reducing the length of the fiber optic link from 26.6 km to within metro network specifications of 20 km.

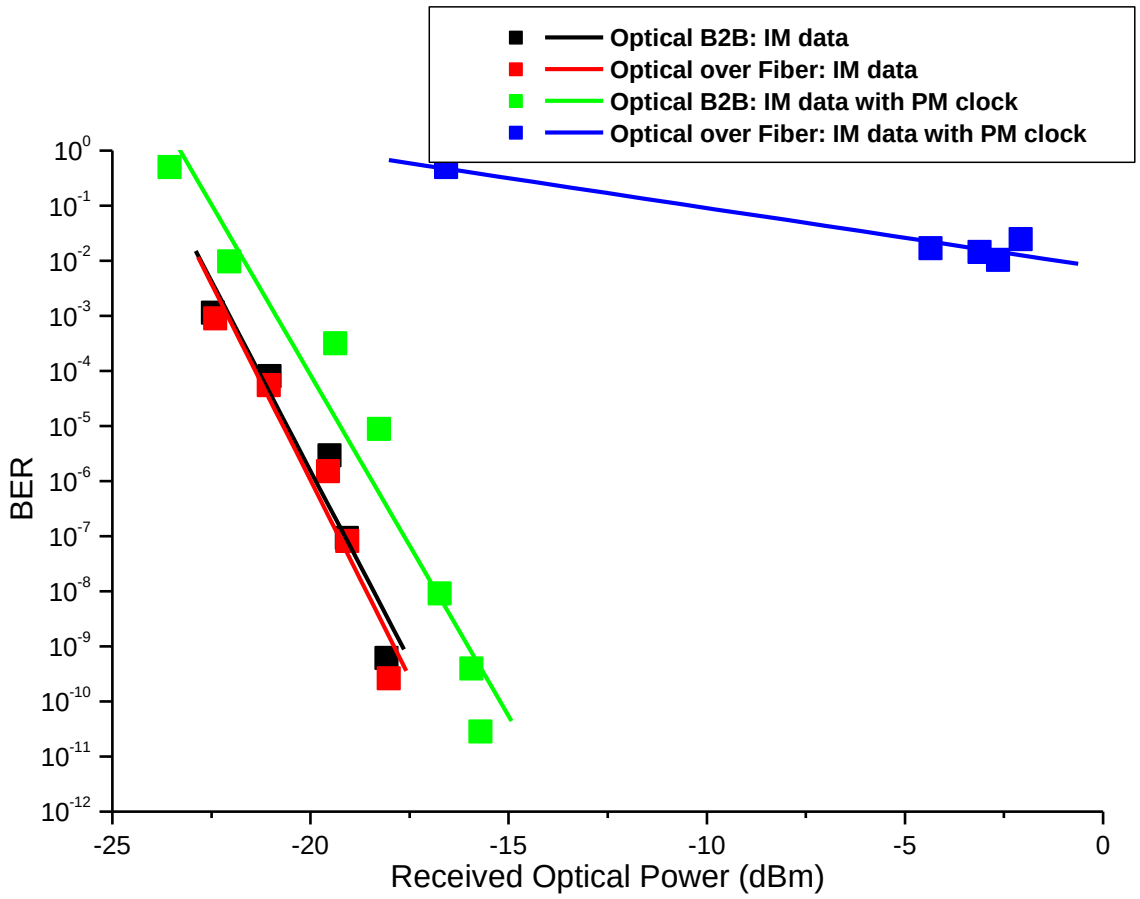

Fig. 11.6. Bit error rate of recovered intensity modulated data.

The clock is delivered over the front-haul network to, e.g., the wireless antenna stations. At this point, the wireless signal could be time stamped before distribution. Accurate time stamps (derived from our optical clock system) can be latched to the individual carrier data channels. For example, switches allow for timestamping of individual packets. This is useful in identifying congestion spots. Further consideration is that the 5G cells are very small hence the wireless latency contribution is not as significant relative to the optical front-haul. The clock is ubiquitously and transparently implemented in the physical layer. The technique is spectrally efficient relative to a conventional 5G data system. Spectral efficiency is achieved by phase modulating the clock onto an already present heterodyne wavelength. Successful transmission of both data and clock was achieved over 26.6 km of NZDSF fiber, demonstrating the suitability of the approach for 5G access networks.

Summary

Continuous monitoring of network data latency is critical in modern networks. Networks such as 5G support high end applications which require information to be delivered at sub millisecond delays. Examples of these applications include self-driving cars, augmented reality, and robotic applications. In this chapter, we experimentally demonstrated a spectrally efficient data latency tracking technique. The method is all-optical, can accurately track <1 ms latency and is spectrally efficient. We experimentally demonstrate generation of a 10 Gbps intensity modulated data signal with 12.3 GHz carrier frequency, embedded with 20 MHz phase modulated clock. The signal is successfully transmitted over 26.6 km of NZDF single mode fiber at 1550 nm. Error free FEC data transmission was archived with 12.05 dB receiver penalty. Phase noise of -40.55 dBc/Hz and -77.84 dBc/Hz were attained at 1 Hz and 1 kHz offsets respectively for the clock.

References

[1] P. Prabesh and A. Bhattarai, “5G Telecommunication Technology: History, Overview, Requirements and Use Case Scenario in Context of Nepal,” 2018.

[2] A. Gupta and R. K. Jha, "A Survey of 5G Network: Architecture and Emerging Technologies," in *IEEE Access*, vol. 3, pp. 1206-1232, 2015.

[3] P. Palacharla, C.W. Barnard, P. Myslinski, J. Chrostowski, R. Neumann and R. Khalil, “Bit Error Rate Analysis of Optical Data Links for Computer Communications,” in Applications of Photonic Technology. G.A. Lampropoulos, J. Chrostowski, R.M. Measures, Eds. Boston: Springer, 1995, pp. 109-113.

[4] E. Säckinger, “Forward Error Correction,” in Analysis and Design of Transimpedance Amplifiers for Optical Receivers. John Wiley & Sons Inc, 2018, ch. G, pp. 477-478. https://onlinelibrary.wiley.com/doi/pdf/10.1002/9781119264422.app7.

[5] J. Coffey, “Latency in optical fiber systems,” 2017. https://www.commscope.com/globalassets/digizuite/2799-latency-in-optical-fiber-systems-wp-111432-en.pdf

[6] K. Nfanyana, S. Wassin, R. Karembera, J. Jena and T. Gibbon, ‘All-photonic 20-MHz clock for latency monitoring in a 5G network at 10 Gbps over optical fiber,’ in *journal of Optical Society of America B*, vol. 37, A202-A206, 2020.

Chapter 12

12.1 Conclusions

In this dissertation, we presented a comparative study between intensity modulation direct-detection scheme and coherent phase modulation. The comparative study was carried out for a bit rate of 10 Gbps through 26.6 km of NZDSF fiber. Coherent BPSK attained better bit error rate performance. At bit error rate of 10^{-9}, the IM-DD system attained receiver sensitives of -12.30 dBm and -10.90 dBm for back-to-back and transmission over fiber, respectively. Basing on the same bit error rate, the coherent BPSK system achieved 18.37 dB and 13.89 dB receiver sensitivity improvement for back-to-back and transmission over optical fiber, respectively. Moreover, equalization of transmission impairments is achievable in the digital domain. We showed equalization of PMD and residual CD by employing the LMS filter. The ability to equalize received information in the digital domain further improves the robustness of the transmission scheme. Therefore, network reach is tremendously improved when using coherent detection. This then makes it ideal for long and ultra-long transmission networks such as the SKA.

Furthermore, we also demonstrated three clock generation and distribution techniques as possible solutions for reference and clock signal distribution in the context of telescope networks. The first technique demonstrated was heterodyning of two lasers at the photodiode. The second technique involved using intensity modulation. Finally, phase modulation was employed to generate the radio frequency signal. All three techniques portrayed good long-term and short-term stability performance. Allan variances in the range of 10^{-10} where attained at 1 second averaging time. The good stability of the generation schemes enables applicability at stratum 3,3E and 4 in the NTP protocol.

Finally, a new all-photonic data latency tracking scheme applicable to 5G specifications was developed. The technique was incorporated in a spectrally efficient manner and was able to track data latency in optical fiber to the nano second scale at 10 Gbps bit rate. This techniques offers continuous tracking of data latency and is easily implemented in the physical layer. Therefore, 5G network re-optimization can be carried out easily with the aid of the data tracking clock.

12.2 Future work

Coherent detection and digital signal processing are fundamental in today's increasing networks and data traffic. With equalization of most transmission impairments achievable in the digital domain, network traffic can be increased by reducing the spacing between adjacent channels. Furthermore, network reach is incredibly improved. By reducing channel spacing, nonlinear effects such as XPM arise. Therefore, it is ideal for implementation of an algorithm which utilizes the NLSE equation for equalization of all impairments encountered in the channel. Therefore, our future work will be on implementing the digital backpropagation algorithm basing on the NLSE equation.

Publication Outputs

Research Outputs in journals, conferences, and other reports

A. Published journal articles
Year 2020:

1. **K. Nfanyana**, S. Wassin, R. Karembera, J. Jena, and T. Gibbon, "All-photonic 20-MHz clock for latency monitoring in a 5G network at 10 Gbps over optical fiber," in *Journal of Optical Society of America B*, vol. 37, issue 11, pp. A202-A206 (2020)
2. R. Karembera, S. Wassin, G. Issoe, **K. Nfanyana** and T. Gibbon, "All-optical flexible 5G signals generation and transmission for spectrum resources optimization," in *Journal of Optical Society of America B*, vol. 37, issue 11, pp. A324-A330 (2020).

B. Presented/published conference articles
Year 2019:

1. **K. Nfanyana**, S. Wassin and T. Gibbon, "Coherent Detection of Data and Timing Signals over Optical Fiber for Telecommunications," in *Southern African Telecommunication Networks and Applications Conference (SATNAC)*, 2019.

APPENDIX 1

Complex modulation formats in conjunction with coherent detection are conducive in signal processing due to the ability to recover full information of the received sent signal. Therefore, common optical fiber transmission impairments such as chromatic dispersion and time varying polarization mode dispersion can easily be equalized for. In this appendix, we present MATLAB script for equalization of PMD as well as calculation of bit error rate without the need for demodulating the signal through the use of error vector magnitude.

```
%%

%MATLAB code for:

%1.Computation of bit error rate

%2.Equalization of PMD using LMS algorithm

%By Ketshabile Nfanyana

%20 August 2020

%%

clc;

close all;

%% Input data

format longEng;

A = importdata('');


%Load the data, IQ signals

time = A(:,1); % time index

I = A(:,2); % In phase data
```

```
Q = A(:,3); % Out of phase data

L = length(time); %length of signal

M = I + j.*Q; %Complex signal

Z = abs(M);

Theta = (180/pi)*(angle(M));%Angle of data in degrees.

Fs = 2e9;% Sampling frequency

% Low pass filter design

pass1 = 1e6/Fs;

b = fir1(50,pass1,'low',chebwin(51,30));

freqz(b);

Mfiltered = filter(b,1,M);

Z2 = abs(Mfiltered); %Filtered signal

Theta2 = (180/pi)*(angle(Mfiltered)); %Angle of filtered signal

%%

%%Bit error rate calculation before equalization

%Instant in time when symbols are detected.

%computation does not include points between symbols.

idx_1 = 1:L;

amp = 0.01;

[pk,loc] = findpeaks(Z2, 'MinPeakHeight',amp,'MinPeakDistance',50);% locate the peaks for optimum signal sampling. Since signal BPSK, these peaks represent the bits.
```

```
for nk = 1:L2


I1 = cosd(Theta2(loc(nk)));

Q1 = sind(Theta2(loc(nk)));

I2(nk) = I1;

Q2(nk) = Q1;


end

%Desired signal

data = randi([0,1],1,L2);

d = pskmod(data,2,-0.90483); %BPSK signal


%Visualize the constellation

figure('Name','Constellation of sampled points','NumberTitle','off');

plot(I2,Q2,'ro');

hold on;

grid on;

plot(real(d),imag(d),'r+','MarkerSize',20);

ylabel('Imaginary');

xlabel('Real');

axis ([-2 2 -2 2]);
```

```
complex_signal = I2 + j.*Q2;


yyy = zeros(1,round(L2/2));

xxx = zeros(1,round(L2/2));


for aa = 1: L2


    if (real(complex_signal(aa))>=0) && (imag(complex_signal(aa))<0)

       xplane = complex_signal(aa);

       xxx(aa) = xplane;


    elseif (real(complex_signal(aa))<0) && (imag(complex_signal(aa))>0)

    yplane = complex_signal(aa);

    yyy(aa) = yplane;

    else

    end

end


%Extract nonzero data

xxxx = xxx(xxx~=0); %positive real, negative imaginary.
```

```
yyyy = yyy(yyy~=0);%negative real, positive imaginary


L3 = length(yyyy);


%EVM calculation for symbols corresponding to bit 0

for k = 1:L3

%ideal symbol locations

up = -617.819263283543e-003 + j*786.320137040748e-003;


Ierrup = real(up) - real(yyyy(k));  %deviation of in phase data from ideal location

Qerrup = imag(up) - imag(yyyy(k));  %deviation of out of phase data from ideal location


Ierrorup(k) = Ierrup;

Qerrorup(k) = Qerrup;

end

Ierror1up = Ierrorup.^2;

Qerror2up = Qerrorup.^2;


for g = 1:L3

    mag = Ierror1up(g) + Qerror2up(g);

    mag2(g) = mag;
```

```
end

mag3 = sum(mag2);

mag4 = mag3/L3;

mag5 = mag4^0.5; %Normalized to outer most state of constellation (EVM for symbols corresponding to bit zero).

%%

L4 = length(xxxx);


%EVM calculation for symbols corresponding to bit 1

for k1 = 1:L4

%ideal symbol locations

down = 617.819263283543e-003 - j*786.320137040748e-003;


Ierrdown = real(down) - real(xxxx(k1));  %deviation of in phase data from ideal location

Qerrdown = imag(down) - imag(xxxx(k1));  %deviation of out of phase data from ideal location


Ierrordown(k1) = Ierrdown;

Qerrordown(k1) = Qerrdown;

end

Ierror1down = Ierrordown.^2;

Qerror2down = Qerrordown.^2;
```

```
for g1 = 1:L4
   magdow = Ierror1down(g1) + Qerror2down(g1);
   ma(g1) = magdow;
end
ma2 = sum(ma);
ma3 = ma2/L3;
ma4 = ma3^0.5; %Normalized to outer most state of constellation (EVM for symbols corresponding to bit 1).

EVM1 = mag5;
EVM2 = ma4;
mag6 = (ma4+mag5)/2;

%Error vector magnitude
EVM = ((ma4+mag5)/2)*100;%Averaged for the two symbol.

EVMdb = 10*log10(mag6);

%Bit error rate calculation
SNR = -EVMdb;%10*log10((1/(mag6^2))); %Signal to noise ratio.
```

```
BER_Initial = erfc((2*SNR)^0.5);

x = complex_signal; %complex sampled point

%LMS parameters

training = 10000;       % Number of repetitions for training

stepsize = 1e-3;       % step size/learning rate

order = 256;           % Order of the equalizer

U = zeros(1,order); % Input frame, 1 (row) by 256 (Columns) matrix

W = zeros(1,order); % Initial Weights, 1 by 256 matrix


%%

%LMS filter algorithm

start = tic;

for kk = 1 : training

   for nn = 1 : L2

      U(1,2:end) = U(1,1:end-1);  % Sliding window (extract information in row 1, column 2 till the end of matrix.

      U(1,1) = x(nn);              % Map the results


      y = (W)*U';       % Complex magnitude vector of equalized signal x(n).

      e = d(nn) - y;     % error estimate between desired symbol and equalized symbol

      W = W +  stepsize * e * U ;  % Update the weights until steady state condition is met.
```

```
        J(kk,nn) = e * e';        % Instantaneous square error
        a(nn) = y; %Output of the equalizer
    end
end
stop = toc(start);
%%
%Filter performance
Filt_Performance = freqz(W); % Spectrum of the designed filter
magnitude_response = 10*log10((real(W).^2)+(imag(W).^2));
phase_response = imag(W)./real(W);
NF = (0:length(W)-1)./(length(W)); %Normalised frequencies

subplot(2,1,1);
plot(NF,magnitude_response);
grid on;
xlabel('Normalised frequency');
ylabel('Magnitude response (dB)');

subplot(2,1,2);
plot(NF,phase_response);
grid on;
```

```
xlabel('Normalised frequency');

ylabel('Phase response(rad)');


%Cost function of the filter

figure('Name','Mean square error','NumberTitle','off');

V = mean(J,2); %Compute mean along dimensions on n, J(k,n)

Vlog = 10*log10(V);

plot(Vlog,'-r.');

grid on;

xlabel('Iterations');

ylabel('Mean square error (dB)');
```